TRIBOLOGICAL AND MECHANICAL STUDIES OF BIO-BASED NOVEL NANO COMPOSITES AND THEIR APPLICATION FOR WASTE WATER TREATMENT

Submitted in partial fulfillment of the requirements for the award of the degree of

DOCTOR OF PHILOSOPHY

In

MECHANICAL ENGINEERING

By

Mr. MANOJ PANCHAL
(Roll No. 716128)

Under the supervision of

Dr. G. RAGHAVENDRA

Assistant Professor

DEPARTMENT OF MECHANICAL ENGINEERING
NATIONAL INSTITUTE OF TECHNOLOGY
WARANGAL-506 004, TELANGANA, INDIA

MAY 2020

TRIBOLOGICAL AND MECHANICAL STUDIES OF BIO-BASED NOVEL NANO COMPOSITES AND THEIR APPLICATION FOR WASTE WATER TREATMENT

Submitted in partial fulfillment of the requirements for the award of the degree of

DOCTOR OF PHILOSOPHY

In

MECHANICAL ENGINEERING

By

Mr. MANOJ PANCHAL
(Roll No. 716128)

Under the supervision of

Dr. G. RAGHAVENDRA

Assistant Professor

DEPARTMENT OF MECHANICAL ENGINEERING
NATIONAL INSTITUTE OF TECHNOLOGY
WARANGAL-506 004, TELANGANA, INDIA

MAY 2020

Dedicated to

my Parents

NATIONAL INSTITUTE OF TECHNOLOGY
WARANGAL (T.S.) INDIA 506 004

DECLARATION

This is to certify that the work presented in the thesis entitled **"Tribological and Mechanical Studies of Bio-Based Novel Nano Composites and Their Application for Waste Water Treatment",** is a bonafide work done by me under the supervision of Dr. Raghavendra Gujjala and was not submitted elsewhere for the award of any degree.

I declare that this written submission represents my idea in my own words and where other's ideas or words have not been included. I have adequately cited and referenced the original sources. I also declare that I have adhered to all principles of academic honesty and integrity and have not misinterpreted or fabricated or falsified any idea/data/fact/source in my submission. I understand that any violation of the above will be a cause for disciplinary action by the Institute and can also evoke penal action from the sources which have thus not been properly cited or from whom proper permission has not taken when needed.

Date:

Place: Warangal

(Mr. Manoj Panchal)
Research Scholar
(Roll No.716128)

NATIONAL INSTITUTE OF TECHNOLOGY
WARANGAL (T.S.) INDIA 506 004

CERTIFICATE

This is to certify that the thesis entitled "**Tribological and Mechanical Studies of Bio-Based Novel Nano Composites and Their Application for Waste Water Treatment**", being submitted by **Mr. Manoj Panchal** for the award of the degree of Doctor of Philosophy in Mechanical Engineering, is the record of bonafide research work carried out under my supervision. **Mr. Manoj Panchal** fulfils the requirement of regulations laid down by the **National Institute of Technology, Warangal**, **Telangana State**. This work has not been submitted elsewhere for the award of any degree.

Dr. G. Raghavendra
Research Supervisor
Department of Mechanical Engineering

Date:
Place: Warangal

NATIONAL INSTITUTE OF TECHNOLOGY
WARANGAL (T.S.) INDIA 506 004

APPROVAL SHEET

This Thesis entitled **"Tribological and Mechanical Studies of Bio-Based Novel Nano Composites and Their Application for Waste Water Treatment"** by **Mr. Manoj Panchal (Reg. No. 716128)** is approved for the degree of **Doctor of Philosophy.**

Dr. S.K. PAL
(External Examiner)
Associate Professor, Department of Ceramic Engineering,
NIT Rourkela, India

Dr. G. RAGHAVENDRA
(Supervisor)
Assistant Professor, Department of Mechanical Engineering,
NIT Warangal, India

Prof. R. N. RAO

(Chairman and Head)
Department of Mechanical Engineering, NIT Warangal, India

Date:

ACKNOWLEDGEMENT

It gives me immense pleasure to express my deep sense of gratitude and thanks to my beloved supervisor **Dr. Raghavendra Gujjala**, Assistant Professor Department of Mechanical Engineering, National Institute of Technology Warangal, for his invaluable guidance, support and suggestions. His knowledge, and suggestions, and discussions helped me to become a capable researcher. He has shown me the interesting side of this wonderful potential research area. His encouragement helped me to overcome the difficulties encountered in my research as well in my life also.

I wish to express my sincere thanks to **Prof. N.V. Ramana Rao**, Director, NIT Warangal for his official support and encouragement.

I am very much thankful to **Prof. N. Selvaraj**, Head, Dept. of Mechanical Engineering for his constant encouragement, support and cooperation. I also express my sincere thanks to **Prof. P. Bangaru Babu** and **Prof. C.S.P Rao**, former Heads, Dept. of Mechanical Engineering for their constant encouragement, suggestions, support and cooperation.

I take this privilege to thank all my Doctoral Scrutiny Committee members, **Dr. K.V. Sai Srinadh**, Professor, Department of Mechanical Engineering, **Dr. V Suresh Babu,** Professor, Department of Mechanical Engineering, **Dr. P. Abdul Azeem,** Associate Professor, Department of physics for their detailed review, constructive suggestions and excellent advice during the progress of this research work

I am highly indebted to **Prof. R. N. Rao,** Design Section Head, Department of Mechanical Engineering for his valuable comments and guidance during semester presentations.

I take this opportunity to convey my special thanks to **Dr. Shakuntala Ojha** for her continuous encouragement, guidance during course of project & moral support.

I am very much thankful to **Dr. Syed Ismail,** Assistant Professor Department of Mechanical Engineering and **Dr. B. Satish Ben,** Associate Professor Department of Mechanical Engineering, for their guidance during course of project.

I would like to place on record my thanks to all the faculty and staff of Mechanical Engineering Department, NIT Warangal for the knowledge they have imparted to me.

I am thankful to my student colleagues **Mr. M. Omprakash**, **Mr. Pratap Naidu**, **Mr. Rajkumar Pittala, Mr. Syamkumar**, for the technical discussions that we had during my course work and research work. I would also like to thank my fellow research scholars from other departments, **Mr. Barghav, Mr. Shekhar, Mr. Vidish**. I would like to also thank M.Tech students (**Mr. Vinay kumar, Mr. Sidhharth**, **Miss Anjali, Mr. Mayank , Mr. Lalit , Mr. Abhinav**) their support while carrying out this research work.

A very special thanks to my dear friend **Mr. Soumya Ranjan Guru**, Research Scholar, IIT Kharagpur, for helping out with my project and providing me the moral support throughout my PhD.

A very special thanks to my dear friends, **Mr. Nitesh Kawadkar, Mr. Abhinav Kumar, Mr. Vivek Janu, Mr. Prasad Mahajan, Mr. Abhisek Tiwari, Mr. Paul Joseph, Mr. Garvit Saxena**. I specially thank **Mr. Sangmesh Gondegaon, Mr. SVB Vivekananda, Mr. Rafaque Ahmad, Mr. Sudarshan Chakravarthy, Mr. Y. Shiva Kumar, Mr. Abeyram Nitin, Mr. Chandrashekar Reddy and Mr. Kranti Kumar** for being my friends throughout this course. A special heartful gratitude to my Juniors **Miss B. Vasavi** and **Mr. Somaiah Chowdary** for being supportive and standing alongside throughout the course.

I heartily thank **Dr. Vishwanathan**, Professor, Humanities and Social Science Department for proof reading my papers and thesis.

I acknowledge my gratitude to all my teachers and colleagues at various places for supporting and cooperating me to complete the work.

Finally, I render my respect to all my family members (my father **Mr. Mahendra Panchal**, my mother **Mrs. Kokilaben Panchal**, my wife **Mrs. Rajni Jha,** my younger sister **Mrs. Vaishali Panchal**, my younger brother **Mr. Dhaval Panchal**, my youngest sister **Miss Amrapali Panchal**, my in laws **Mr. Jairam Jha** and **Mrs. Saroj Jha**) for giving me moral support and inspiration. They have motivated and helped me in my life. Also, I take this opportunity to thank all my relatives, friends and well-wishers who are part of this journey directly and indirectly.

Manoj Panchal

ABSTRACT

Owing to globalization and ecological concerns over the last decade, the research has been oriented towards development of biocomposites. Moreover, critical climate change and environmental pollution not only demand the use of biodegradable material in the composite field but also the utilization of biowaste to convert them into value-added products. Biowaste materials being natural materials are available in huge stock and are landfill materials. Dumping these biowastes material in an open environment, provide a safe passage for bacteria growth which in turn leads to bacterial disease. However, these waste materials could be of economic value when used in a sensible manner. Agricultural wastes contain cellulose, hemicellulose and lignocellulose which can be readily converted into useful material in the form of carbon. Further this carbon can be utilized in a number of ways (for air or water filtration, as filler material in composites). Beside agricultural waste, other such materials are avian products such as eggshells which are generated in tons or insect's cuticle such as crab shells, fish scales which are readily available and could be a potential source of fabrication of value-added products.

In this work, an attempt has been made to utilize these biowastes. The first material was eggshell. The eggshell particles were analyzed for its chemical and physical characteristics with the aid of different characterization techniques (XRD, CHNOS analysis, SEM, TEM, FTIR and TGA). After thorough characterization of particles, the composites with unboiled eggshell microparticle and boiled eggshell microparticle were made with epoxy as matrix material. Then the environmental behavior, and the erosion behavior of unboiled eggshell and boiled eggshell microparticulate composite was investigated. Based on analysis it was found that unboiled eggshell microparticulate reinforcement provides better results compared to boiled eggshell microparticulate. Then unboiled eggshell nanoparticulate epoxy composites with different weight percentages of eggshell nanoparticles concentration were made and their environmental behavior, mechanical behavior and erosion behavior were analyzed. The experimental analysis shows affirmative results for mechanical and erosion behavior.

The second material chosen was activated carbon. Activated carbon was prepared from one most produced biowaste, coconut shell. A novel method was developed for the preparation of activated carbon. Unboiled eggshell nanoparticulate which were used in composite fabrication here again used for preparing the activated carbon from coconut shells. Eggshell nanoparticles were used as a template as well as an activating agent for the synthesis of ordered porous carbon, while coconut shells act as a precursor. The synthesized activated carbon

particles were characterized with the aid of X-ray diffraction analysis (XRD), Raman Spectroscopy, thermogravimetric analysis (TGA), Scanning electron microscopy (SEM), transmission electron microscopy (TEM), and Surface area analysis. The adsorption capacity of synthesized ordered porous carbon was investigated with UV-vis spectroscopy.

This synthesized activated carbon was utilized for making composites. Composites with different percentage of activated carbon viz. 1 wt.%, 2 wt. %, 3 wt.%, were made. The environmental and erosion behavior of composites was investigated. Studies show the fruitful result of erosion wear resistance.

The third material chosen was chitosan. The chitosan nanopowder was prepared and characterized from crab shells. The powder was characterized using X-ray diffraction analysis, FTIR, ^{1}H-NMR Spectroscopy, TGA, SEM, TEM analysis and UV-vis Spectroscopy.

The synthesized chitosan nanoparticles could be employed in waste-water treatment as they have a tendency to absorb and adsorb toxic materials such as dyes. The size reduction provides the added advantage during filtration due to the presence of micropores. The antimicrobial ability of chitosan makes it a suitable candidate in textile industries as it inhibits the growth of microorganisms on textile. The prepared chitosan nanopowder was further used to make a pellet.

Finally, a novel composite sample was made for water filtration. A composite sample with silica, activated carbon, and eggshell nanoparticles, was fabricated using gel casting technique. The filter was characterized by SEM-EDAX and XRD analysis for elemental and morphological analysis. Prepared composite sample made from silica, activated carbon, and eggshell nanoparticles, was used along with chitosan pellet to check the dye adsorption ability of composite filter. TDS concentration and pH value were also checked before and after analysis. UV-vis Spectroscopy results revealed that the prepared filter (composite sample and chitosan pellet in combination) reduced the concentration of dye in the water solution hugely. The filtration through the composite filter reduced TDS concentration in water and also made the water from slightly acidic to basic. The use of composite filter purifies the polluted water and converts it into potable water.

Table of Contents

LIST OF FIGURES

LIST OF TABLES

LIST OF ABBREVIATIONS

SEM	Scanning Electron Microscope
TEM	Transmission electron microscope
TGA	Thermogravimetric Analysis
FTIR	Fourier Transform Infrared Spectroscopy
BET	Brunauer-Emmett-Teller
NMR	Nuclear Magnetic Resonance

Chapter 1

Introduction

1.1 Background

Over the last few decades, due to globalization, the ultimate objective of a material scientist is to find a novel material that would be economically sustainable and non-hazardous. This has led to the extensive use of polymer composites in automobile, aerospace, and defense and in many other mechanical applications. Extensive interest has been shown in the fabrication of polymer composites because of their extraordinary and tailorable properties, such as mechanical properties, thermal stability, and economical sustainability.

However, in the present age of advanced materials, products with commercial value in addition to sustainability to the ecosystem are becoming a potential topic for research. The concept of zero wastage is gaining importance for making new engineered materials with optimum properties with a reduced cost of fabrication. Transforming various natural materials into useful products for commercial applications has gained importance in the past few decades due to their abundant availability and better compatibility with conventional materials. Moreover, being biodegradable, these materials are not a threat to the environment. Critical climate change and environmental pollution not only demand the use of biodegradable material in the composite field but also utilization of biowaste to convert them into value-added products.

As far as natural materials are concerned, they are available in huge stock and are landfill materials and require a large area for dumping. One major pollution risk due to such huge stock is a major source of pathogens growth. However, they could be of economic value when used in a sensible manner. Most agricultural waste contains cellulose, hemicellulose and lignocellulose, which is a complex carbohydrate that can be converted into useful material in the form of carbon. This carbon can be used after activation for filtration purpose or used as reinforcing material in composites. Beside agricultural waste, other such materials are avian products such as eggshells which are generated in tons, or marine insect's cuticle such as crab shells, fish scales which are readily available and could be a potential source of fabrication of value-added products.

1.2 Eggshells

The basic function of an avian eggshell is to protect the egg against physical damage and microbial activities, provide passage for transfer of fluids (water and gas) and calcium for the embryo growth [1]. The eggshell is inorganic material which comprises a three-layered

structure with the outer layer called cuticle layer, the middle layer being calcareous layer and the inner layer being the mammillary layer. Eggshell is usually composed of calcium carbonate (by weight) ~94 %, calcium phosphate ~1 %, organic matter ~4 %, such as type X collagen, polysaccharides and other protein and magnesium carbonate ~1 % [2]. The annual production of eggs in India was about 82.929 billion units in years 2015-2016 [3]; if we see the statistics each year, egg production is growing. Eggshells contain 11% of the total egg weight [4]. If we calculate eggshell waste for the year 2015-2016, it would be 547331.4 tons. Statistics show huge egg production worldwide. Although the eggshells are biodegradable, huge production of eggs on a daily basis requires a large area for dumping and one of the major pollutions risks due to such huge eggshell stock is a potential source of pathogen growth. Eggshells have been used for numerous applications such as solid catalyst, limestone, correction of pH in agriculture, agricultural fertilizer, dental preparation, bone implantation and calcium supplement [4].

1.3 Activated carbon

Activated carbons are man-made materials known for their high porosity, high surface area and a broad range of surface functional group account for synergistic adsorptive characteristics. Porous or activated carbons have gained worldwide popularity and are seen as commercially viable options as adsorbents, catalyst, filters etc. due to their high adsorption capacity [5].

Porous carbon is produced by the activation of carbonaceous material. Activation is a process of eliminating certain functional groups, opening new inaccessible pores and broadening existing pores as well. Activated carbon can be prepared by two methods viz., physical activation and chemical activation [5]. The former involves the utilization of a gas such as carbon dioxide or steam, while the latter employs certain chemicals such as KOH, NaOH, $ZnCl_2$ [6] etc. Industries have been using activated carbon for decades for various applications such as wastewater treatment [7,8], medicinal use [9], gas separation [10], removal of pollutant and odors from the air (air purification [10–12], energy storage device [13,14], as filler material in composites [15] and the spectrum of application that porous carbon covers is immense.

1.4 Chitosan

Chitin is a natural polysaccharide like cellulose. It has multiple units of D-glucosamine. Crustaceans (lobsters, crabs, shrimp etc.) shells, insect cuticle, fish scales and cell wall of fungi

[16,17] are some of the sources of chitin. Chitin is a natural polymer consisting of β (1→4)-linked D-glucosamine and *N*-acetyl-D-glucosamine [18]. Chitosan is prepared by de-acetylation of chitin. Chitosan has a unique set of physiochemical characteristics such as, biodegradability, biocompatibility, hydrophilicity, antifungal and antibacterial properties [16,18,19]. These aforementioned properties open up the path for numerous applications of chitosan in tissue engineering, agriculture, nutritional enhancement, pharmaceutical industries and wastewater treatment.

1.5 Polymer composite

For the last few decades, polymers and polymeric materials have found their way into engineering applications and have become an important class of material. For decades, polymers have been tremendously used in everyday life due to their applicability in routine work. The inception of the polymers can be traced back to the early 19th century. The term polymer was first introduced by J. J. Berzelius [20]. The common chemical property which distinguishes polymers from another kind of materials is a high molecular weight, due to repeating units of covalent bonds. Some very important physical characteristics owing to high molecular weight are high viscosity, a wide range of elasticity, good strength etc. One of the first polymers was synthesized in the 19th century, by adding camphor to nitrocellulose, thus forming a polymer called celluloid [20]. The rapid growth of polymers began in the early 20th century with the development of Bakelite, polyester, PVC and later polyethylene, epoxies, and PEEK etc.

The industrial production of polymers began during world war II, with the production of PVC for insulation [20]. Polymers have a wide variety of applications ranging from household applications to space applications. Some applications of polymers are as consumable goods, food and packaging, medical applications (capsules and tablets), insulators, pipe and pipe fittings, constructions (doors, windows, ceilings), automobile body parts, coatings, sealings etc. Polymers lack certain properties such as strength, hardness, wear resistance and they have a low thermal resistance. They provide good compatibility with other materials when used in combination.

With the advent of composites, polymers have been extensively used for fabrication of polymer matrix composites. A composite is called a polymer composite when the matrix material is polymer while the reinforcement is fibers or particulates. The objective of polymer

composites is to exploit the superior properties of both matrix and reinforcement and form new tailormade properties.

Owing to the availability of a wide variety of matrix and reinforcements, polymer composites provides much more options in terms of design parameters to play with compared to the metal matrix and ceramic matrix composites. The reinforcement can be fiber or particulate. Furthermore, the fiber can be natural or synthetic fibers. Some examples of synthetic fibers are carbon fiber, glass fiber, aramid fiber, boron fiber etc. While naturals fibers are obtained from natural resources such as bamboo fiber, jute fiber, hemp fiber, coir fiber etc. Besides, fiber particulates are also used for enhancement of certain properties such as wear resistance, thermal stability, hardness etc. Sometimes these filler materials are used in combination fibers to make hybrid composites.

The filler materials are also can be divided into two categories conventional fillers and biofillers. Conventional fillers are TiO_2, SiC, SiO_2, calcium carbonate, Al_2O_3, ZrO_2 etc. while biofillers are particulates produced from natural waste. Polymer composites have a wide range of engineering applications due to special characteristics of polymers such as lightweight, corrosion resistance, self-lubrication some of the applications are gears, bushes, cams etc.

1.6 Nanocomposites

A composite is called Nano composite, when a constituent material in nanophase is introduced into the continuous phase (matrix material). The inception of nanomaterial can be traced back to the 9^{th} century in Mesopotamia. This was when craftsmen were supposed to have introduced silver and copper nanoparticles into the ceramic to get the glittering effect [21]. The first scientific application was traced back to 1857, where the preparation of gold nanoparticles was called ‘Activated gold’ by Michael Faraday[21].

The first industrial fabrication of silica nanoparticles was reported in the 1940s. Since the inception of nanomaterials, the nanocomposite field has been revolutionized. The reason behind the drastic growth in nanocomposite field is the attractive properties of nanomaterials.

A nanomaterial is divided into three different classes based on their dimension. When all the dimensions of material are in the nanometer range i.e. within 100 nm, such nanomaterials are said to be zero dimensional; these are nanoparticles, some examples of such nanoparticles are nanoparticles of TiO_2, SiC, Al_2O_3 etc. When two dimensions are in nanometers range while the third dimension is considerably bigger than other two, the material may be said to one

dimensional nanomaterial; such materials are in the form of elongated wires or tubes as shown in figure 1.1 (b) examples of such materials are nanowires, carbon nanotubes, nanofibers etc. When one dimension of material is in nanometer range i.e. within 100 nm, it is said to be two-dimensional nanomaterial; such materials are in the form of sheet or ribbons or they form plate like structure as shown in figure 1.1 (c); the examples are nanoplatelets and graphite flakes.

Nanomaterials boost electrical, physical, thermal and mechanical properties of the base material. Polymer nanocomposite has multiple constituents, where the primary constituent is polymer while the second constituent is filler, which has at least one dimension below 100 nm [22].

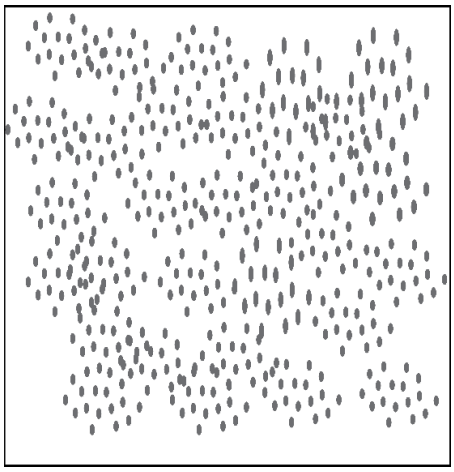

(a) Nanoparticles

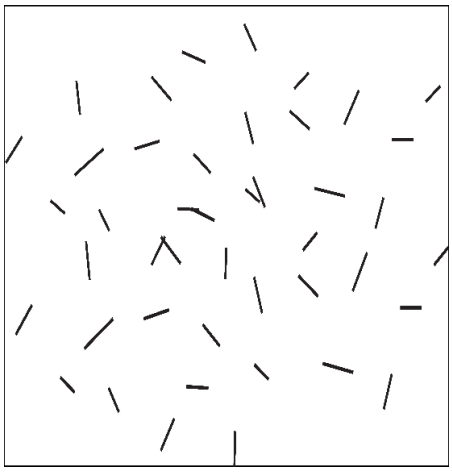

(b) Nanowires

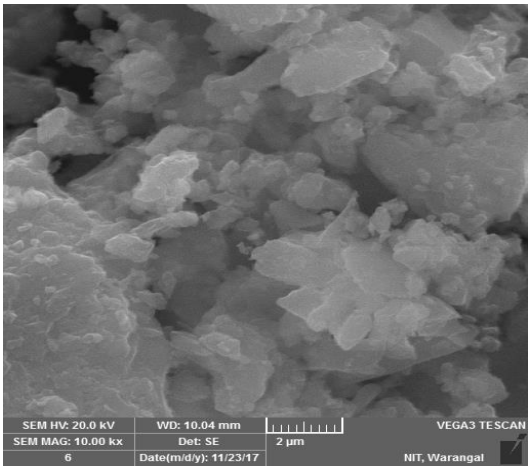

(c) Graphite flakes

Figure 1.1 Type of nanomaterials

1.7 Water filtration

Everything in nature that exists is made of five basic elements of life on the planet; water, earth, air, fire, space. If someone tries to alter their form, it will have an adverse effect on life in any form i.e. humans, animals or plants. It is our duty to protect our environment but the most intellectual form of life (human) has invested every effort in destroying nature in exchange for money and power. With the advent of globalization and industrialization, the human race has put the environment in jeopardy and conceive advancements as a way of technological evolution. Among these five elements of life on the planet, clean water which was easily available in earlier days, has become a scarce commodity owing to industrialization and several other factors, involving human activities, such as exponentially growing human population, deforestation, urbanization etc.

The runoff of unprocessed industrial wastes, dumping of industrial waste, human waste and agricultural runoff [23] in water are hazardous to aquatic life as it pollutes natural water sources. According to WHO Joint Monitoring Program (JMP) in 2015, it was estimated that 660 million people globally do not have access to drinking-water sources. Drinking water sources which have been contaminated by faecal matters used by at least 2 billion people [24].

Contaminated water causes several diseases such as cholera, dysentery, typhoid, diarrhea, and polio etc. It is predicted that 58% of diarrheal disease alone was responsible for 8,42,000 deaths per year, due to contaminated water supply, sanitation and hygiene[24]. Only 2.5% of water is freshwater from the global water reserve while the rest is saline and out of 2.5%, only 0.007% of water is directly available for use [25]. Based on an estimation approximately 2.4 billion people are living in highly water-scarce areas [26].

Ongoing research aims to make use of technology for water treatment more energy efficient, cost-effective and easily available in order to provide potable water to everyone. Development of new materials, new design and modification of existing water facilities has a major role in achieving the above-mentioned role. There are a number of techniques which have been developed for water treatment over a period of time; the very basic method starts with boiling, then further development leads to different techniques such as coagulation and flocculation, deionization, adsorption, membrane technologies etc. These processes can be categorized as physical or chemical, based on treatment phenomenon, for example, membrane technology such as reverse osmosis falls under the category of physical technique while

adsorption is categorized as chemical or surface phenomenon. Treatment with a certain chemical such as chlorination comes under the category of chemical technique.

However, techniques such as reverse osmosis, ultra-filtration, ozonation are costly and require huge investment would not be feasible for everyone. Development of innovative techniques is very much needed which will not require much power and would be easily available and cheap.

1.7.1 Factor affecting water quality

- **Total Suspended solid**: particles which are bigger than 2 microns are come under suspended solids. Anything floating in water such as gravel, sand particles, silt, organic particles comes under the category of suspended solids. These particles can be seen with naked eyes when floating in the water column. Some heavy particles such as gravel and sand particles can be separated by sedimentation while light particles which do not settle in still water requires a filtering medium for removal. Suspended solids also contribute to the turbidity of water.
- **Turbidity**: Turbidity is the opacity of water due to the presence of suspended particles such as silts and clay, suspended chemicals such as manganese and iron, and organic matter such as plant remains and microorganisms. It is an indicator of the aesthetical appearance of water that as the turbidity increases, clarity of water reduces. Turbidity is an important parameter pertaining to water quality. According to the World Health Organization, the turbidity of drinking water should be below 1 NTU (nephelometric turbidity units)[27].
- **Total dissolved solids**: Total dissolved solids (TDS) broadly describes the dissolved salts and organic matter in water. The main constituents are salts of calcium, sodium, potassium, magnesium and metals. The primary sources of TDS in water are industrial discharge, agriculture or residential discharge etc. According to BIS (Bureau of Indian standards), the maximum permissible limit of TDS is 500 ppm.
- **Heavy metals**: the presence of metals that have a significantly high density such as mercury, lead, cadmium, arsenic, zinc, nickel, copper, iron etc. in water is a health hazard as these metals are toxic in nature. Mining is a major source of water pollution due to heavy metals. Out these metals, cadmium, lead and mercury are very toxic in nature and even a small amount is hazardous to human health [28].
- **Fluoride**: According to WHO guidelines the maximum allowable limit of fluoride in drinking water is 1.5g/L. Higher intake of fluoride carries a risk of skeletal fluorosis. A

compound of fluoride used for aluminum, steel and glass production. Industrial effluents which carry fluoride are a major source of high concentration of fluoride in water.

- **Hardness**: water is characterized as hard or soft depending on the presence of ions of calcium and magnesium. Moderately hard water does not have any effect on human health. The hardness of water varies depending on geographical location. Sometimes calcium and magnesium ions in drinking water are beneficial to people who have a deficiency of minerals [29].
- **Microorganism:** There are several bacteria which are invisible to naked eyes; these are called microorganism (such as Shigella, Escherichia coli, Vibrio, and Salmonella), these bacteria can cause diseases such as typhoid, diarrhea, cholera etc. the most common is E. coli bacteria which originate from the feces of warm blooded animals causing diarrhea, stomach pain, bloody diarrhea etc. Diarrhea alone is responsible for thousands of deaths each year[30,31]. According to WHO it must not be detected in a 100ml of the water sample.
- **pH value**: The acidic or basic nature of water is determined by its pH value. The pH value describes the reaction of hydrogen ion in water. Based on pH value a liquid is characterized as acidic or basic. If the pH value of an aqueous solution is less than 7 it is identified as acidic while solution with a pH value of more 7 than it is characterized as basic. Generally weak acid or base does not have any health effect on humans, WHO does not provide any specific limit for pH value in drinking water, however, lower pH value i.e. acidic water results in corrosion in pipelines, which could contaminate the water. In general drinking water has a pH value between 6.5-8. According to EPA (Environmental Protection Agency) guideline, the pH value should be between 6.5-8.5. [32]

1.7.2 Source of water pollution

There are several sources of water pollution such as agricultural runoff, industrial wastewater, residential runoff etc. While agricultural runoff and residential runoff also pose threat, the scale of pollution of industrial waste runoff is much higher compared to the other two. There are several kinds of industries which are responsible for water pollution; textile industries, chemical manufacturing industries, printing industries, petroleum refining industries, leather industries, paper manufacturing industries, construction industries, metal industries and pharmaceutical industries etc. [33,34]. These industries produce different kinds of wastes such as dye waste, acid and bases, toxic chemicals, heavy metals, inks, paint waste,

hydrocarbons etc. [33,34]. One major effluent that causes water pollution is dye waste. For example, textile industries produce millions of liters of dye toxic wastes.

Oily layer and organic matter present in dye waste increase the turbidity of water, giving it a foul smell and changing its color. Textile waste is also very harmful to aquatic life as it reduces dissolved oxygen in water owing to restriction to photosynthesis [35]. Moreover, when the effluent flows through fields resulting in clogging of the pores in soils it consequently hampers the soil efficiency for agriculture.

1.8 Organization of thesis

The second chapter discusses literature to briefly explain, work related to natural fillers i.e. eggshells, activated carbon, and chitosan in the field of composite and water treatment.

In the third chapter a detailed discussion about the synthesis and characterization of eggshell micro and nanoparticles, activated carbon, and chitosan is presented.

The fourth chapter gives a detailed description of environmental behavior under different environmental conditions, solid particle erosion behavior and mechanical behavior of eggshell micro and nanoparticulate epoxy composite.

The fifth chapter deals with environmental and solid particle erosion behavior of activated carbon epoxy.

In the sixth chapter, the preparation and characterization of Silica-Activated carbon-eggshells composite filter for water filter applications has been presented.

The seventh chapter presents concluding remarks of findings and states the scope for future studies.

Chapter 2

Literature Review

2.1 Introduction

The rationale behind the review of literature is to gather necessary information connected with research as well as discusses recent trends in the research area. Also, the review relates the present work with past research, cements evidence of present research and carries forward the past work. The literature presented here is mainly concerned with natural biofillers, their properties and use in different application i.e. composite and water purification.

2.2 Biocomposite

Since the inception of research in the composite field, synthetic fibers or inorganic particles with high modulus have been points of attraction and have been used for decades, however, high cost and environmental hazard of aforementioned reinforcement has led to growing research and development of biocomposites. A composite is called a biocomposite when one constituent is derived from renewable resources, such as avian products or cellulose fibers such as rice husk, rice straw, bamboo, coconut shell, jute, hemp, eggshell etc. There are quite a few examples found in literature where agricultural waste is used as reinforcing material for composite applications.

For example, Lee, S. et al. [36] studied the interfacial adhesion between polylactic acid (PCA) and polybutylene succinate (PBS) with bamboo fiber and also the tensile properties and water absorption behavior of bamboo fibers reinforced polymer composite.

Pirayesh, H. et al. [37] investigated the mechanical and physical attributes of urea–formaldehyde (UF) resin reinforced with walnut and almond shells in different particle ratios. It was found that the addition of walnut/almond particle significantly improved water-resistance of the composites. However, flexural properties decreased with increase in walnut/almond shells content.

Mishra, S. C. et al. [38] used chicken feathers as the reinforcing phase in an epoxy matrix. The effect of alkali treatment of chicken feathers on mechanical properties was investigated. It was concluded that the bending strength and elastic modulus of the composite made with alkali-treated feather was more than that of untreated feather.

Prithivirajan, R et al. [39] analyzed the mechanical properties of coir pith, rice husk and groundnut shell reinforced epoxy composite. It was concluded that the hybrid reinforcements improved the mechanical properties of the composite.

Khan, M Z et al. [40] investigated mechanical properties and thermal properties of Pinus and Shorea Robusta reinforced epoxy composites with different weight percentages. It was noted that the composite with equal weight fractions showed optimum results for mechanical and thermal properties.

Mounika, M. et al. [41] examined mechanical properties and textural properties of nanocellulose (extracted from pistachio shell powder) polyester composite. It was observed from the analysis that the reinforcement of cellulose enhanced thermal stability and mechanical properties.

Mounika, M. et al. [42] analyzed mechanical properties of polyester reinforced with nano cellulose extracted from green gram husk. The comparative analysis of mechanical properties of nanocellulose reinforced in polyester nanocellulose/banana fiber hybrid composites has been done. It was found that hybrid composite showed improved properties compared to nanocellulose reinforced polyester.

Rao, T. V. et al. [43] investigated the mechanical properties of polypropylene reinforced with banana fiber/ fly ash. It was observed that the mechanical properties of composite increased addition of fiber and biofiller.

Baby, A. et al. [44] analyzed the mechanical properties of the carbonized eggshell and borassus fiber reinforced polyester composites. Enhancement in mechanical properties was observed owing to incorporation of a fixed ratio of treated borassus fiber and 2 wt. % carbonized eggshell.

Sajith S et al. [45] examined mechanical properties of biowastes (coconut shell, rice husk and teakwood) reinforced epoxy biocomposite. Biocomposite samples were prepared with 2.5 and 4.5 weight percentage of biowastes. Different mechanical properties i.e. deformability, stiffness, elasticity and strain energy were examined. It was discovered through experimental analysis that different fillers favored different properties due to different amounts of lignin and cellulose. High amount of lignin enhances stiffness while high amount of cellulose favored deformability and provided better interfacial adhesion.

D.J. Kang et al.[46] characterized SEBS (poly(styrene-b-ethylene/butylene-b-styrene)) composite reinforced with variable percentage of eggshell and silk fibroin. FESEM results revealed that SEBS/eggshell/silk composites show better dispersion of particles than SEBS/eggshell composites. The DSC thermogram results showed that thermal stability also improved due to the addition of eggshell and silk fibroin. It was concluded that silk fibroin helps to enhance adhesion between eggshell and SEBS matrix.

Khraisheh, M. et al.[47] investigated the photocatalytic removal of three pharmaceutical and personal care products pollutants using novel TiO_2– Coconut Shell Powder (TCNSP) composite. It was found that UVC/TCNP combination resulted in 99% removal compared to 30% for TiO_2.

Among the fillers, eggshell is avian filler, which has a very high tensile modulus (47.4 to 53 GPa) [48], impact strength, toughness, and good lubricating properties, excellent wear resistance due to the presence of $CaCO_3$. Eggshell has a density of around 2.1 g/cc, there are few reports in the literature where eggshells have been reported to be used as reinforcing material.

Mičicová, Zuzana, et al. [49] prepared polymeric rubber blend using eggshells as filler material. The effect of various factors on curing characteristics was evaluated. Also, the mechanical properties of the prepared samples were compared with a reference blend. The results obtained from testing mechanical properties suggested that eggshells could be a possible replacement of carbon black.

Rahman, GM Shafiur, et al. [50] investigated the effect of a variable percentage of viz. 5 wt.% ,10 wt.% ,15 wt.% ,20 wt.% and 25 wt.% eggshell filler addition on the physical and mechanical properties on eggshells particulate reinforced polyester composite. It was observed that 10 wt. % of eggshell powder filler composite showed optimum mechanical properties. Water absorption test showed that the water absorption of composite films was time-dependent function and it was found to be optimum at 10 wt. % with eggshell powder addition.

Toro, et al. [2] evaluated tensile strength of the polypropylene eggshell composite and compared polypropylene eggshell composite with different size and proportion of fillers and with commercial talc and calcium carbonate filler. It was observed that Young's modulus was found to improve with an increase in eggshell content.

Ji, Genzhong, et al. [51] studied the effect of the surface area of particles in epoxy resin. In their study, it was found that eggshell particle filler in epoxy resin improves the toughness of the composite. It was postulated the reason behind this synergic improvement in toughness was increased surface area of eggshell particles, which results in more sites of interfacial adhesion and proper bonding between the eggshells and epoxy powder particles. The Scanning Electron Microscope pictographs of fracture surfaces showed that voids, cavities, plastic

deformations and deboning were predominantly seen, leading to a decrease in the mechanical attributes of the composite.

Bootklad, et al. [52] studied the water resistance and thermal stability of chicken eggshell filler and thermoplastic starch composite. It was found that the addition of eggshell particulate in thermoplastic starch improved water resistance and thermal stability. On the other hand, it was observed that calcium carbonate and thermoplastic starch composite, compare to eggshell and thermoplastic composite had lower resistance to water and thermally stable. This happened because eggshell filler has strong adhesion compared to calcium carbonate, as observed by scanning electron microscope (SEM) and different micrographs.

2.3 Potential of eggshells as water filtration agent

Eggshells and eggshell membrane are often used in the removal of impurities, they used as catalysts for biodiesel production, as reinforcing materials in composites, use of eggshells is also common in the medical field due to the high percentage of calcium carbonate for the synthesis of hydroxyapatite and as a calcium supplement.

In earlier days, calcium carbonate was the usual choice for water purification. It is generally observed the water flowing through capillary cracks in the rock is filtered water; these rocks generally contain calcium carbonate. Calcium carbonate is a major constituent of eggshells as described in the previous chapter beside calcium carbonate; it contains small amounts of organic protein and other chemical compounds (calcium phosphate, magnesium carbonate). Eggshell generation is huge every year, as mentioned in the previous chapter; therefore, the environmental aspects should be taken into consideration in order to add value to eggshell and avoid their dumping in an open atmosphere. Moreover, the use of eggshells as a substitute for calcium carbonate may reduce the burden on nonrenewable natural sources of calcium carbonate. There are a few examples found in the literature where research work has been carried using eggshells for water treatment.

For example, Vijayaraghavan, K. et al. [53] used eggshells for the removal of copper from aqueous solution. W.T. Tsai et al. [54] had tested adsorption of dyes (blue 9 and orange 51) from aqueous solution using eggshells. Köse, T. E., & Kıvanç, B [55] used eggshells for adsorption of phosphate. Eggshells also used for the removal of heavy metals from contaminated water [56–58]. Use of eggshells for the removal of pharmaceuticals wastes also

found in literature [59,60]. Based on the literature it may be concluded that the eggshells could be a potential material for water filtration application.

2.4 Activated carbon

There are numerous examples in the literature where agricultural and industrial wastes have been utilized on a continuous basis for the extraction of carbon. Nowadays finding a cheap, easily available, potential agricultural waste material as a precursor for extraction of carbon is an exciting area of research. The secondary area of research is finding optimal parameters (activation methods, activating agent, activation time, activation temperature etc.[61], to get high pore size, high surface area and finding novel applications for porous carbon.

2.4.1 Method of activation

Method of activation for preparation of activated carbon are categorized into two types viz. physical activation and chemical activation. Both methods have some advantages and disadvantages.

2.4.1.1 Physical activation

A physical activation is a two-step process, comprises carbonization or pyrolysis and thermal activation. In the first step the carbonaceous material heated in an inert atmosphere at elevated temperatures, this process is pyrolysis. Pyrolysis results in decomposition of organic materials; during this process the carbon and other elements are separated (hydrogen, oxygen). Upon pyrolysis, crystalline graphite structure is formed. The second step, thermal activation, involves oxidation of biochar produced from pyrolysis of carbonaceous material. Oxidation of char is done by carbon dioxide or steam or a combination of both. Microwave heating also can be used for thermal activation. Oxidation of char results in the formation of new pores, broadening existing pores and removing the blockage from pores.

2.4.1.2 Chemical activation

Unlike physical activation which involves two steps; pyrolysis and activation, respectively, chemical activation is a single-step process. The chemical activation combines both the steps, carbonization and activation. Chemical activation requires a relatively lower temperature for activation compared to physical activation. In chemical activation, the carbonaceous material is mixed with a dehydrating agent such NaOH, KOH, $ZnCl_2$, H_3PO_4

etc.,[6] and pyrolyzed at elevated temperatures. Then the pyrolyzed product is washed with deionized water or dilute acid to remove the activating agent.

2.4.2 Natural biomaterial as a source for carbonaceous material

Broadly speaking, plants made up of three parts, namely, roots; leaves and stem, each of which has their own specific function. Their reproduction results in the growth of nutrition rich flowers or fruits or both. Each of these is made of several plant tissues, which in turn made up of plant cells. The plant cells consist of different organelles most of which are the same as human organelles. However, plants do have some features that humans don't. These are cell walls, cell membrane, central vacuole and plastids. The function of the cell wall is to provide structural support; protection and act as transferring media that allow the transfer of fluids such as water, CO_2 and O_2. The cell wall is a composite structure containing hemicellulose, cellulose, lignin and pectin; it comes under the category of lignocellulosic material [62]. Some intracellular substances also come under the category of lignocellulosic material. These intracellular substances are called extractives. Each of these chemical compounds has a variable concentration of carbon. Thus, the amount of carbon content in char is dependent on the carbon present in these aforementioned compounds i.e. cellulose, hemicellulose, lignin etc. Lignocellulosic materials are most abundant materials found in the world and readily used as a precursor for the synthesis of activated carbon.

Activated carbon or porous carbon can be extracted from various agricultural residues. A number of examples are found in literature where various agriculture wastes such as corn cob, wood apple shell, bagasse, wheat, rice husk, rice straw, coconut shell, bamboo, date stone, olive stone, peach, apricot, raspberry seeds, rice hull etc. [6] are precursors for extraction of activated carbon.

For example, Nabais, J et al. [9] used the almond shell as a precursor for activated carbon production. The surface properties and physical properties were also examined. The results from the FTIR analysis showed that activated carbon has several surface functional groups such as hydroxyl, ester, pyrones, lactones, Si-H etc. The results from BET analysis shows that the micropores appear due to the activation process.

Sekirifa, ML et al. [63] investigated the surface properties, adsorption capacity, and element analysis of activated carbon derived from date stones. It was found from adsorption results that the activated carbon obtained from date stones could be a potential adsorbent for 4 chlorophenol. BET analysis shows that micropores are observed in activated carbon from date

stones. It was concluded that different varieties of date stones have the different adsorptive capacity and could be used as heterogeneous catalysis.

Torres-Perez et al.[7] used sugar beet pulp and peanut hulls for activated carbon preparation using steam as an activating agent and analyzed the adsorption properties of obtained activated carbon for arsenic removal.

Hong, Seok-Min, et al. [64] derived activated carbon from wheat flour by activation with various ratios of KOH. The highly porous activated carbon thus obtained was investigated for carbon dioxide adsorption. It was concluded that micropores with a pore diameter of less than 0.8 nm have a significant effect on CO_2 adsorption as compared to larger pores.

Li, Bingjing, et al. [65] used three types of activated carbons viz. coal, a fruit and coconut shell activated carbon for batch and column adsorption test for de-chlorination of water.

Jain, Akshay et al. [66] presented a review on heating biomass utilizing hydrothermal process and subsequently converting biomass into activated carbon with high porosity using the chemical activation process.

Gaya et al.[67] synthesized doum palm shell activated carbon using three activating agents i.e. KOH, NaOH and $ZnCl_2$. The synthesized activated carbon analyzed for cadmium and lead adsorption from wastewater.

Abioye, A.M. and Ani, F.N. [68] have reviewed the potential applications of activated carbon synthesized from various agricultural waste.

Zhang, YJ et al. [69] had investigated the effect of different process parameters such as activation time, temperature, activation agent on pore structure, surface chemistry activated carbon (AC) extracted from bamboo waste. Optimum temperature and activation time were found to be 850ºC, and 120 min respectively for steam activation. Fourier transform infrared spectroscopy (FTIR), and X-ray photoelectron spectroscopy (XPS), results showed that steam activation changed the content of oxygen-containing group in comparison with pyrolyzed char. Activated carbon obtained using optimum process parameters showed exceptional potential for methylene blue adsorption.

Smets, K et al. [70] studied the influence of activation temperature, activation time and activating agent (steam and CO_2) on the surface properties of activated carbons obtained from rapeseed cake and raspberry seed cake. The results obtained from BET analysis showed that

the longer the activation time and the higher temperature, the higher was porosity of activated carbon irrespective of activating agent used (steam and CO_2). It was concluded that raspberry seed cake is a better raw material than rapeseed cake. Moreover, activated carbon from raspberry seed cake prepared by steam activation at optimum conditions (900^oC for 90 min) showed results which were as well as commercially available activated carbon in a phenol batch adsorption test.

Among all aforementioned agricultural residue, coconut shells are one of the major wastes produced worldwide. The coconut shell has a very high amount of cellulose and lignin content. A section on the literature on the preparation of activated carbon from coconut shell is given below.

Yang, K et al. [71] utilized coconut shell to synthesize activated carbon via physical activation method. Activated carbon synthesized using microwave heating has a very high surface area. Results of BET analysis confirmed highly porous activated carbon. Different activating agents have been compared viz. steam and carbon dioxide with microwave heating. It was found that microwave heating provides better results than the other two activation methods. However, the activation time is longer than the other two activating agents.

L. Yue et al.[12] characterized activated carbon doped with nitrogen derived from coconut shell. The synthesis process begins with the carbonization of coconut shells followed by urea modification and K_2CO_3 activation. It was found that derived porous carbon displays high CO_2 removal at 1 bar, even sorption capacity, at 0^oC. From kinetic studies, it was established that the obtained porous carbon had fast adsorption kinetic. Finally, it was concluded that nitrogen-doped porous carbon derived from coconut shells could be a potential substitute for CO_2 sorption.

2.4.3 Applications of Activated carbon

Activated carbon has a broad area of applications such as in water treatment, air purification, as an energy storage device, and as filler material in composites. Carbon has been used for water purification for ages. Nowadays carbon is used in a slightly different form and surface variety, for water treatment. Numerous examples have been found in literature where activated carbon is used for purification of different impurities present in dyes, phenols, heavy metals, turbidity, microorganism etc. which are found in sewage water and industrial waste water. The following section reports recent trends in applications of activated carbon.

Amuda, O. S. et al. [72] had studied heavy metal removal capability of activated carbon removal from industrial waste water. Khalil, HPS Abdul, et al [73] had investigated the mechanical, and the physical properties of Carbon black and activated carbon polyester composites. Din, A. T. M et al. [74] also made similar studies for Carbon black and activated carbon polyester composites.

Ojha, S et al. [15] investigated the mechanical and tribological properties of wood apple carbon black and coconut shell carbon black particulate polymer matrix composite.

Isah A. et al. [75] had evaluated the adsorption capacity activated carbon for the removal of reactive blue 19 dye from aqueous solution. K.G. Raj and P.A. Joy [76] had fabricated nanocomposite adsorbent material fabricated using coconut shell-activated carbon and iron oxide nanoparticles and tested for an oil adsorption.

Tahir, D et al. [77] had investigated the molecular properties, structural properties, and chemical composition of the activated charcoal polymer composite.

Giorcelli, Mauro, et al. [78] had tested the mechanical properties of biochar-epoxy polymer composite.

Based on literature it may be concluded that activated carbon has a broad area of application, however, the use of activated carbon in composites is limited, which requires further exploration.

2.5 Isolation of chitosan and its applications

Chitin is a natural polymer, as described in chapter 1. Chitin can be extracted from fish scales, shrimp shell or crab shells. Crustacean shells are made of chitin, protein, and $CaCO_3$.

Many researchers have prepared chitosan from crustacean shells, fish scales and crab shells with varying concentration of acid (HCl) and base (NaOH) through the de-acetylation process. The concentration of NaOH decides the degree of de-acetylation.

M. Mahdy Samar et al.[79] produced chitosan from shrimp waste by de-acetylating waste under microwave irradiation. It was concluded that higher concentration of NaOH results in an increased degree of de-acetylation and that separation time decreases hugely when compared to thermal heating. A similar observation has been made by F.A. Al Sagheer et al.[80] for extraction of chitosan from α and β Chitin from different marine crustaceans.

Kucukgulmez et al. [81] isolated chitosan from shrimp shell and compared the fat and water holding capability of chitosan with commercial chitosan. It was concluded that isolated

chitosan showed better fat and water holding capability comparable to commercial chitosan. E.S. Abdou et al.[82] attempted to extract chitosan from chitin using autoclave heating. Autoclave heating reduces the time of de-acetylation hugely.

Paul, Sneha, et al. [83] prepared Chitosan from prawn waste (shell). The chitosan thus prepared was studied for its suitability in pharmaceutical applications. Kumari, S. and Rath, P.K [84]extracted chitosan from fish scales. Chitosan was studied by FTIR, XRD and SEM analysis. M. T. Yen et al. [85] prepared chitosan from crab chitin by de-acetylation at different periods of time (60, 90 and 120 min). It was concluded that the more the reaction time, the higher the DD (degree of de-acetylation).

M. Hamdi et al.[86] isolated chitosan from blue crabs and shrimp shells employing CO_2 for deproteinization followed by de-acetylation. They eliminated the demineralization process.

There are quite a few methods available in the literature for the preparation of nanoparticles of chitosan. These methods are ionotropic gelation, polyelectrolyte complex, microemulsion, reverse micellar method, and emulsification solvent diffusion [87]. Out of these, ionotropic gelation and polyelectrolyte complex are the most common methods for the preparation of chitosan nanoparticles.

Ball milling is another approach which can be used for nanoparticle preparation. There are certain benefits of ball milling such as retention of chemical properties and structure of prepared chitosan.

Jothimani B et al. [88] synthesized and characterized the nanoparticles of the substituted derivative of chitosan and N-(Thiophene-2-acetyl) chitosan. It was confirmed that modified chitosan has easy processability.

Chen, Xi, et al. [89] examined the effect of various modification methods on chitin. It was observed that ball milling was the most effective method to change crystallinity and hydrogen bonding amongst all methods.

Zhang W et al. [90] analyzed the influence of ball milling on chitosan. They concluded that the milling time of more than 8 hrs. does not affect particle size. It was also observed that the crystalline structure was destroyed due to milling.

Sari K et al. [91] studied the influence of varying milling time on the microstructure of chitosan and concluded that the milling changes the crystalline size, but there was no change in chemical structure.

Tran, Thang Hong, et al. et al. [92]combined ball milling and chemical method for synthesis of chitin nanofibers and they further employed Chitin nanofibers with poly (L lactic acid) for composite preparation and investigated the mechanical properties.

2.6 Summary

The above literature survey summarized the studies that have been carried out on natural biofillers, their properties and use in different applications. Three materials were selected after thorough literature review for preparation of composite in order to improve mechanical and tribological properties and their use for water treatment. Very limited work is available on using eggshells as filler material for mechanical and tribological properties, although eggshells have attractive properties. Very limited work is done on using activated carbon as filler material for tribological properties. There is plenty of research available on using activated carbon as filter material. No work has been done using a combination of material such as silica, eggshells and activated carbon composite in conjunction with chitosan.

2.7 Proposed Work

Natural fillers or biofiller are abundant in nature, their availability makes them a potential source for many applications, also the relative cost of these fillers is low compared to expensive metallic fillers which allow them to rival alternate materials for particular uses. The strong interfaces, bonding, and miscibility are key factors for the improved properties of natural filler polymer composites.

This research focused on achieving the following objectives.

1. Synthesis and characterization of the eggshell (micro and nanoparticles).
2. Synthesis and characterization of activated carbon from coconut shell.
3. Synthesis and characterization of chitosan from crab shells.
4. Investigation of environmental and tribological properties of eggshell epoxy composite.
5. Investigation of mechanical properties of eggshell epoxy composite.
6. Investigation of environmental and tribological properties of activated carbon epoxy composite.
7. Preparation and characterization of silica/activated carbon/eggshell nanoparticulate composite to be used in conjunction with chitosan pellet for water treatment application.

.

Chapter 3

Synthesis and characterization of eggshell (micro and nanoparticles), activated carbon and nano-chitosan

3.1 Introduction

Nanometer-scaled materials are those materials which have at least one dimension of less than 100nm as already described in chapter 1. Nanoplates, nanowires, nanoparticles, and quantum dots, in general come under the category of nanomaterials. For the last few decades, nanomaterials have been a very area of research owing to their distinct properties, which are not typical to materials in bulk. Those outstanding properties may be mechanical, electrical, optical and many more. The reason behind these astounding properties compared to bulk material is the high volume to surface ratio. Nanomaterials can be zero dimensional (nanoparticles); one dimension (nano wires) or two dimensional (nanometer-thin films). They occur in dispersed or agglomerated form with different shapes such as round, tubular, and uneven shape [93].

3.1.1 Nanoparticle Synthesis

Methods of synthesis of nanoparticles are divided into two categories.

1. **Top down Approach**: As the name suggests, this method produces fine particles from bulk material. This method is a conventional way of preparing nanoparticles through the grinding of bulk material. Ball milling is typical top down approach.
2. **Bottom up approach**: The term "bottom up" implies building nanoparticles from atoms or molecules. Bottom approach can produce very tiny nanoparticles compared to top down approach.

There are several types of bottom up techniques which are used for nanoparticle preparation.[94,95]

1. Electron (or ion) beams technique
2. Ultrasonic dispersion
3. Sol–gel
4. Inert gas condensation
5. Vacuum arc deposition
6. Chemical/physical vapor deposition
7. Molecular self-assembly
8. Molecular beam epitaxy
9. Metal–organic chemical vapor deposition
10. Electrodeposition

3.1.1.1 High energy ball milling

Ball milling is a top down approach. It uses impact force to reduce the size of particles. Milling time, milling speed, size of container, types of balls used, ball to weight ratio and grinding medium are some of the factors that determine the final size of particles. Ball milling is of two types depending on the reduction of size of particle. The first one is commonly used in industries with a cylinder rotating about its own axis either in horizontal or vertical direction. The balls continuously rotate inside the cylinder at a certain speed and crush the material. The second is a planetary ball mill that utilizes the principle similar to the sun and planet gear mechanism. An outer disc rotates at a certain speed and the slot for containers is fixed with the disc near the periphery of the disc. The weight of the container, balls and samples are balanced by placing counterweights accordingly. Planetary ball mills are generally used for laboratory purpose. The former helps in size reduction in micron range and later may reduce the size to nano scale.

3.2 Materials

3.2.1 Eggshells

Eggshells are natural sheaths that form on egg during their evolution and are thrown away while eating them; the eggshells have no commercial value and can be used as filler material. Eggshells have been collected from institute food court of NIT Warangal.

W.T. Tsai et al.[96] prepared eggshell powder through planetary ball milling by varying different process parameters such as rotational speed, milling time and mass loading. Different samples have been characterized by XRD, SEM and BET analysis for surface properties. It was found that the ball milled eggshell powder has a larger BET surface area than un milled sample. It was observed from XRD analysis that the crystallinity of eggshell particles reduces with milling and pore generation can be achieved.

Francis, A. A., & Rahman M.[97] prepared different samples of calcium phosphates by milling eggshells with different concentrations of phosphoric acid in the presence of gelatin. They attempted to explore the possibilities to prepare tailormade calcium phosphates for bio-medical applications.

Wu, Shih-Ching, et al. [98]synthesized hydroxyapatite powder using eggshells as a precursor via ball milling followed by heat treatment. Pure hydroxyapatite phase was observed

when sintering milled sample for of 10 hours at 1000ºC. The results obtained from the FTIR analysis showed the presence of a and b-type carbonates.

3.2.2 Coconut shells

Coconut (Cocos nucifera) belongs to a species of palm tree. Since ancient times coconut leaves have been used for decoration and culinary purpose. Coconut shell is waste part of the coconut, which is lignocellulosic agricultural waste. The outer part of the coconut is made up of fibers called coir while the inner part is referred to as endocarp, the hard part of coconut. The outer structure protects the pulp and water inside the coconut. India is third largest coconut producing country with annual production of 11,930,000 tons [99] . The shells can be used as fuel and as a source of charcoal. Activated carbon prepared from coconut shell is believed to be very effective for elimination of impurities.

3.2.3 Crab shells

Crabs are decapod crustaceans, the scientific name being Brachyura. They exist in fresh water and in oceans. They generally have a pair of claws and a very thick exoskeleton. This exoskeleton is made up of chitin, mineral and protein. Protein and chitin in the exoskeleton tissue form a protein-chitin matrix and calcification of this matrix results in hard shell.[100]

3.3 Methods

3.3.1 Preparation of eggshell microparticles

There are two different categories of eggshells considered in the studies, one being boiled egg shell (200^0 C) (treated) and the other unboiled (untreated) eggshells. These eggshells are thoroughly cleaned with normal water and dried in oven for 4 days to get moisture free eggshells. Dried eggshells are crushed into micro range using a laboratory ball mill.

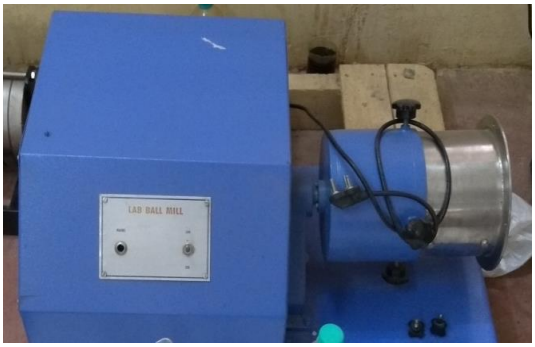

Figure 3.1 Laboratory ball mill

3.3.2 Preparation of unboiled eggshell nanoparticles

Nanoparticle preparation of unboiled eggshell particles was done using a planetary ball mill. Stainless-steel vials and 100 balls of 10mm diameter were used with a ball to weight ratio of 20:1 for milling eggshell particles. The rotation rate of the vials was fixed at 400 rpm. The total milling time was 8 hours at an interval of 30 minutes. The milled powder was stored in containers for further experimentation.

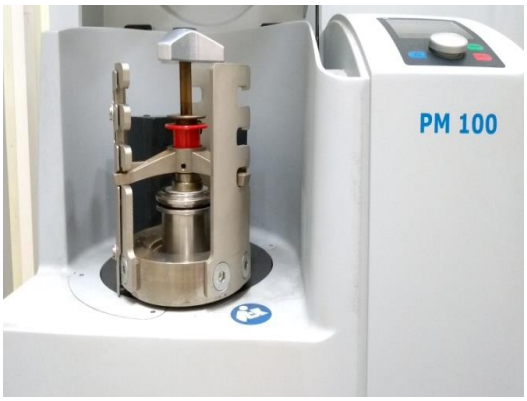

Figure 3.2 Planetary ball mill

3.3.3 Preparation of activated carbon

Activated carbon can have microporosity or combination of micro, mesoporosity and/or macro porosity. The combination of micro, meso and/ or macropores is called ordered or hierarchical porous carbon [101]. The preparation of ordered porous carbon requires the use of template material such as Silica [101], MgO [102] as in hard template, while polymers such as polystyrene, polyurethane, polymethyl methacrylate [101], OMMT (organically modified montmorillonite) [103] are used as soft template. The hard templates are required to be isolated or dissolved after the activation while soft template is thermally degradable. The template material will produce mesopores or macropores while activation results in microporosity. Beside agricultural waste there have been attempts to use polymer wastes to produce the hierarchical activated carbon. Ordered porous has better capacitance over microporous carbon, consecutively provide better options for energy storage devices. There have been attempts to use ordered or hierarchical activated carbon for water treatment as in capacitive deionization [104].

Here we have used a novel approach for single step synthesis of ordered porous carbon. Two of most produced biological wastes are used together to produce ordered porous carbon.

The two materials are coconut shell and eggshell. Eggshell as already well-known as it contains around 95% of $CaCO_3$, while coconut shell is rich in cellulose. Here we have used eggshell nanoparticles to generate mesopores. Eggshell particles used were unboiled eggshell nanoparticles.

Eggshells and coconut shells are both washed with deionized water and subsequently with ethanol. Cleaned eggshells and coconut shells were dried in sunlight for 2 days to get rid of moisture. The drying of shells results in crispy flakes, which in turn facilitate easy breaking of flakes during milling. Both unboiled eggshell nanoparticles and coconut shells were milled in the laboratory ball mill and sieved into fine powder. In order to find the optimum amount, the eggshell and coconut shell powders were mixed in different weight ratios viz. 1:1, 2:1, 3:1 and 4:1. Various ratios of eggshell unboiled nanoparticles and coconut shell powder were milled in the planetary ball mill.

To find the optimum temperature for activation, the powder was milled in the ratio of 1:1 and pyrolyzed on the Carbolite horizontal tube furnace at different temperatures viz. 600-1000^o C. Single step activation was carried out under a continuous flow of argon gas. After analyzing the samples, the mixture of coconut shell and eggshell in different ratios viz. 2:1, 3:1, 4:1 were pyrolyzed at 800^o C. New method for synthesis of activated carbon was developed using eggshell and coconut based on the principle given below.

$$CaCO_3(Eggshell) + CoconutShell \rightarrow CaO\ (Template) + CO_2(gas)\uparrow + Char \quad (3.1)$$

$$CaO\ (Template) + CO_2(gas)\uparrow + Char \rightarrow 2CO\ (AC)\ +\ CaO \quad (3.2)$$

$$AC + CaO + 2HCl \rightarrow Ordered\ Porous\ carbon + CaCl_2 + H_2O \quad (3.3)$$

The thermal decomposition of eggshells releases carbon dioxide gas and calcium oxide while the decomposition of coconut shells results in char. The carbon dioxide released from the decomposition of eggshells was directly utilized for activation of char as in physical activation. Calcium oxide produced during the decomposition of eggshell acts as a hard template which will further produce the mesopores and macropores.

The obtained powder was washed with HCl to remove hard template (CaO). This method provides a single step synthesis process unlike physical activation. The activated carbon was further washed with ethanol and deionized water. The sample Ids used throughout the paper are given in table 3.1.

Table 3.1 Nomenclature for different samples

Sample ID	Description
1:1	Eggshell and coconuts powder in 1:1 weight ratio pyrolyzed at 800º C
2:1	Eggshell and coconuts powder in 2:1 weight ratio pyrolyzed at 800º C
3:1	Eggshell and coconuts powder in 3:1 weight ratio pyrolyzed at 800º C
4:1	Eggshell and coconuts powder in 4:1 weight ratio pyrolyzed at 800º C
ESCS	Eggshell and coconuts powder mixture
Raw CS	Raw coconut shell powder

3.3.4 Preparation of nano-chitosan

3.3.4.1 Sample preparation

The base substance used for isolation of chitosan were Crab shells (collected from the local fish market) , are shown in figure 3.3. The crab shells were initially washed 3-4 times in tap water and then cleaned with ethanol for further removal of bacteria and contamination. The shells were also additionally cleaned with deionized water to remove the traces of the ethanol. The crab shells were dehydrated in the sun for three days and kept in vacuum oven for 1 day at 50° C to remove moisture.

3.3.4.2 Chitosan preparation

The entire procedure is divided into 5 stages:

A. Demineralisation

B. Deproteinization

C. Decoloration

D. Deacetylation

E. Ball Milling

A. Demineralization

In this process excess and waste minerals are removed from crab shells. Dried Crab shells and 2N HCl were poured in a conical flask. This mixture was heated for 8 hours on a magnetic

plate at 60^{o}C with continuous stirring. Crab shells began to lose their colour; which was an indication of completion of the process. The resulting product was then thoroughly rinsed with distilled water till the pH was 7. During this process the bonds between different compounds in the shells were broken due to the action of concentrated hydrochloric acid. Before advancing to the next stage of the process, the sample was further dried in an oven overnight at a temperature of 50° C.

Figure 3.3 Raw Crab shells

B. Deproteinisation

In this process crab shell flakes were heated to 60^{o}C with 2N sodium hydroxide solution in a ratio of 10:1 for 3 hours in a conical flask. After demineralization, the shells became weak and the organic compounds easily disbanded with this process. The samples were then kept at room temperature for 3 hrs.

This process was carried out to remove protein and other protein related compounds in the shells. These deproteinised scales were then treated with distilled water to remove any traces of sodium hydroxide. The pH level was maintained at 7. The product formed in the reaction is called "chitin".

C. Decoloration

After deproteinisation, the obtained powder was sticky. The product was further subjected to decoloration process. The product was treated with acetone in a ratio of 10:1 in a reflux condenser for 12 hrs. It is further dried in an oven to remove moisture and turn them into dry flakes for easy breaking.

D. Deacetylation of Chitin

The organic compounds are then removed by reacting the chitin obtained with 50% (W/V) NaOH solution at 90-95 degree centigrade for 4hrs and then it is kept at room temperature for 12 hrs. This process ensures the removal of the N-actyl group and only chitosan is left behind as a residue. Again the flakes are treated with deionized water to retain the required pH level.

E. Ball Milling

Chitosan flakes are first crushed using mortar and pestle and then converted from micro particles to nanoparticles by the planetary ball mill process. After milling, the powder is stored in a sealed container for further characterization. The parameters used for planetary ball milling of chitosan particles are given in table 3.2.

Table 3.2 Milling parameters

Parameters	**Details**
Diameter of balls	3mm
Ball material	Tungsten Carbide
Ball to weight ratio	20:1
Milling time	12hrs.
Milling Speed	400 rpm.

3.3.5 X-ray diffraction

X-Ray Diffraction (XRD) is a non-destructive technique for identifying concentrations of different phases present in a given sample. It may also be used for calculation of d spacing for the crystal structure of the material. A clear understanding of the composition of the material is obtained by XRD analysis.

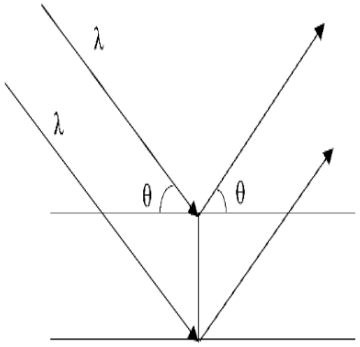

Figure 3.4 Bragg's law for diffraction

Bragg's Law is the main principle for XRD analysis. If d is the lattice spacing between two atomic planes of a crystal and x rays with wavelength λ impinges on the crystal at an angle θ, then according to Bragg's Law the path difference between two beams may be given by equation 3.4

$$2dsin\theta = n\lambda \tag{3.4}$$

where n is the integral multiple of wavelength λ. In XRD, the X ray impinges at a different angle θ on the sample and hence the intensities of the reflected light are recorded accordingly. The diffractogram obtained in XRD gives peak for constructive interference.

The position of peaks represents the constituents present in the material, distance between peaks identifies the crystal spacing and the area under peak represents the concentration of the different constituent present. The crystallite size may be calculated using the Scherrer equation[105]. The degree of crystallinity or percentage crystallinity may be calculated using equation 3.5.

$$\% \text{ Crystallinity} = \frac{\text{Area of crystalline peaks}}{\text{Total area of all the peaks}} \tag{3.5}$$

Figure 3.5 X-ray diffraction machine

X-Ray Diffraction (XRD) of different samples (eggshells milled powder, activated carbon and chitosan) was conducted on Malvern X-pert Pro X-ray diffraction machine, shown in figure 3.5 for quantification of element present in the sample for crystal analysis. Samples were scanned with 2θ angle which varies from 6^{o}-90^{o} with a step size of 0.008 degrees per second. X-pert software was used to investigate any change in crystalline structure and size transformation.

3.3.6 CHNSO analysis

A CHNSO(CHN-932) analyzers calculate the percentage of Carbon (C), Hydrogen (H), Nitrogen (N) and Sulphur (S) present in organic material.

This analysis works on the principle of the Dumas method which involved the complete combustion of the sample. The sample is placed in CHNSO analyzer and burnt in the presence of excess oxygen, which results in generation of nitrogen dioxide, water, sulphur dioxide and carbon dioxide. These compounds are then further detected by a thermal conductivity detector (TCD). [106].

3.3.7 FTIR analysis

Fourier- Transform Infrared Spectroscopy abbreviated as FTIR is a technique that uses infrared rays to probe. It works on the principle that different functional groups have different molecular 'fingerprint' and based on transmitted spectra the functional group can be identified. On the incidence of infrared radiation, the molecules absorb certain radiations and transmit others. The relation between the energy absorbed (E) and wavelength (λ) may be given as

$$E = \frac{hc}{\lambda} \tag{3.6}$$

where h is Plank's constant and c is the velocity of light. Thus, as the wavelength is reduced the energy absorbed is increased. It may be concluded that peaks for single bond are obtained at a lower wave number while double and triple bonds are obtained at higher wave number. This way transmission spectrum is observed. The spectrum may be divided into two regions. First one is the fingerprint region from 400-1400 cm^{-1} and it is difficult to interpret due to complicated spectrum. The second spectrum is from 1400-4000 cm^{-1} and is used for the identification of various functional groups present in the sample.

Figure 3.6 FTIR Spectrophotometer

For sample preparation of powdered sample, KBr is used with sample powder to make the circular pellet. PerkinElmer FTIR spectrophotometer with spectra range 4000-400cm^{-1} was used to analyze the sample as shown in figure 3.6

3.3.8 TG-DT analysis

Thermal Gravimetric Analysis, abbreviated as TGA, is used to study the thermal degradation of materials. It gives details of both the physical and chemical changes that a material undergoes while subjected to temperature changes.

Differential Thermal Analysis, abbreviated as DTA, is a technique in which the changes in temperature of a given substance and reference material at the inert condition are recorded. Thus, DTA is helpful in identifying the type of reaction (exothermic or endothermic) at a defined temperature range. The area under DTA curve is the representation of enthalpy change of the material. Exothermic reactions may be due to crystallization and oxidation of sample while endothermic reactions are due to decomposition, vaporization, reduction, fusion, etc. The uphill peaks are representation of exothermic reactions while the downhill peaks are typical of endothermic reactions.

Thermo gravimetric analysis (TGA) is conducted using NETZSCH STA 2500 thermo gravimetric analyzer as shown in figure 3.7. The parameters used were viz. temperature varying from 27-1000^{o} C at a heating rate 10^{o}C/min; argon gas flow rate was kept at 60 ml/min.

Figure. 3.7 Thermogravimetric analyzer

3.3.9 Raman Spectroscopy

Raman Spectroscopy is an analytical technique which gives complete detail about chemical structure, phase, morphology, crystallinity and molecular interactions of the sample. It works on the principle of transmittance of light upon the incidence on sample material.

Raman spectroscopy of activated carbon samples was carried out on T64000 Jobin Yvon Horiba Raman spectrometer with spectra varies between 1100 to 2000 cm^{-1} a laser source of 514 nm was used for excitation.

3.3.10 SEM-EDX analysis

A scanning electron microscope (SEM) generates the image of a sample by scanning with the concentrated electron beam. The electrons come in contact with atoms in the sample, which results in emission of secondary electron from the atom or back scattering of electron or transmission of electron. The secondary electron contains information about the surface topography and configuration of the sample.

EDAX (Energy-dispersive X-ray spectroscopy) is analytical for identification of elements present in the sample. EDX generally is an accessory of SEM.

For powdered sample very small quantity of sample was taken and attached to carbon tape. For non- conducting sample, a coating of conductive materials is required, gold being a very common material for coating purpose. SEM analysis was performed with the aid of Vega 3 Tescan and Zeiss scanning electron microscope.

3.3.11 TEM analysis

A transmission electron microscope uses transmitted electron unlike scanning electron microscope which uses secondary electron or back scattered electron. The sample is a very thin film through which an electron beam is transmitted. TEM provides details about crystal structure, grain structure and grain boundaries. High resolution can also be used to analyze the quality, shape, size of nano wires, quantum dots, nanoparticles etc.

TEM analysis of samples was conducted on JOEL 3010 High resolution Transmission Electron Microscopy Analysis as shown in figure 3.8. For TEM imaging of powdered sample, the powder has to be drop cast on carbon coated copper tape. Initially the powder sample was dispersed in ethyl alcohol; the solution was then cast onto the tape. Ethyl alcohol in dispersed sample evaporates at room temperature, resulting in a thin film of powder on tape. The tape is then analyzed with TEM for particle size and morphological studies.

Figure 3.8 Transmission electron microscope

3.3.12 Surface Area and pore size

Total surface of particles is the sum of the total area of open surfaces of particles per unit mass. The total surface area is calculated from Nitrogen adsorption of a powder. Brunauer, Emmett, and Teller (BET) method is most commonly used method to calculate the surface area. The pore size of particle can be calculated from the formula given in the equation below.

$$d_{BET} = \frac{6}{S_{BET} \times \rho} \tag{3.7}$$

Where d_{BET} is pore diameter, S_{BET} is total surface area and ρ is the theoretical density of the sample.

The surface area and the average pore size were analyzed using Quanta chrome Autosorb Automated Gas Sorption System. The surface area and average pore size of particles was calculated using BET analysis while BJH (Barrett-Joyner-Halenda) analysis was used to calculate the pore distribution. The adsorption and desorption analysis were performed using nitrogen gas with p/p_0 values varying from 0.1 to 0.99.

3.3.13 ^{1}H-NMR Spectroscopy

Nuclear magnetic resonance spectroscopy, most commonly known as NMR spectroscopy, is a spectroscopic technique to identify organic compounds, proteins and other complex molecules. There are two most common kinds of NMR, H-NMR (proton-NMR) and

C-NMR (carbon-13 NMR) spectroscopy. The sample to be tested is placed in a constant magnetic field and nuclei are excited by radio waves, which results in magnetic resonance of nuclei. Magnetic resonance signals are detected with radio receivers, which provides details about the electronic structure of the molecule and its functional group.

^{1}H-NMR spectra were performed on chitosan sample using Bruker Bio Spin GmbH NMR spectrometer to find out the degree of De-acetylation. 5mg/ml chitosan particles were dissolved in 2% deuterated acetic acid solution for NMR Spectroscopy. The spectral range of the measured data was 0 to 10 ppm. For the determination of Degree of De-acetylation, ASTM F2260-03 standards were used. The Degree of De-acetylation was estimated using equation 3.8. [107]

$$DD\% = \frac{H1-D}{H1-D+(H-AC/3)} * 100 \quad (3.8)$$

Where H1-D represents the integral at δ=3.17 ppm and H-Ac is the integral at δ=1.88 ppm.

3.3.14 UV- Vis Spectroscopy

UV-visible spectroscopy measures concentration based on absorbance of ultraviolet or visible light by a sample. UV-visible spectroscopy covers spectral range from 200-800 nm. UV-visible spectroscopy was used for both qualitative and quantitative evaluations of samples. The absorption of visible spectrum of light results in a change of color of certain chemicals, which then help in the identification of the chemical compound. The absorbance of visible or Ultra violet light based was beer lambert law which provides details of concentration of a particular chemical compound.

Dye adsorption test of the methylene blue dye solution was conducted using Beckman DU640 UV/Vis spectrophotometer. A 100 ml of dye solution was prepared with various initial concentrations (100mg/L-500mg/L) of methylene blue dye. An adsorbent (activated carbon) dose of 0.1 gram was added in 100ml solution. Solution then stirred at 200 rpm for 5 hours to attain the equilibrium.

The adsorption uptake at equilibrium is calculated by following equation [108].

$$q_e = \frac{(C_i - C_e)V}{M} \quad (3.9)$$

Where q_e adsorption of dye at equilibrium, C_i is the initial concentration of dye in solution C_e is the final concentration of dye in solution at equilibrium, V is the volume of solution and M is the mass of adsorbent used.

Kinetic studies were conducted to find out the rate of adsorption process. The dye uptake at time t, q_t (mg/g) was calculated using following formula [109].

$$q_t = \frac{(C_i - C_t)V}{M} \tag{3.10}$$

Where q_t (mg/g) adsorption of dye at time t, C_t (mg/L) is dye concentration of solution at time t.

3.4 Result and discussion

3.4.1 Eggshells microparticles and nanoparticles

3.4.1.1 X-ray diffraction

XRD data was analyzed on x-pert software. Figure 3.9 shows the comparative analysis between unboiled, boiled eggshell and chemically obtained $CaCO_3$. From figure 3.9 it is evident that the intensity of the peaks is little high in case of boiled eggshell when compared with unboiled eggshells; however, for both the cases, the peak intensity is still lower than pure $CaCO_3$. The little difference in intensity of peaks of unboiled and boiled eggshell is due to impurities present in the unboiled egg shell. boiling results in removal of the outer layer of the egg shell (cuticle layer), which is removed from the surface with some weak bonded impurities. The $CaCO_3$ percentage is around 95% which matches with results obtained by Rivera, Eric M., et al. [110]. Due to boiling of the egg shell, the amount of $CaCO_3$ obtained is almost equal to pure $CaCO_3$ (chemically obtained). Figure 3.10 shows the XRD analysis of eggshells powder with different milling time. It was observed from figure 3.10 that peak intensity of eggshells powder decreases and peak broadening increases with increases in milling time, which uncover the fact that the crystalline size decreases with increase in milling time. The crystallinity was found to be 91.96 % for 2hrs. milled sample. The decrease in the percentage crystalline of eggshells reduced by 27% for milling time of 8hrs. Boiling also causes removal of membrane from the eggshell surface that has certain functional group such as amine. The crystallite size for different samples is given in table 3.3

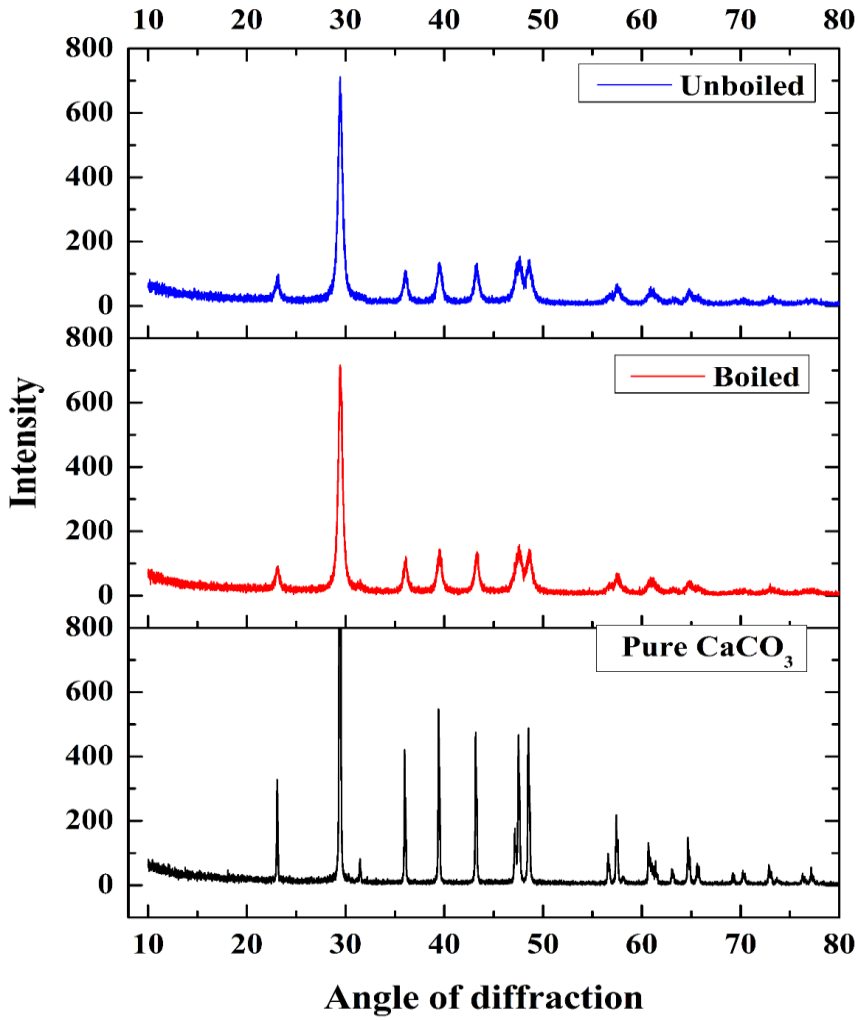

Figure. 3.9 Comparative XRD analysis of unboiled, boiled eggshells and pure $CaCO_3$ sample

Table 3.3 Variation of crystalline size with milling time

Milling time (hrs.)	Crystalline size
2	2μm
4	0.3μm
6	0.1 μm
8	14nm

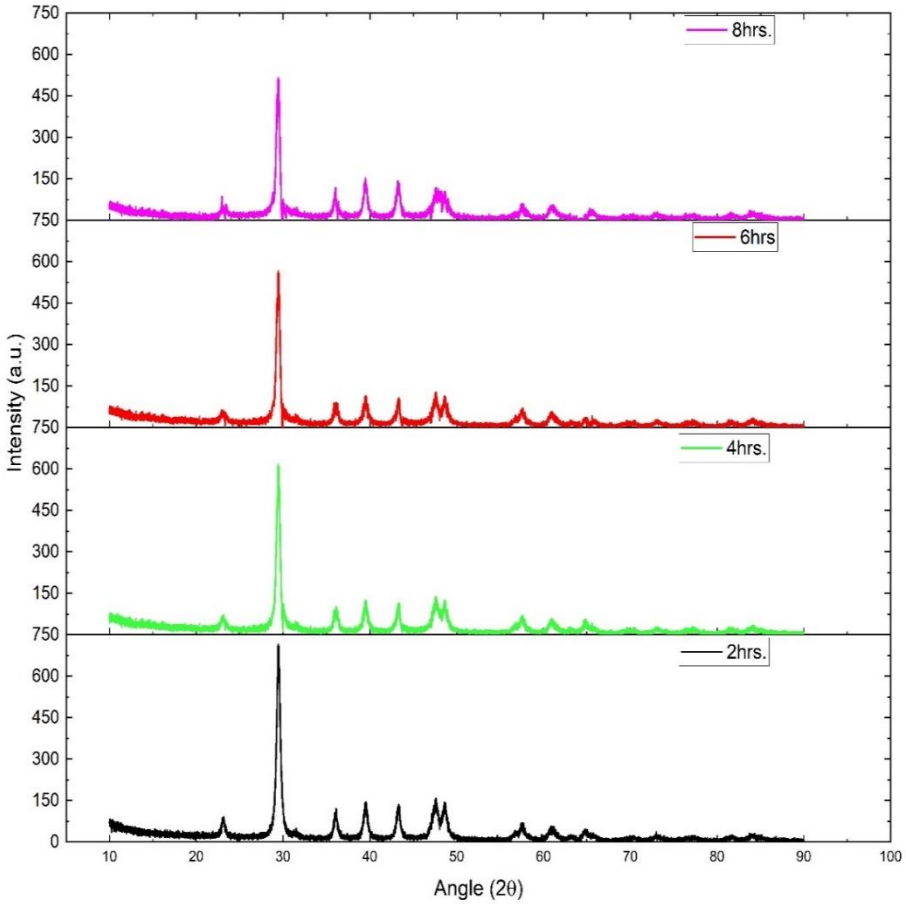

Figure 3.10 X-ray diffractograms of the milled eggshells powder

3.4.1.2 Ultimate analysis or CHNSO analysis

The results of ultimate analysis of egg shell of boiled and unboiled are shown in the table 3.4. From the results it was found that due to boiling, carbon percentage increases while hydrogen and sulphur content decrease, on the other hand, in both the results of eggshell particle, other elements like S, N, and H are very low. Boiling causes removal of cuticle layer from the shell. This soft non-calcined layer is made up of glycoprotein and carbohydrate. Removal of this layer will leave calcareous layer for direct exposure. Hence the analysis shows more amount of carbon in the boiled eggshell.

Table 3.4 Elemental analyses of eggshell particles

Sample	C (wt. %)	H (wt. %)	N (wt. %)	O (wt. %)	S (wt. %)
Un boiled egg shell	14.25	0.47	0.63	31.25	0.05
Boiled egg shell	15.25	0.35	0.65	33.24	0.02

3.4.1.3 Morphological studies of eggshell microparticle

Closer observation of SEM analysis in figure 3.11 (a) and 3.11 (b) reveals that due to boiling, outer layer (cuticle layer) of the eggshell is removed from the surface of the egg shell. The surface also becomes porous due to heating.

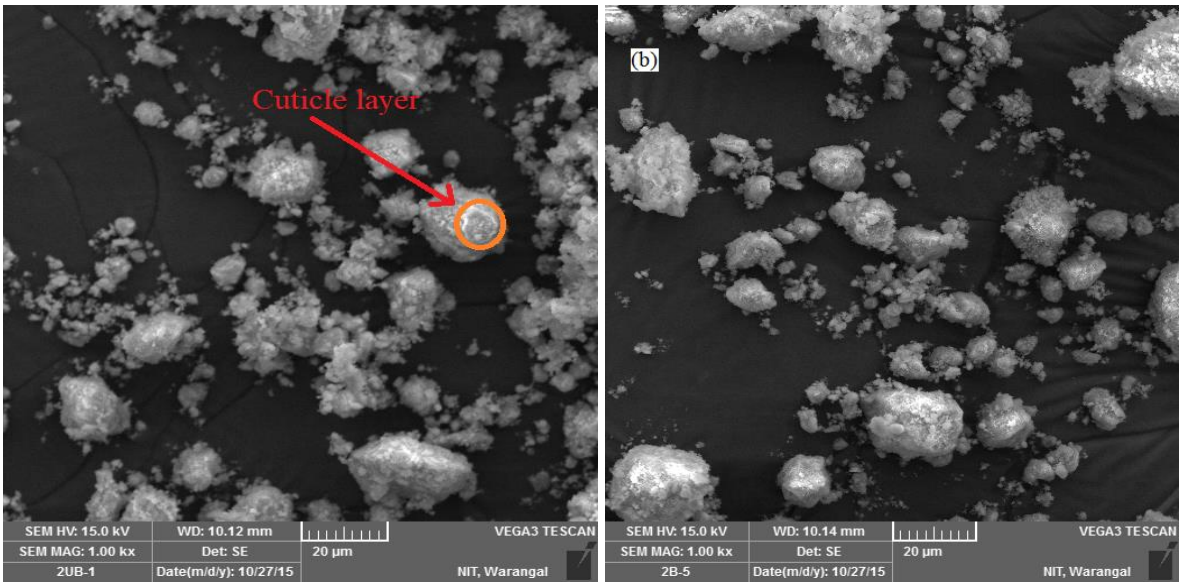

Figure 3.11 SEM pictograph (a) unboiled eggshell particles (b) boiled eggshell particles

It is observed through SEM analysis that boiling lead to removal of eggshell membrane, which leads to removal certain chemical compound and functional groups. which will be helpful in enhancement of adhesion with resin consecutively enhancement of mechanical properties. Based on results of SEM, XRD, and CHNSO analysis, unboiled particles were chosen for further characterization.

3.4.1.4 TGA analysis of unboiled eggshell nanoparticles

The results of the study of mass loss with respect to temperature change are shown in figure 3.12. This figure depicts the different stages of weight loss. One stage at temperature below 650ºC and another between 650ºC and 805ºC.

The initial mass loss which started from 25-200^{o}C was about 2% may be due to the evaporation of adsorbed water and the presence of some hygroscopic molecules. Further the mass loss occurred between the temperature range of 200-650^{o}C due to the disintegration of organic protein materials into small molecules. The next step involves the maximum weight loss of 42% between 650ºC and 805ºC. This drastic change in mass is observed, due to the decomposition of calcium carbonate into CO_2 and CaO [111].

Process was continued to ensure complete conversion of CaO. The decomposition of carbonate is an endothermic reaction as given below.

$$CaCO_{3(s)}\ (\text{Eggshells}) \rightarrow CaO_{(s)} + CO_{2(g)}$$

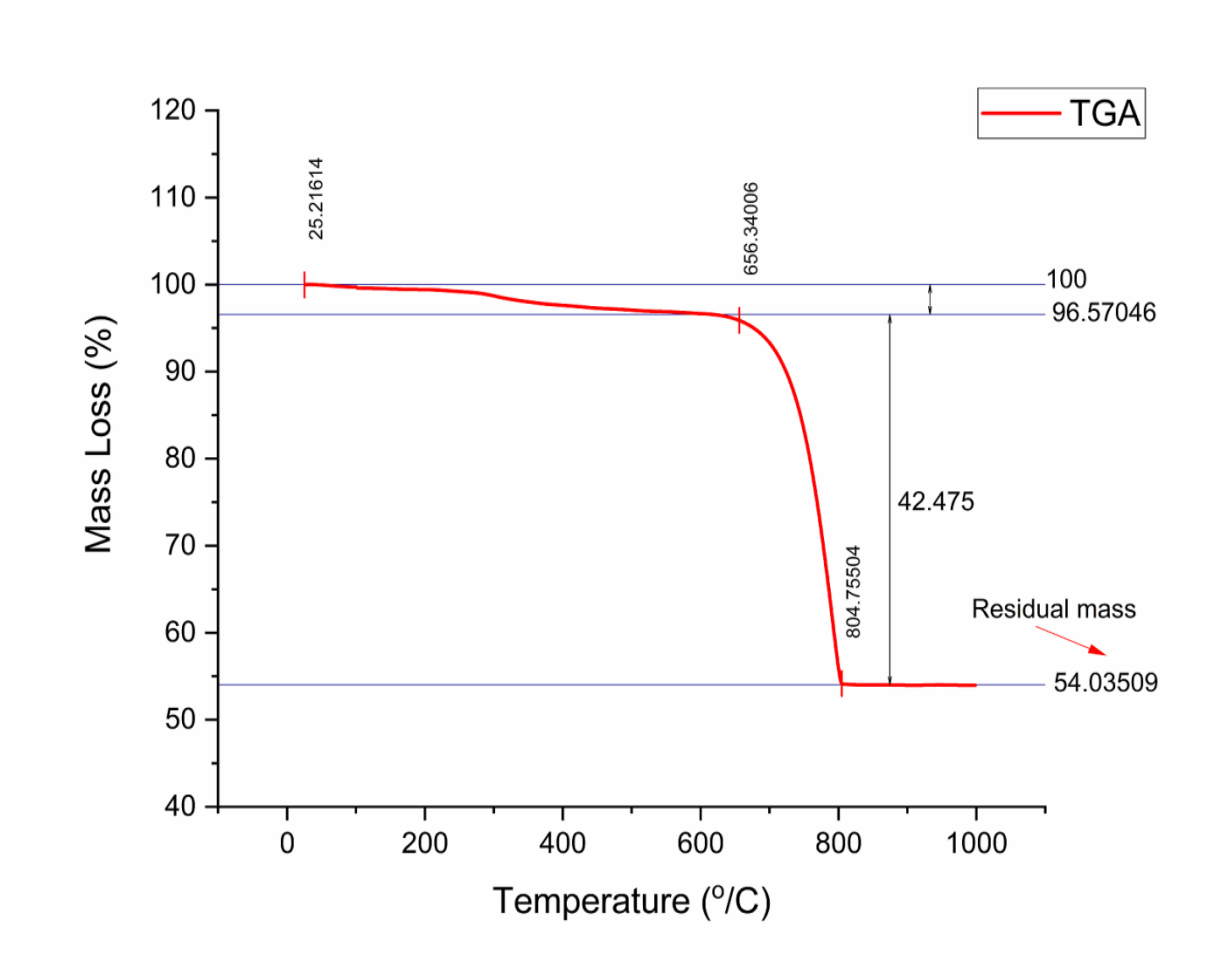

Figure 3.12 Thermal decomposition of unboiled eggshell powder

3.4.1.5 FTIR analysis of unboiled eggshell nanoparticles

FTIR spectroscopy was analyzed for eggshell powder sample. FTIR spectra of the eggshell particles are shown in figure 3.13. Figure exhibits the characteristic absorption bands at 3411 cm^{-1} (O-H stretching), 2866 and 2927 cm^{-1} (C-H stretching) which shows the presence of organic layers of proteins in particles of eggshell. The Absorption band at 2517 cm^{-1} is molecular fingerprint of Amine salt. The absorption bands at 1797 cm^{-1}, 1421 cm^{-1}, 1078 cm^{-1},873 cm^{-1} and 711 show the absorption bands of CO_3^{2-} ions which confirm the existence of $CaCO_3$. A similar observation was made by Carvalho, J et al.[112].

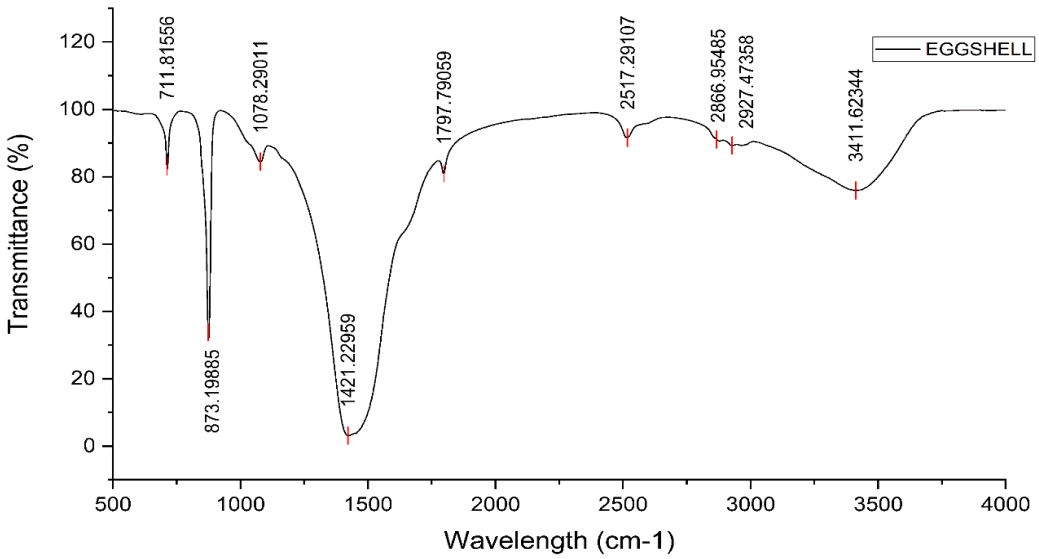

Figure 3.13 FTIR analysis of unboiled eggshell nanoparticles

3.4.1.6 Morphology analysis of unboiled eggshell nanoparticles

There are many clusters of particles visible in SEM image as shown in figure 3.14, a big cluster was enlarged to see the morphology of particles. The enlarged SEM image shows that the particles are irregular in shape. TEM images taken for the eggshell particles are shown in figure 3.15. From TEM images, it was confirmed that the particle size was well within 20 nm. The TEM images also suggest that particles are crystalline in nature and have hexagonal structure similar to that of calcium carbonate.

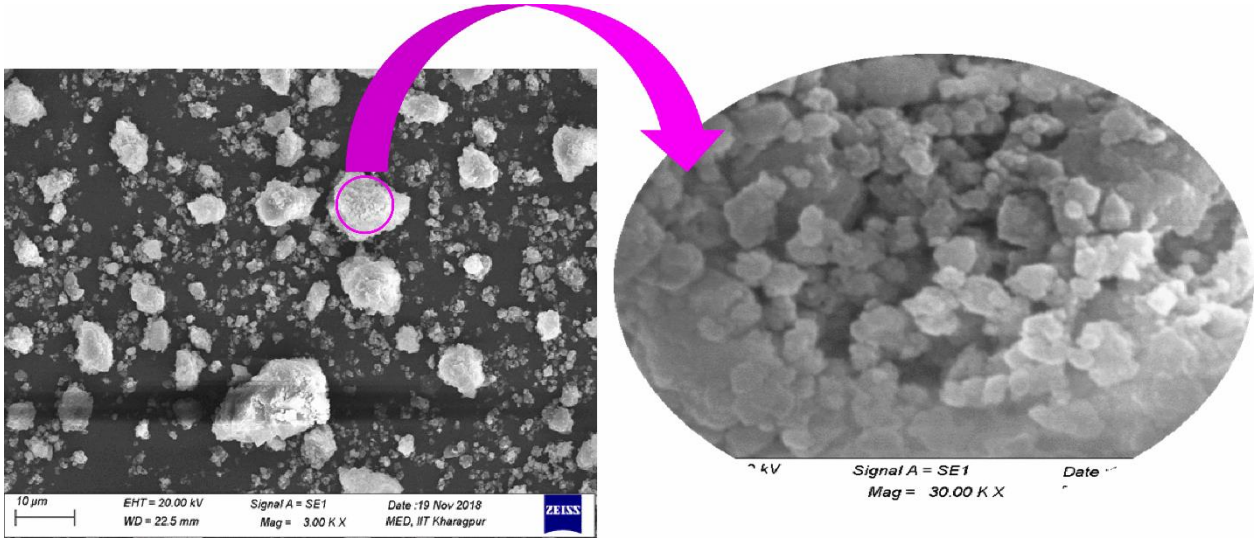

Figure 3.14 SEM image of unboiled eggshell nanoparticles

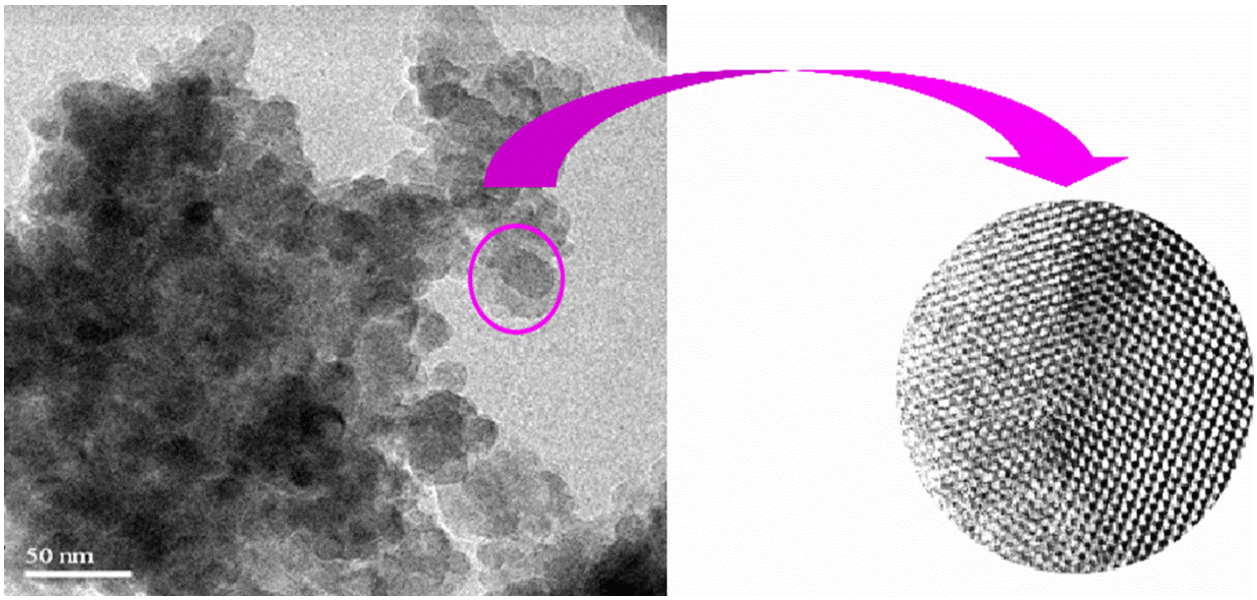

Figure. 3.15 TEM image of unboiled eggshell nanoparticles

3.4.2 Activated carbon

3.4.2.1 XRD analysis

XRD patterns of a mixture of coconut shell and eggshell pyrolyzed at different temperatures is illustrated in figure 3.16.

It is noted from the figure that the pyrolyzed coconut shell and eggshells mixture shows the peaks at 2θ value around 23º, 26º, 29º and around 43º. Out of these peaks around 23º and around 26º are mainly of crystalline cellulose[113]. Phases of these peaks are C, SiO_2. The peak around 29º is due to the presence of calcium carbonate in the mixture. As is evident from TGA analysis of the eggshells, calcium carbonate present in the eggshell does not decompose at 600°C. As the temperature increases the peaks around 26º and 29º begin to disappear due to decomposition of cellulose and decomposition of calcium carbonate present in eggshell. However, at 700ºC the peaks are still appreciable, which suggest the presence of calcium carbonate and another compound. Further increase in temperature leads to total decomposition of calcium carbonate and cellulose.

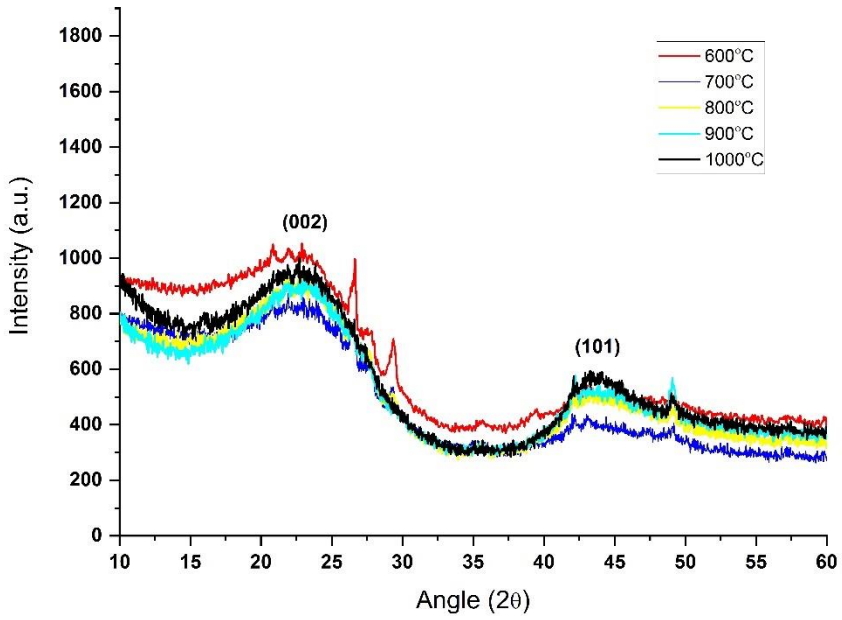

Figure 3.16 X-ray diffraction analysis of 1:1 eggshells and coconut shells mixture at different temperatures

Figure 3.17 shows, the XRD pattern of different ratios of eggshells-coconut shells pyrolyzed at 800°C. As seen in figure 3.17, only two peaks are evident around 23 degrees and around 43 degrees, which confirm the presence of carbon in form of graphite [114]. Another observation is the peak shift with increase in eggshells-coconut shell ratio. The two peaks, one at 23 degrees and another around at 43 degrees are identical to (002) and (101) replication of graphite. This implies the presence of partially graphitic crystal structure [114,115]. With the crystalline peaks there is lot of noise observed in XRD analysis which is due to the combination of crystalline and amorphous nature of carbon. The minor peak around 26 degrees may due to the presence of SiO_2 [116] in activated carbon. The peak at around 29 degree shows traces of calcium in activated carbon. The minor peaks around 42 degree and 49 degree may be due to traces of chlorine and calcium [117,118]. These small traces of Ca and Cl are observed may due to the presence of $CaCl_2$, which was obtained with activated carbon during activation process. One further observation is that the intensity of peaks decreases with increase in the ratio, which suggests the amorphous nature of carbon. The peak intensity of eggshell-coconut mixture in the ratio of 1:1 pyrolyzed at 800°C is highest. It suggests more pronounced and porous activated carbon.

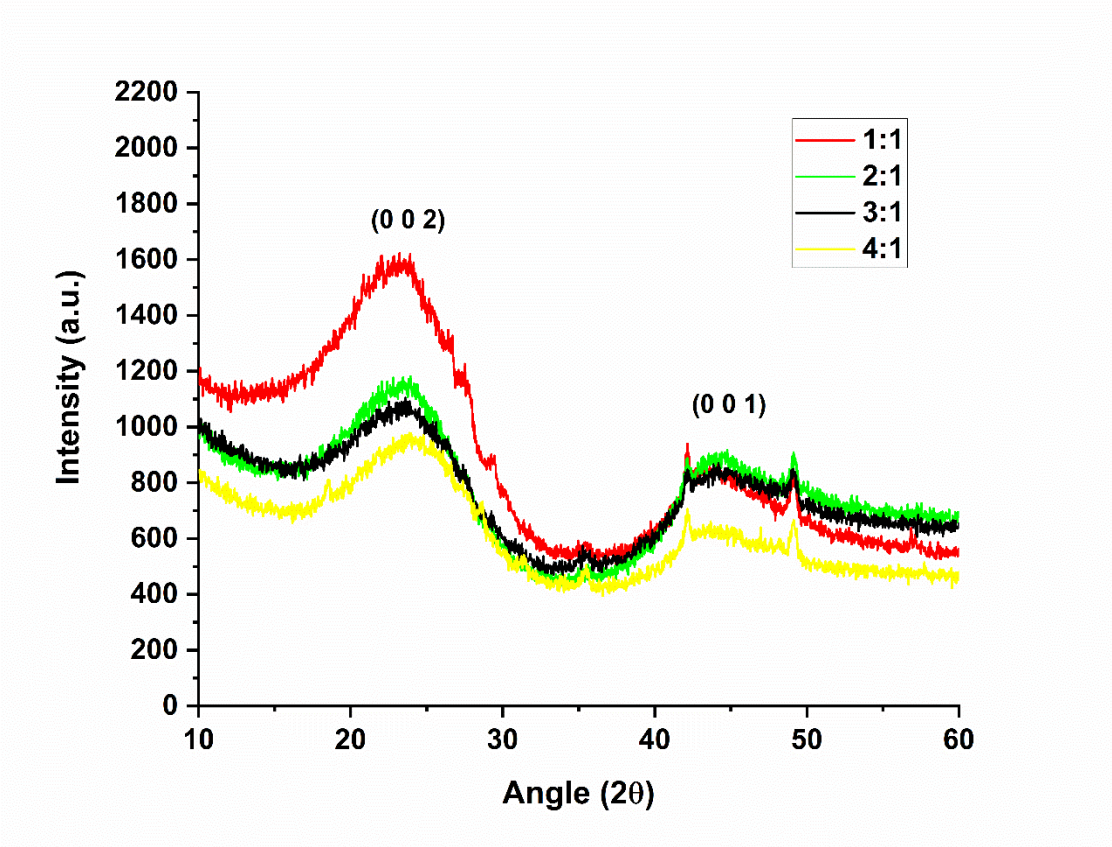

Figure 3.17 X-ray diffraction analysis of different ratio of eggshells and coconut shells mixture pyrolyzed at 800^{o} C

3.4.2.2 Raman Spectroscopy

Raman spectra of different sample of ordered porous carbon is illustrated in figure 3.18.

Crystalline graphite only displays one peak at around 1582 cm^{-1} which is characterized as graphite peak or G peak while amorphous carbon or disordered carbon shows one more peak called D peak around 1350 cm^{-1} (disordered induced peak) along with G peak [119]. The figure demonstrates two peaks, G peak and D peak at 1584 cm^{-1} and 1350 cm^{-1} respectively, proving that the material has disordered structure. The intensity of D peak shows the degree of disorder. From figure 3.18 it is evident as the ratio of coconut shell and eggshell powder increases, FWHM (Full width at half maximum) value of G band and D band also increases; due to broader peaks. The ratio of integrated intensities of D band and G band (I_D/I_G) increases with an increase in ratio of coconut shell and eggshell powder, which establishes the fact that activated carbon becomes more amorphous in nature with an increase in ratio of coconut shell and eggshell powder. The amorphous nature of activated carbon was also revealed by XRD analysis.

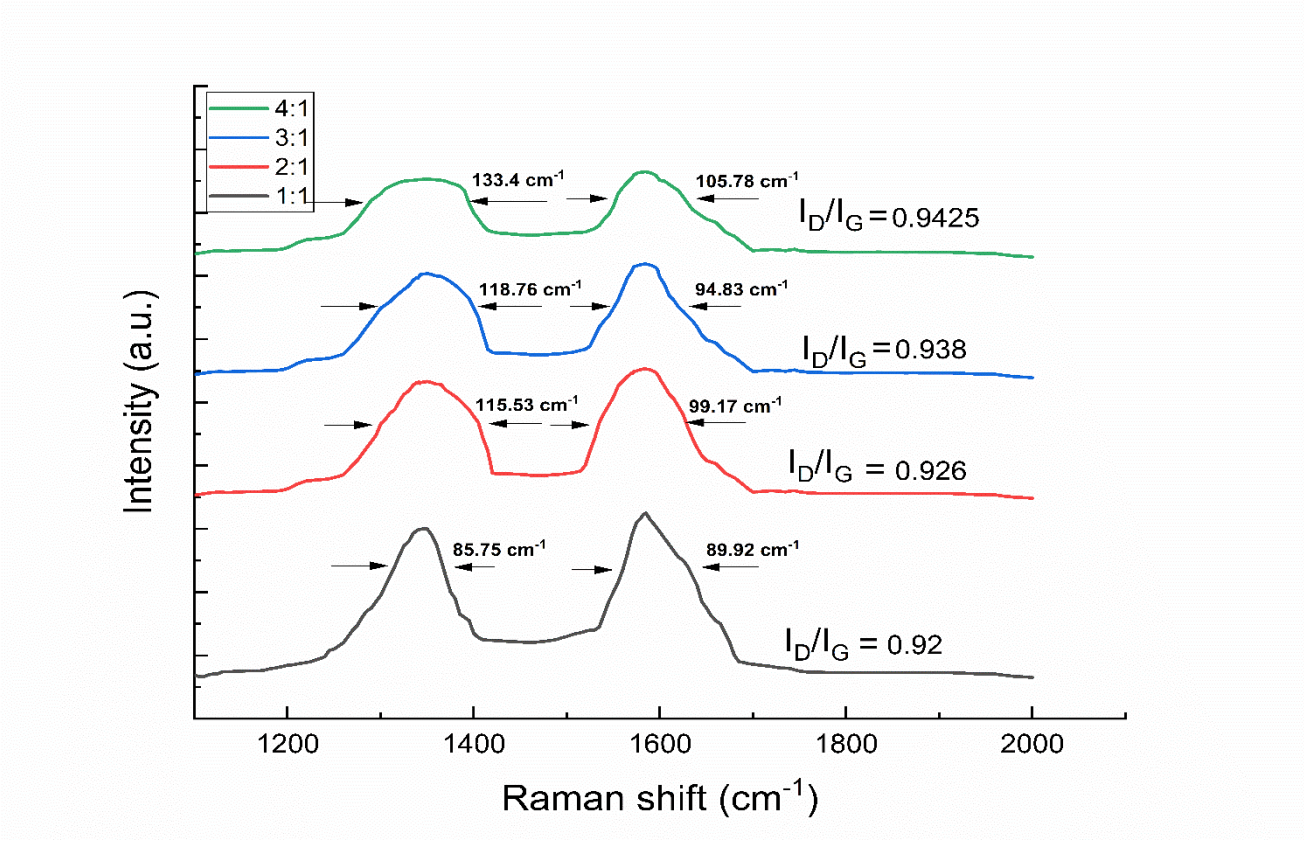

Figure 3.18 Raman Spectra of various different ratio of eggshells and coconut shells mixture pyrolyzed at 800° C

3.4.2.3 FTIR analysis

From figure 3.19 it can be seen that functional groups at 3396, 2927, 2877, 2515, 1800, 1731, 1607, 1428, 1265, 1036, 876 and 719 cm^{-1} were present in eggshell-Coconut shells mixture. The primary surface functional groups present in the raw coconut shell- eggshells mixture was hydroxyl groups at 3396 cm^{-1}, C-H stretching at 2927 cm^{-1} and 2877 cm^{-1}, which suggest the presence of cellulose and hemicellulose. Surface functional groups such as carbonyl group (ketone, aldehyde) present in the raw mixture suggest the presence of lignin in mixture. The peaks at 1428 cm^{-1}, 876 cm^{-1} and 719 cm^{-1} suggest the presence of carbonate group which suggest the presence of calcium carbonate [111,120]. From the figure it is clearly visible that as temperature increases, carbonyl groups start disappearing at 800°C and there are no traces of carbonate, suggesting total decomposition of calcium carbonate, which is supported by XRD and TGA analysis as well. Peak at 1582 cm^{-1} suggest the presence of amine groups (N-H). Presence of the amine group in activated carbon greatly influences its pollutant adsorption capacity. The peaks of 800°C activated carbon are more pronounced and one other observation is that any further increase in temperature results in the disappearance of peaks.

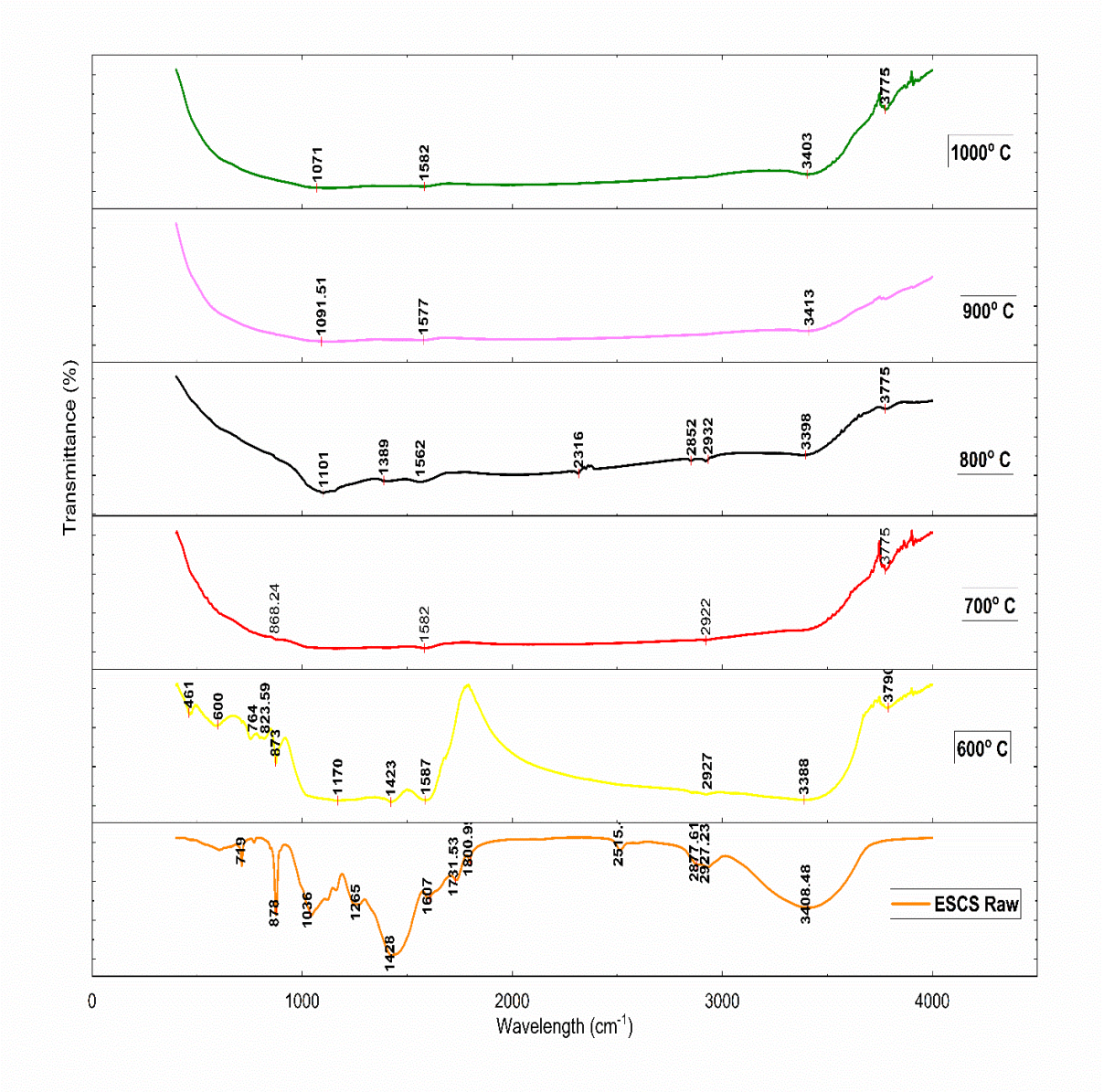

Figure 3.19 FTIR analysis of 1:1 eggshells and coconut shells mixture at different temperatures

Figure 3.20 shows activated carbon prepared with different ratios of coconut shells and eggshells. When comparing with peaks of different samples of activated carbon, almost all samples except the sample with a 4:1 ratio has peaks at ~2850 cm^{-1} and ~2950 cm^{-1} which correspond to CH-stretching. All the samples show the presence of the amine group and nitro compound. It is observed that bonds break further with an increase in the ratio which is due to the breaking of pores. When comparing different samples, 1:1 and 2:1 do not show much difference which is due to the fact that the bonds are still intact. The amount of oxygen during activation is significant, sufficient amount helps in formation of microporosity during the formation of char [121]. However the excess amount of oxygen causes the fall of the aliphatic

and aromatic network, which in turn results in rearrangement of carbon layer and consecutively the destruction of pores [121,122]

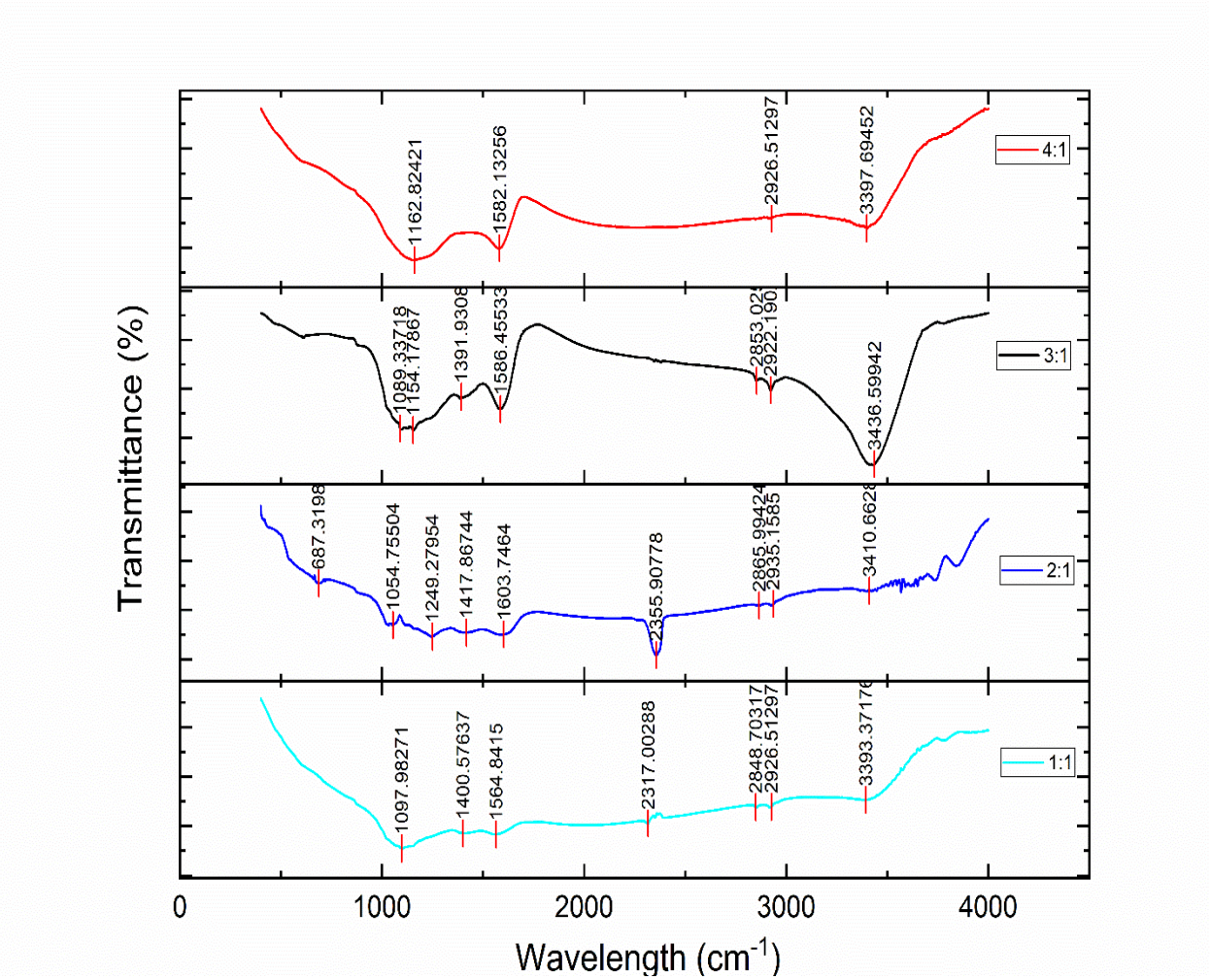

Figure 3.20 FTIR analysis of different ratios of eggshells and coconut shells mixture pyrolyzed at 800^{o} C.

3.4.2.4 TGA analysis

Thermal decomposition analysis of raw coconut shell powder was carried out to find out the range of temperature where major decomposition occurs. From figure 3.21 it is evident that for temperatures from 27°-105°C, the mass loss from 100% to 94% is due to the evaporation of water molecules. The thermal degradation of biomass starts after that. Thermal degradation starts slowly from 105°-229°C with lignin, although lignin decomposition goes beyond 500^{o}C.The major mass loss is due to decomposition of hemicellulose and cellulose. The decomposition of hemicellulose starts from 229°-300°C. The weight loss occurred at a temperature range of 320°–390°C as a consequence of cellulose decomposition [123,124]. The major mass loss occurs between temperature ranges of 230°-400°C, which is an indication of

the degradation of biomass. After decomposition of all three compounds i.e. cellulose, hemicellulose, and lignin; the residual mass which remains is biocarbon.

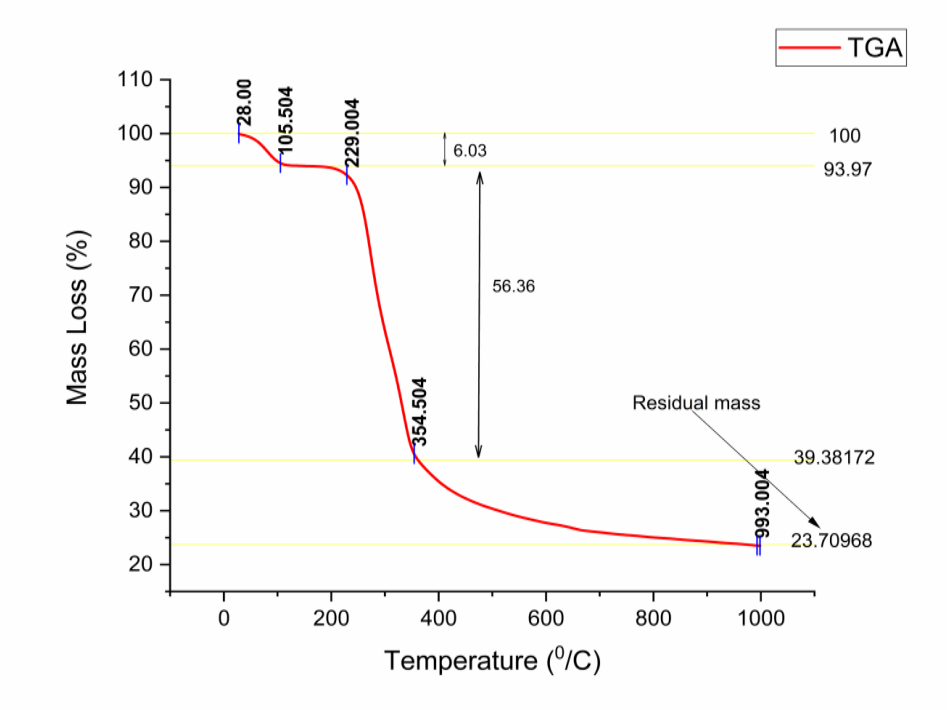

Figure 3.21 Thermal decomposition of coconut shell powder

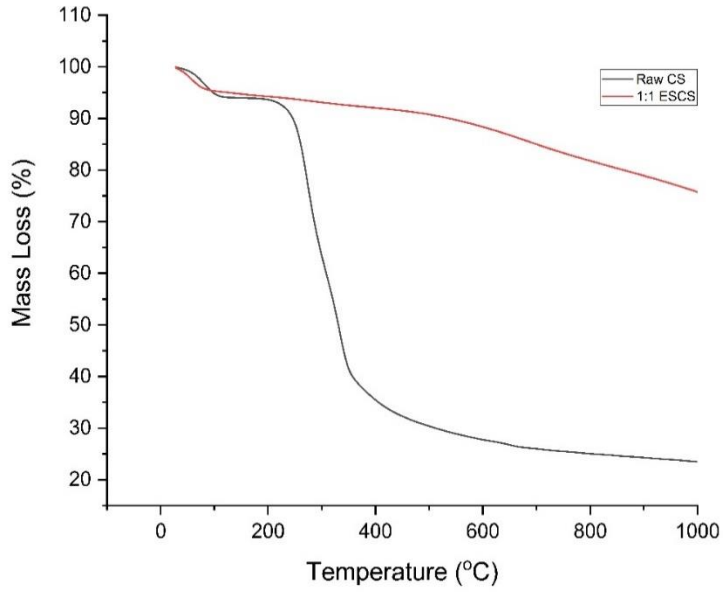

Figure 3.22 Comparison between thermal decomposition analysis of 1:1 activated carbon and raw coconut shell powder

Figure 3.22 shows a comparison of thermal decomposition between raw coconut shell and activated carbon sample. It is observed from 3.22 that mass loss of activated carbon is very much less than raw coconut shell.

3.4.2.5 Morphology analysis

Figures 3.23 (a)-3.23 (b) show SEM image of raw and pyrolyzed coconut shell particles. It is observed from figure 3.23 that upon carbonization of raw coconut shell particles which are round in shape converted in the form of flakes which suggest the presence of graphite.

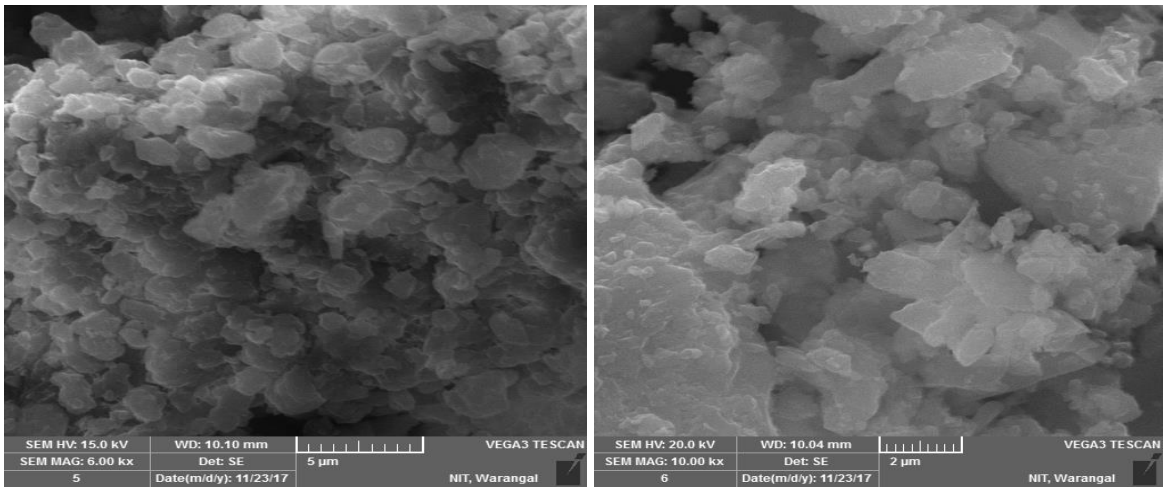

(a) (b)

Figure 3.23 SEM image of (a) Raw coconut shells powder (b) Coconut shell pyrolyzed at 800ºC

The carbonization of a mixture of eggshell and coconut in the ratio of 1:1 at 800^{o}C results in plenty of pores as shown in figure 3.24 (a). The pores are clear, strong and transparent. The SEM images shown in figure 3.24 (a) prove that the activation is successfully done using eggshell as activating agent and hard template. The SEM images presented in figure 3.24 (a) also suggest the presence of both micro and mesoporous carbon implying that the carbon obtained is hierarchical activated carbon. However, as the eggshell content increases, the porous structure suddenly weakens and the carbon material became rough.

For the eggshell to coconut shell ratio of 2:1, the pores are weak compared to 1:1 ratio sample. Further increase in eggshell content results in the breaking of pores as can be easily recognized from scanning electron microscopy images shown in figure 3.24 (b)-3.24 (d). TEM images 1:1 is illustrated in Figures 3.25 (a)-3.25 (d). Figure 3.25 (a) show that the thin walls

connect the three-dimensional systems of mesopores. Figure 3.25 (a) also reveals the presence of graphite ribbons. Figure 3.25 (d) shows the presence of microchannel. TEM images of different samples viz. 2:1, 3:1 and 4:1 is shown in figures 3.26 (a)-3.26(c). TEM image of 2:1 sample from figure 3.26 (a) shows the presence of graphite ribbon and thin walls just like 1:1 sample; however, there are fewer pores compared to 1:1 activated carbon sample.

TEM image of 3:1 show the broken pores as in figure 3.26 (b). For 4:1 sample, it is observed from figure 3.26 (c) that excess amount of carbon dioxide results in breaking pores as well as burning of activated carbon and formation of tar. It is clearly observed from TEM image shown in figure 3.26 (c) and SEM image shown in figure 3.24 (d), that tar formed due to excess carbon dioxide resulted in blockage of pores.

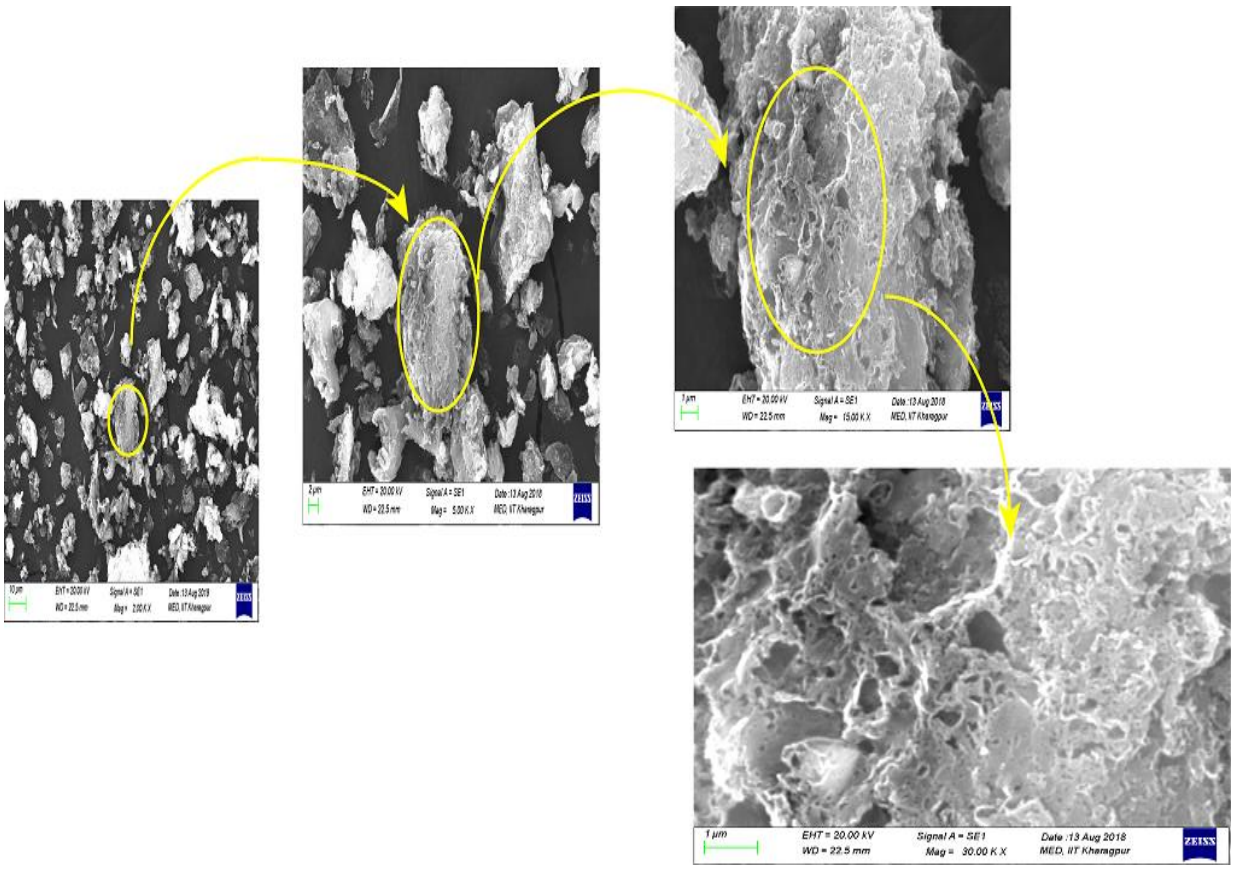

(a) 1:1

Figure 3.24 SEM images of different samples of ordered porous carbon (a) 1:1

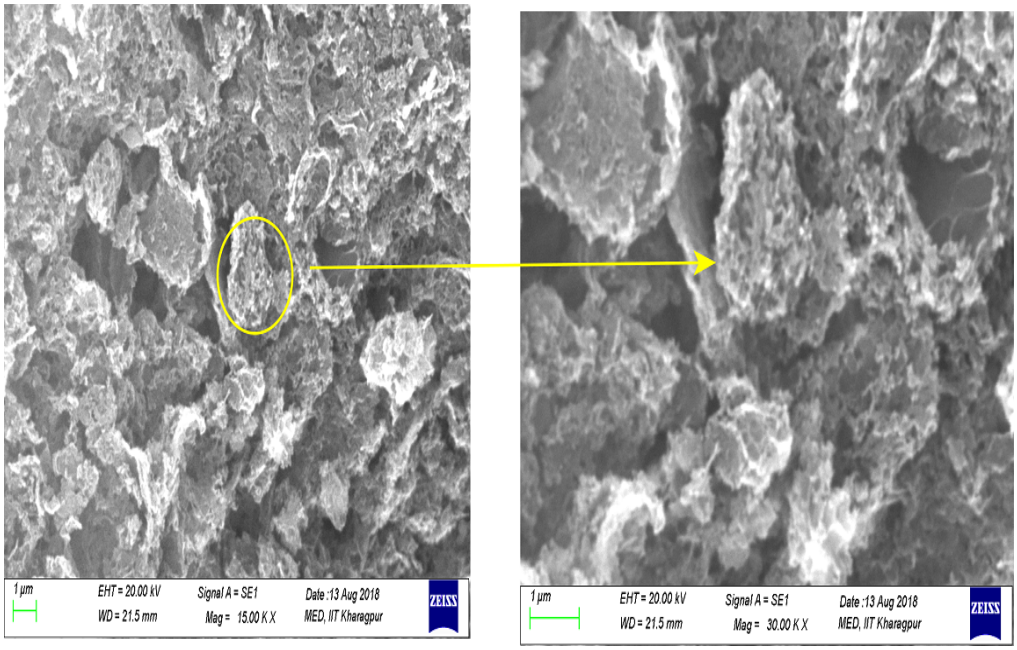

(b) 2:1

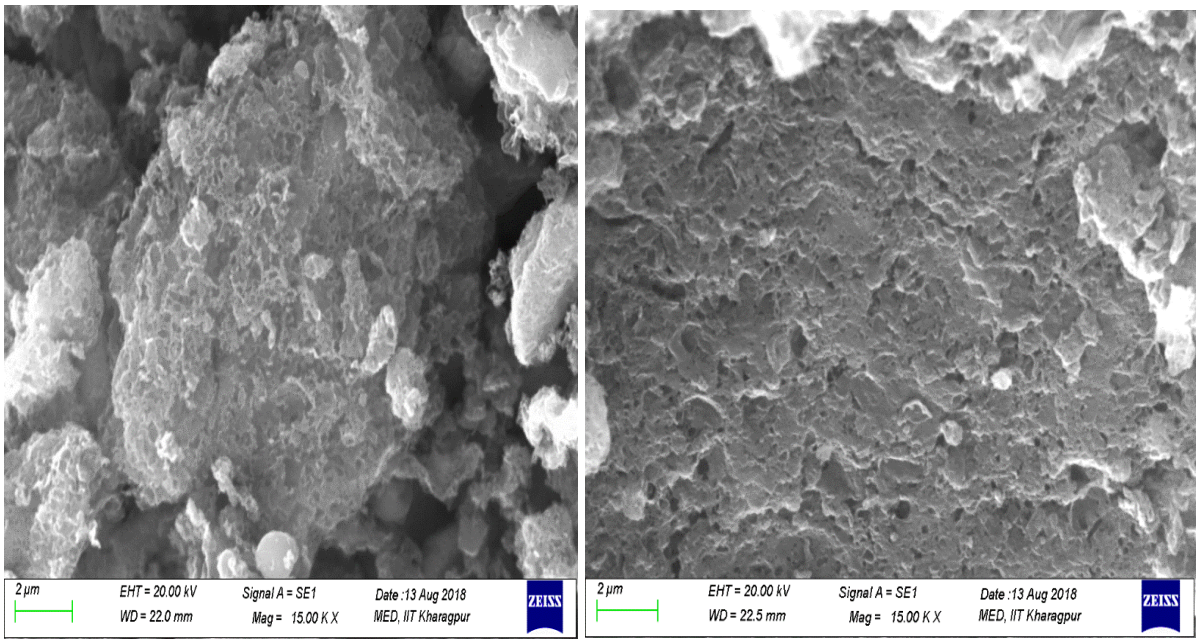

(c) 3:1 (d) 4:1

Figure 3.24 SEM images of different samples of ordered porous carbon (b) 2:1 (c) 3:1(d) 4:1

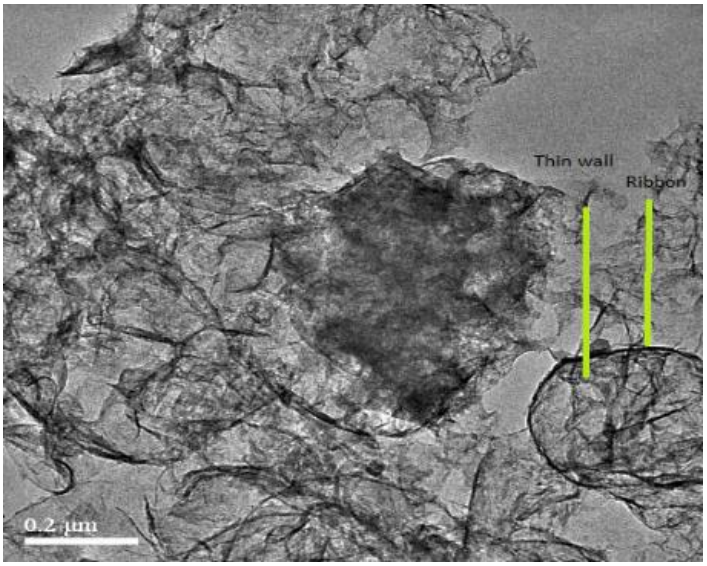

(a)

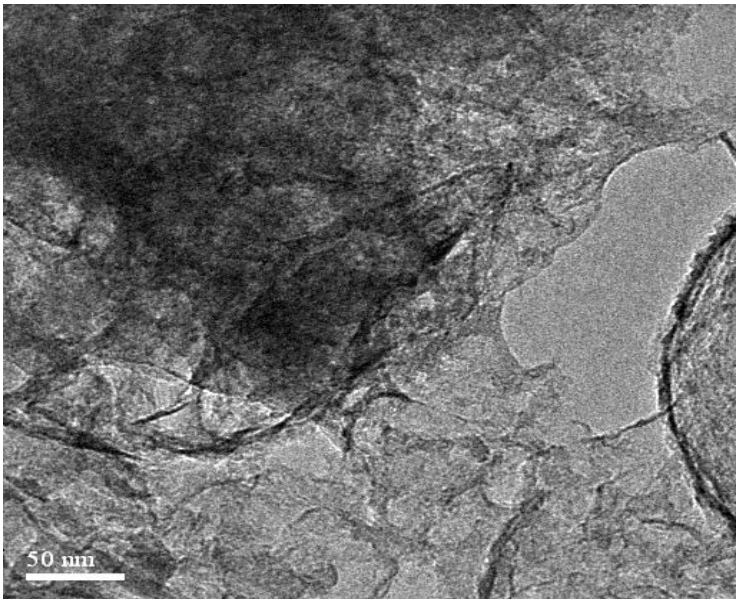

(b)

Figure 3.25 TEM images of 1:1 sample of ordered porous carbon at different magnification (a) 2 μm (b) 50 nm

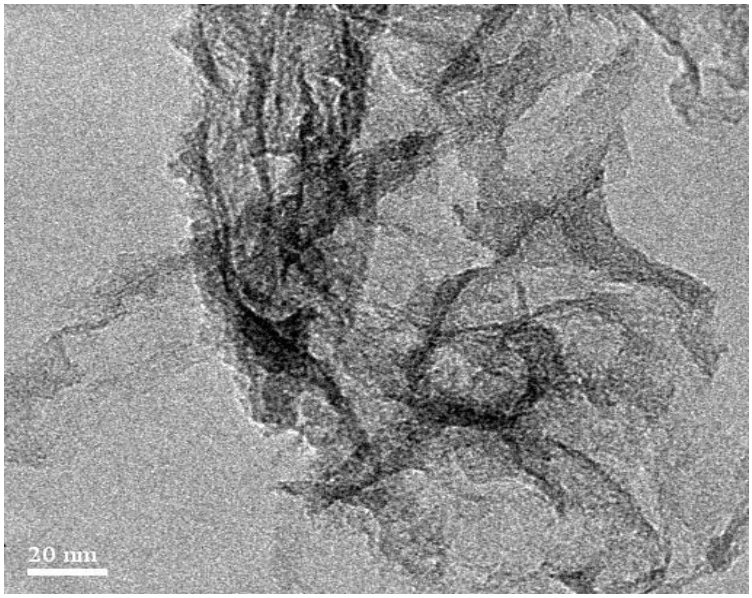

(c)

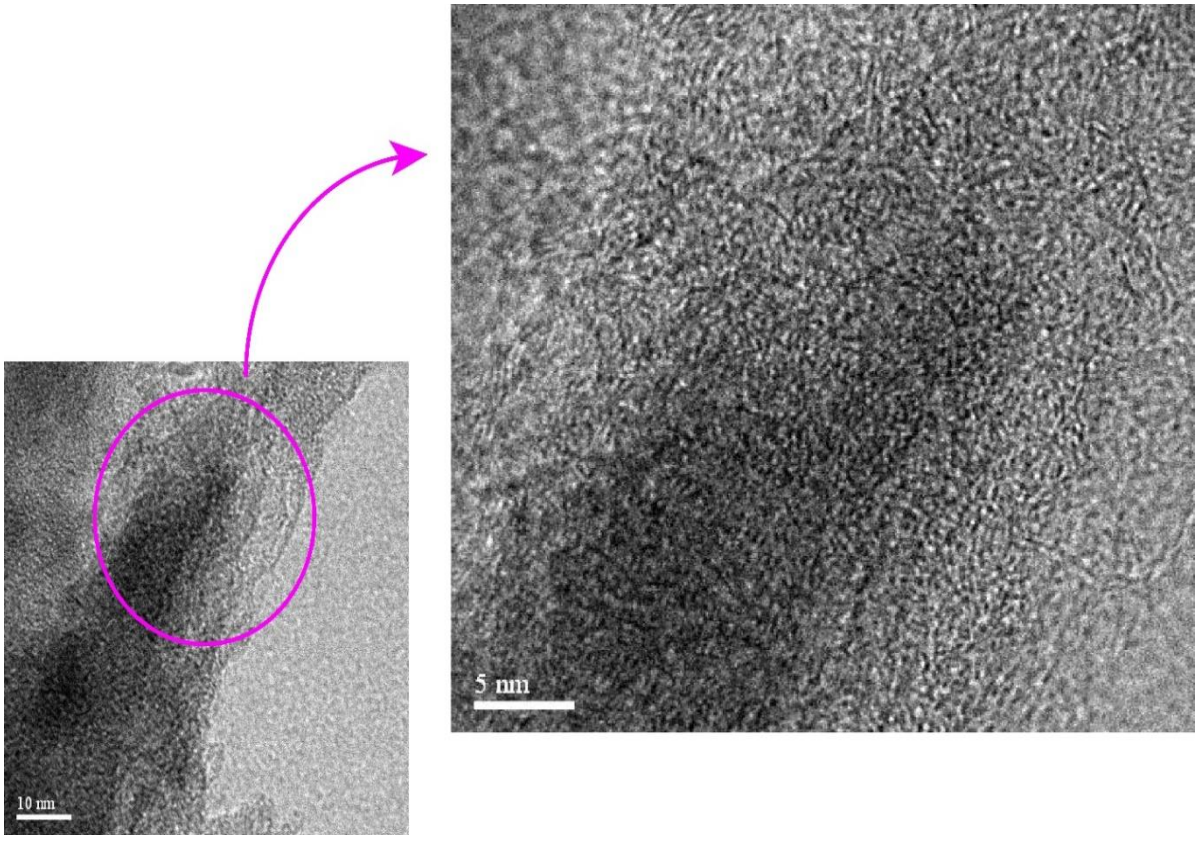

(d)

Figure 3.25 TEM images of 1:1 sample of ordered porous carbon at different magnification (c) 20 nm (d)10 nm

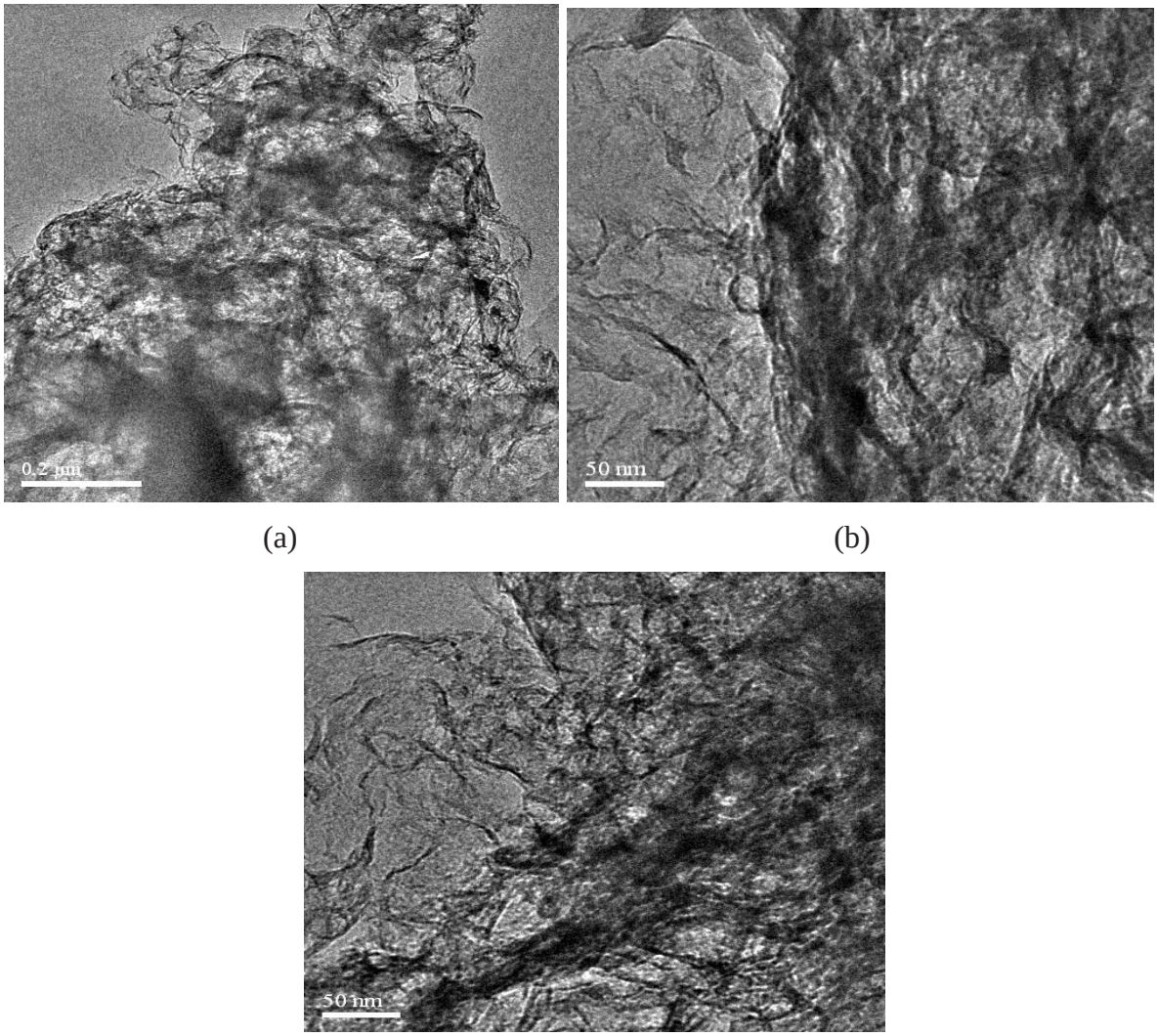

(a) (b)

(c)

Figure 3.26 TEM images of (a) 2:1 (b) 3:1 (c) 4:1 sample of activated carbon at different magnification

3.4.2.6 BET analysis

The total surface area and pore volume of 1:1 at 800°C were 375.4 m^2/g and 0.2478 cm^3/g respectively. The 1:1 sample has the highest total pore volume and micropore volume with a micropore percentage of around 73%. As evident from table 3.5, further increase in eggshells powder content results in a drop in the total pore volume as well as micropore volume. The reason behind the drop-in pore volume and surface area is due to the collapse of pores which can be gathered from scanning electron microscopy images. The reason behind the decrease in pore volume and surface area may be due to increase in eggshells contents. More amount of eggshell present in mixture increases the amount of CO_2 released while the amount of precursor material reduces. The excess quantity of CO_2 causes burning of porous carbons,

which has a detrimental effect on pores generation. Burn out of results in broadening of present micropores, and external burning of the particle causes tar formation which hampers the creation of new porosity break the pores which in turn results in less surface area [121,122].

Table 3.5 Pore properties of different activated carbon samples

Sample	**S_{BET} (m^2/g)**	**Langmuir Surface Area**	**V_{TOTAL} (cm^3/g)**	**V_{Micro}(cm^3/g)**	**Average pore diameter(nm)**	**% micropores**
Raw CS	2.74	1.95	0.005	0.0024	-	
1:1	375.4	570	0.2478	0.182	2.64	73.44
2:1	357	448.2	0.2307	0.1527	2.585	66.18
3:1	260	309.9	0.2649	0.075	4.075	28.31
4:1	158.1	247.7	0.1013	0.0754	2.563	74.43

3.4.2.7 Pore size distribution study

Figure 3.27 (a) shows the adsorption-desorption curve of raw and activated carbon sample. For the raw sample, which does not have pores, adsorption-desorption curve shows a straight line. The other samples have sharp capillary condensation at high pressure due to the presence of meso-pores and macro pores.

The high capillary condensation at low pressure ($p/p< 0.1$) suggests the presence of micropores, which were activated by CO_2 obtained from the decomposition of eggshells. The results display type-I adsorption isotherm which implies that the activated carbon has a microporous nature [64,125]. Another important observation comes from N_2 adsorption/desorption isotherm which is 1:1 ESCS sample has more adsorption than 2:1,3:1 and 4:1 sample, which supports the fact that 1:1 ESCS sample has more pores than other three samples.

The pore-size distribution of different samples is presented in figure 3.27 (b). It can be seen that from the figure that there are three major regions, the region below 2nm corresponds to micropores, the region between 2nm to 10nm corresponds to meso-pores and the region above 10nm corresponds to mesopores. Similar kind of observation is made by Shen, Feng, et al. [126].

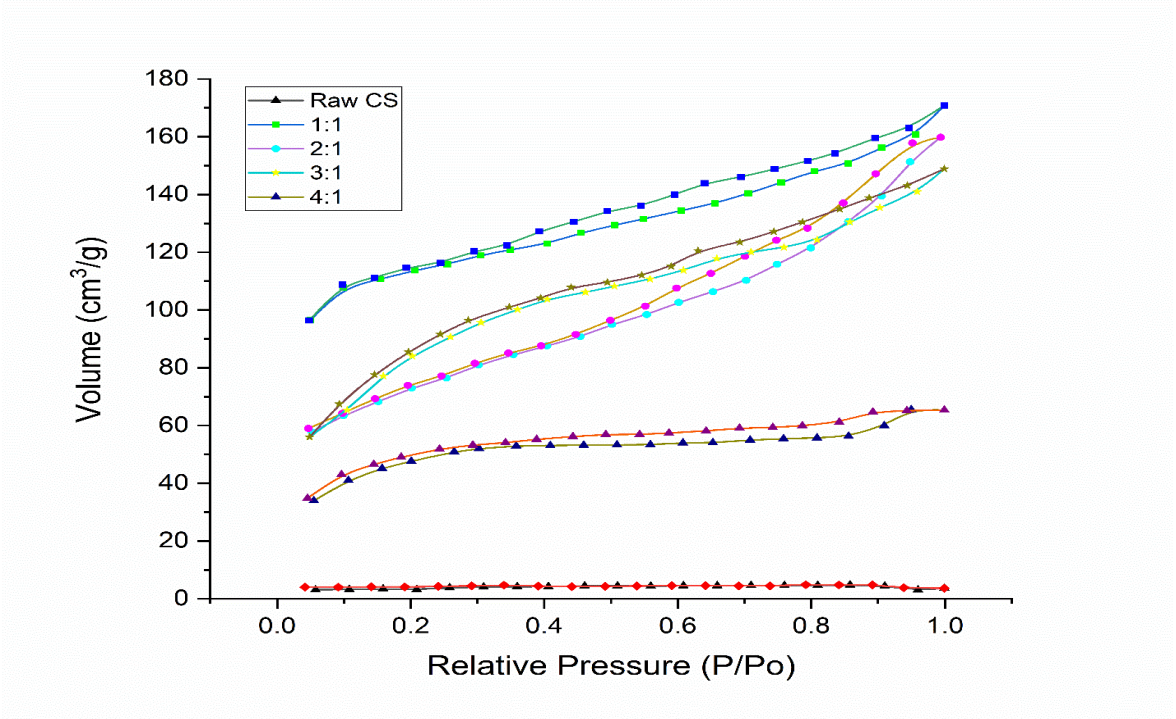

(a)

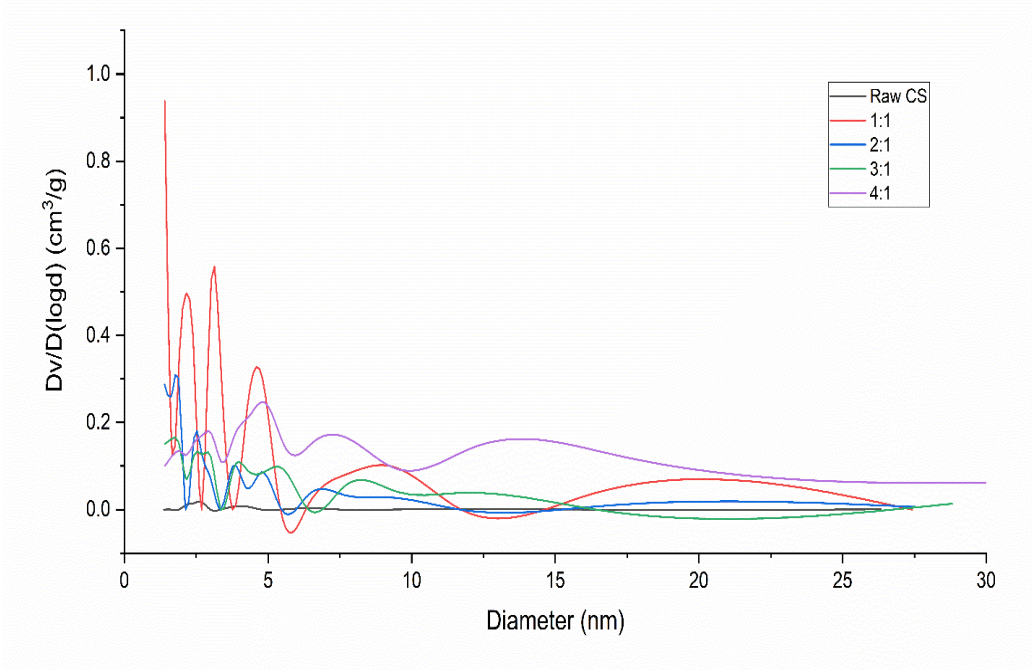

(b)

Figure 3.27 (a) Nitrogen adsorption/desorption isotherms and (b) Pore-size distribution of prepared activated carbon.

3.4.2.8 Adsorption studies

3.4.2.8.1 Effect of contact time

Figure 3.28 illustrates the influence of time on adsorption rate of activated carbon for various initial of concentrations of dye solution. It is recognized from figure 3.28 that dye adsorption increases with increase in contact. The equilibrium was attained after 5 hours of contact time with highest dye adsorption of 299.63 mg/g for 500 mg/L of the initial concentration. The figure depicts the fast adsorption at initial time periods, which may be due to the availability of unfilled pores with a higher diffusion rate of methylene blue ions on the surface of activated carbon. However, as the time goes on, the pores gets filled with methylene blue ion and equilibrium is attained.

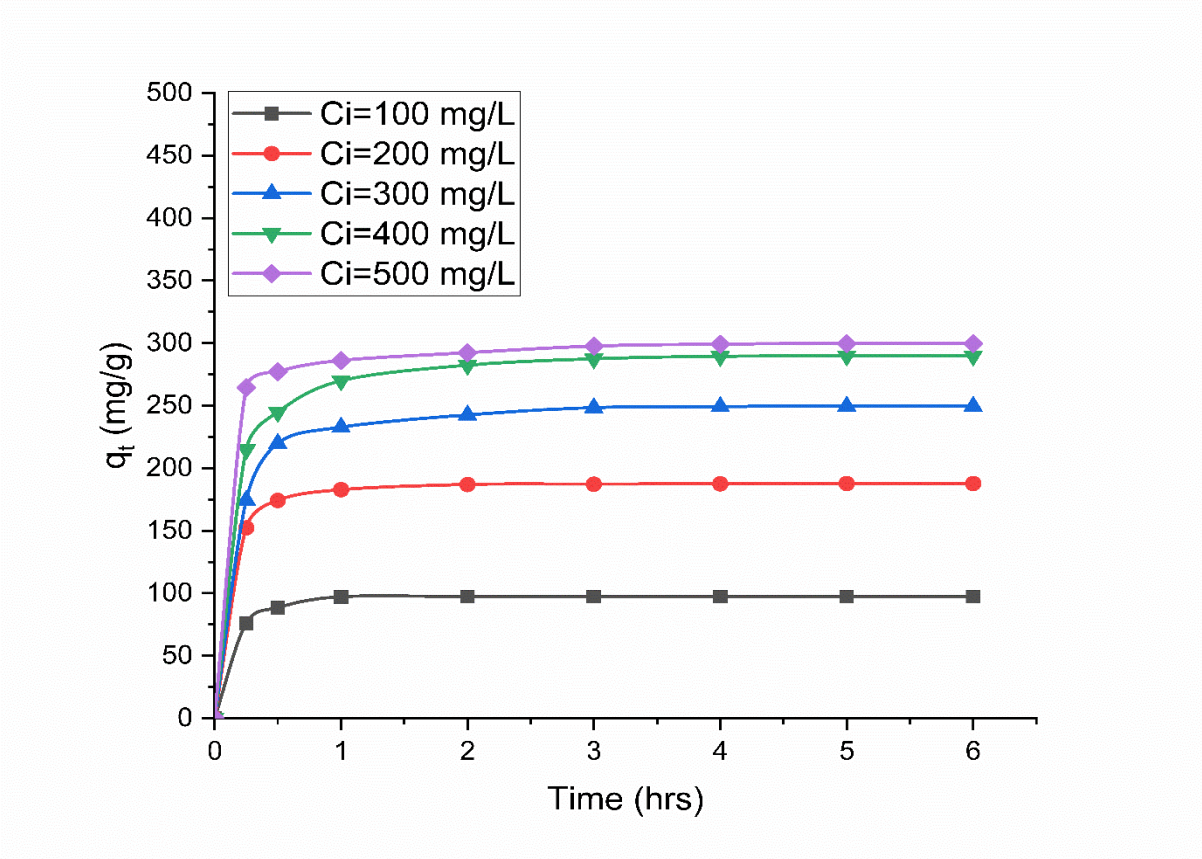

Figure 3.28 Effect of time on adsorption of methylene blue dye at various initial concentrations.

3.4.2.8.2 Adsorption isotherms

Figure 3.29 represents the adsorption experimental data fitted with Langmuir [127] and Freundlich [128] isotherms calculated from following formula.

$$q_e = \frac{q_m \times K_L \times C_e}{1 + K_L \times C_e} \tag{3.11}$$

$$q_e = K_F \times C_e^{1/n} \tag{3.12}$$

where q_m (mg/g) and K_L (L/mg) are Langmuir constants related to adsorption capacity and rate of adsorption, respectively. K_F (mg/g) $(L/mg)^{1/n}$ and 1/n are the Freundlich adsorption constant, and a measure of the adsorption intensity respectively.

Langmuir constant K_L *is* related to R_L by following relation [129].

$$R_L = \frac{1}{1 + K_L \times C_i} \tag{3.13}$$

Where, R_L is dimensionless number, called equilibrium constant.

It is observed from figure 3.29 that Langmuir isotherms provide a better fit with R^2 value of 0.9913 suggesting, the monolayer adsorption of methylene blue onto the ordered activated carbon surface. The values for Langmuir and Freundlich parameters are given in table 3.6. Value of The R_L is found from equations to be 0.0134 ($0<R_L<1$, favorable) which suggest the favorable condition for dye adsorption.

The prepared ordered activated carbon shows better adsorption capacity compared to some previous work [130–133] with highest adsorption value of 305.76 (mg/g).

Table 3.6. Langmuir and Freundlich isotherms parameters for methylene blue adsorption by activated carbon

q_m	R_L	R^2	K_L	K_F	N	R^2
305.76	0.0134	0.9913	0.14766	104.52	4.728	0.913

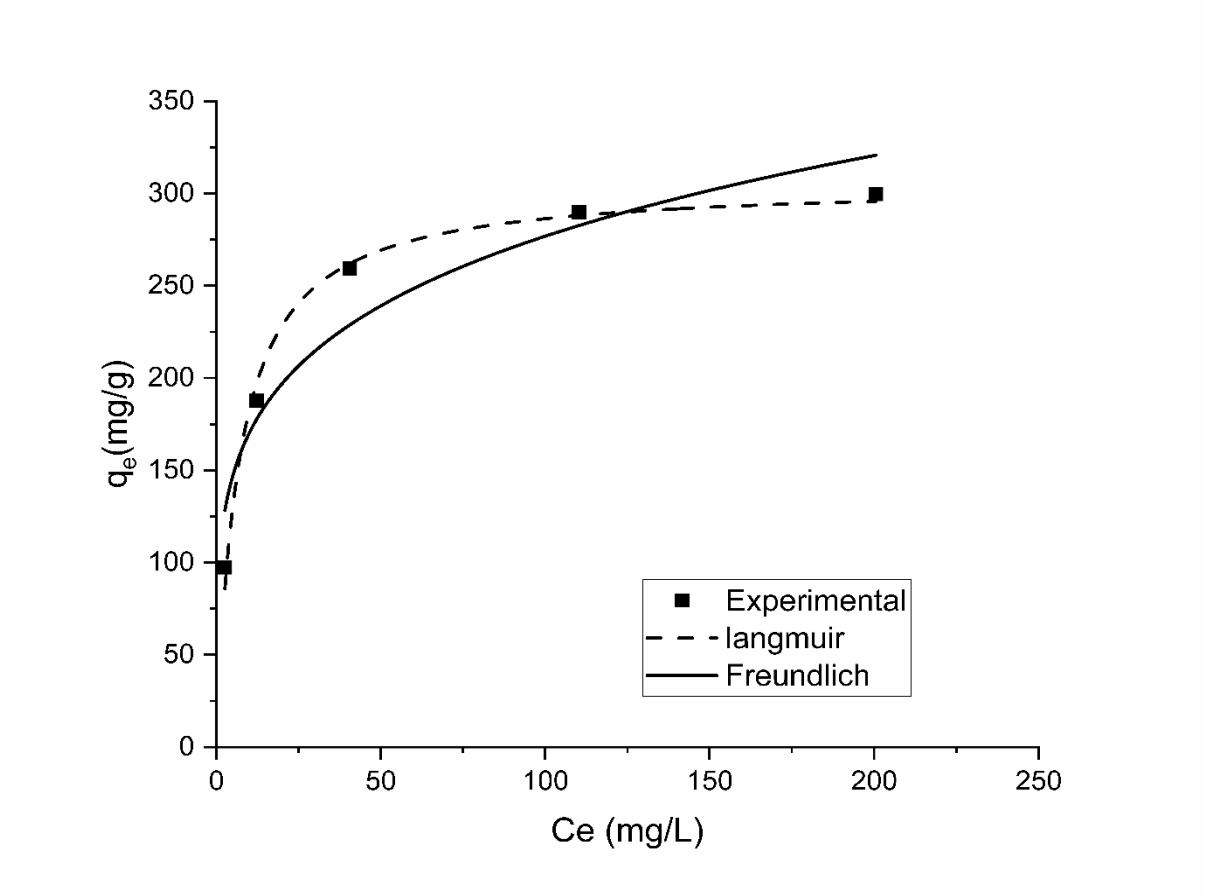

Figure 3.29 Adsorption isotherms of methylene blue dye on activated carbon

3.4.3 Chitosan

3.4.3.1 XRD analysis

X-ray diffractogram of the Chitosan nanoparticle is shown in figure 3.30. The first most prevalent peak appeared at 2θ=19.3º, which is the characteristic peak of chitosan nanoparticles, as reported by Wu J et al. [134] Closer observation of the graph reveals that there is one more peak around 9.7º. The intense and sharp peak around 19.3º represents high crystallinity of chitosan. The crystallinity of chitosan is a significant factor influencing the accessibility of water or metal ions in the internal sites. A polysaccharide structure shows two different crystal forms viz. hydrated crystalline and anhydruous crystalline of the two peaks wherein the peak at 2θ=10º exhibits crystal forms I (hydrated crystalline) while the peak at 2θ=20º exhibits crystal forms II, which corresponds to anhydruos crystalline in an amorphous zone[134–136]. The derived chitosan strongly represents anhydruos crystalline in an amorphous zone.

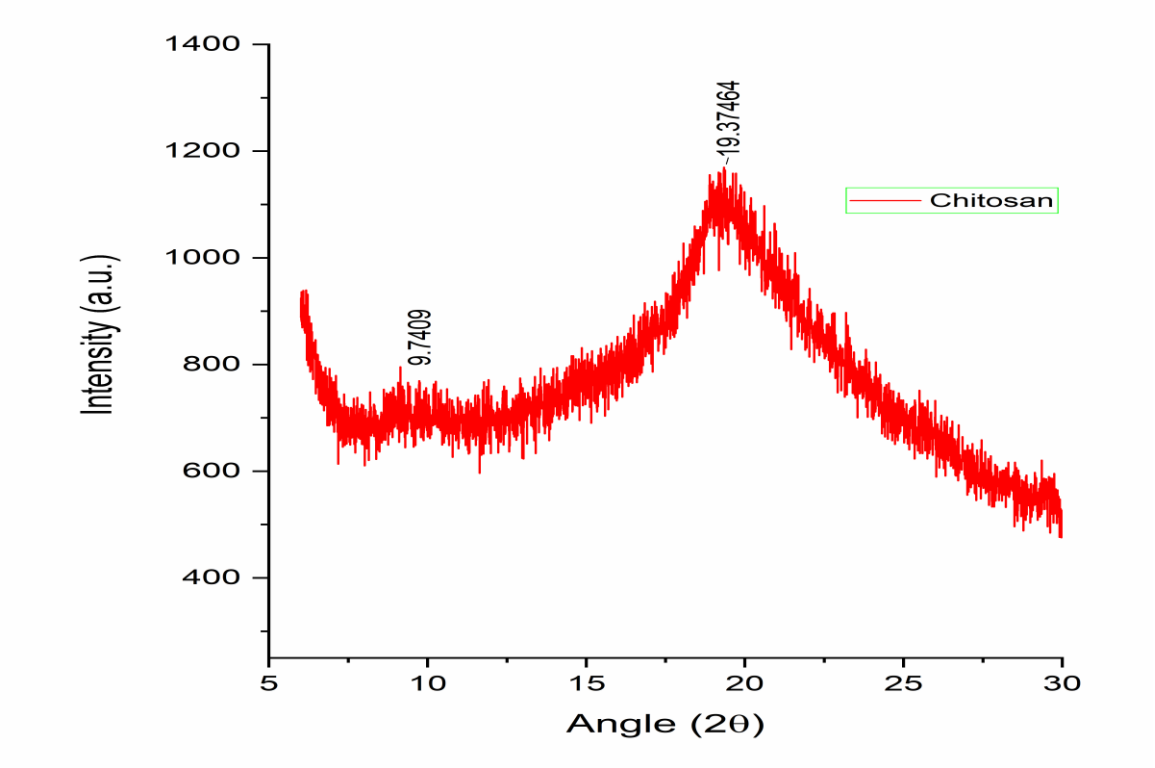

Fig 3.30 X-Ray Diffraction pattern of chitosan

3.4.3.2 FTIR (Fourier Transform Infrared Spectroscopy) analysis

Figure 3.31 illustrates the transmitted spectra of chitosan nanoparticle. The peak at 3428 cm^{-1} indicates O-H stretching. The wider O-H stretching peak represents better hydrogen bonding in chitosan nanoparticles and it represents alcoholic and phenolic groups. The peaks at 2882 cm^{-1} and 2924 cm^{-1} exhibit CH-stretching. The peak at 1655 cm^{-1} confirms the presence of amide I. The presence of Nitro groups is confirmed through the peak at 1377 cm^{-1}. These transmitted spectra (1655 cm^{-1} and 1377 cm^{-1}) imply that chitosan is partially de-acetylated.

The Spectra at 1560 cm^{-1} corresponds to $–NH_2$ bending. The presence of amine group is confirmed by transmitted spectra at 1316 cm^{-1}. Typical saccharide structure in chitosan is confirmed with bands at 1156 cm^{-1} (C-O-C stretching), 1067 cm^{-1} and 1030 cm^{-1}(C-O stretching) . The presence of OH and an amine group confirms the presence of glucose amine. The amine and amide group present in chitosan greatly influences its pollutant adsorption capacity[137]. The functional groups Obtained were anticipated as they are characteristic of chitosan. The degree of de-acetylation (DD) of chitosan was 70.26 %. The degree of de-acetylation of chitosan is a major parameter influencing tangible and biological attributes of chitosan.

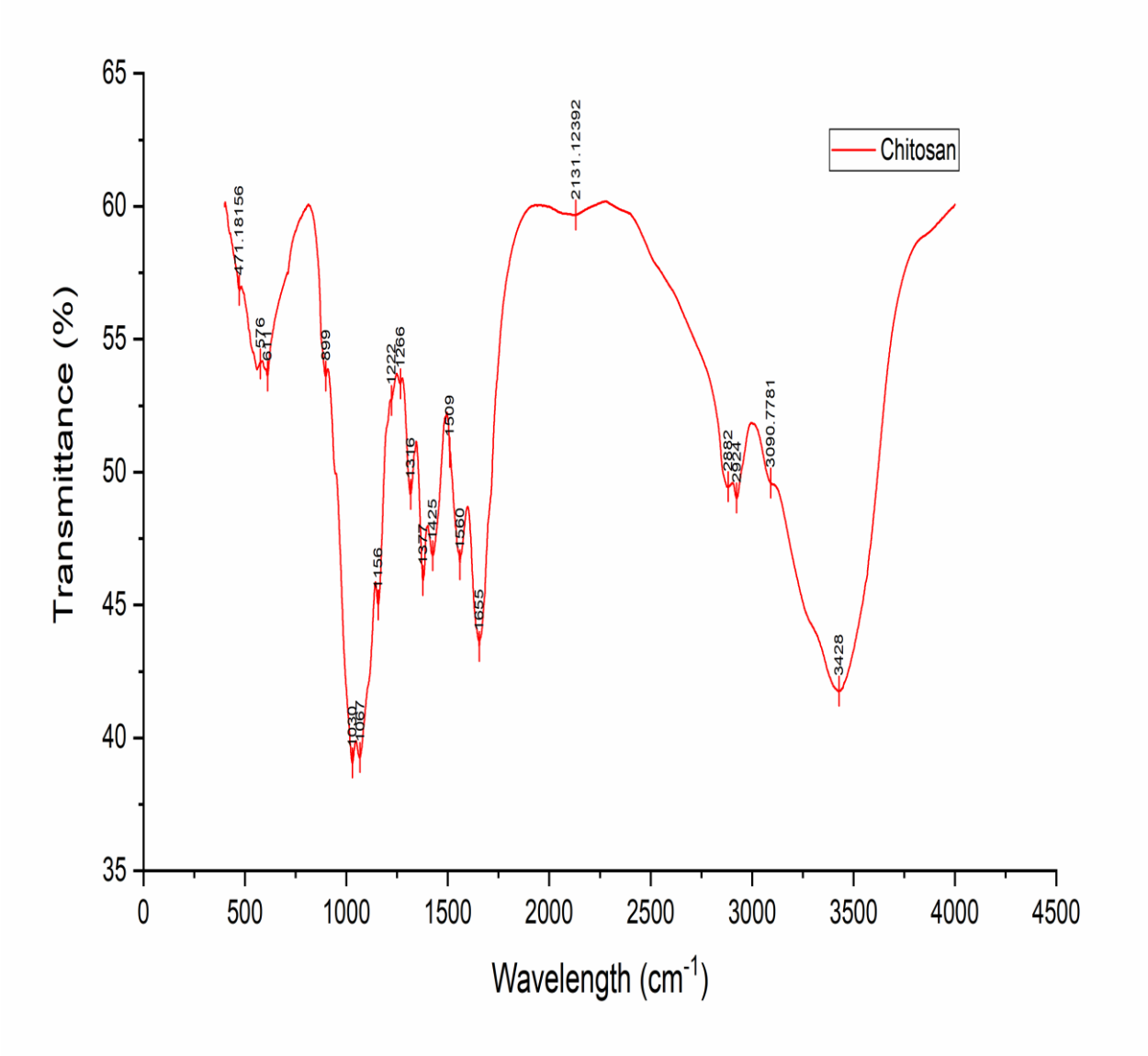

Fig 3.31 FTIR Spectra of chitosan nanoparticle

3.4.3.3 ^{1}H-NMR Spectroscopy

The characteristic peak of chitosan nanoparticle is illustrated in figure 3.32 through ^{1}H-NMR spectroscopy. Three protons of acetyl group around δ=1.8 ppm and peak at δ =3.2 ppm is from Glucosamine, δ=3.3 ppm indicates that the CH group protons are coupled to the functional group of nitrogen. δ=0.9 ppm indicates the presence of – CH_3 group. The degree of De-acetylation was found to be 83.4% based on equation 3.8.

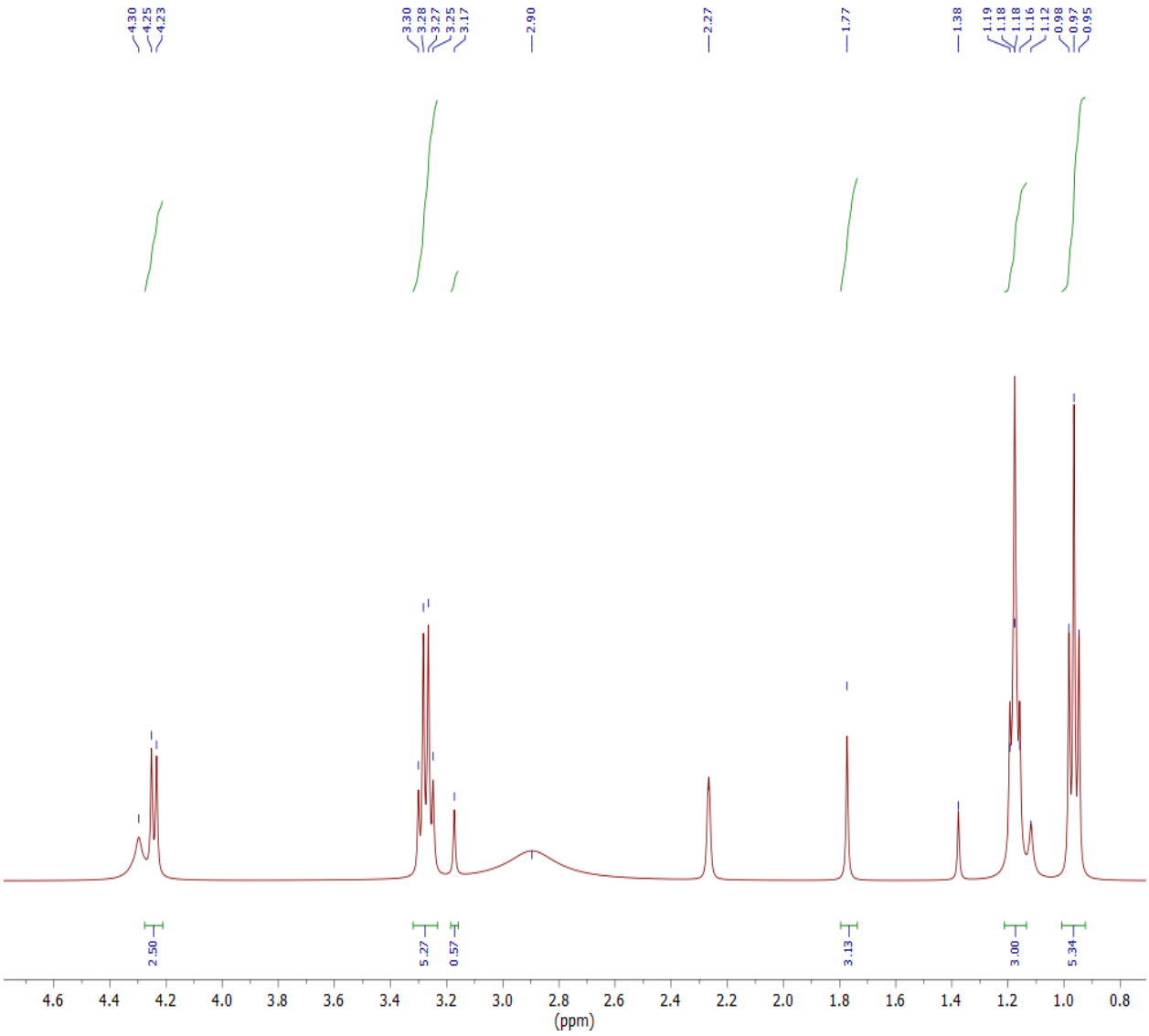

Fig 3.32 ^{1}H-NMR Spectroscopy of chitosan nanoparticle

3.4.3.4 Morphology analysis

Scanning electron and transmission electron micrographs of chitosan nanoparticles are shown in figure 3.33 and 3.34. From figure 3.33 it is clearly observed that chitosan micro particles are distributed on the surface in the form of flakes and that the shape of particles is uneven and forms an agglomeration. The particle size varies from 1-40 micron. Further analysis shows that the particles are in the form of a layered structure.

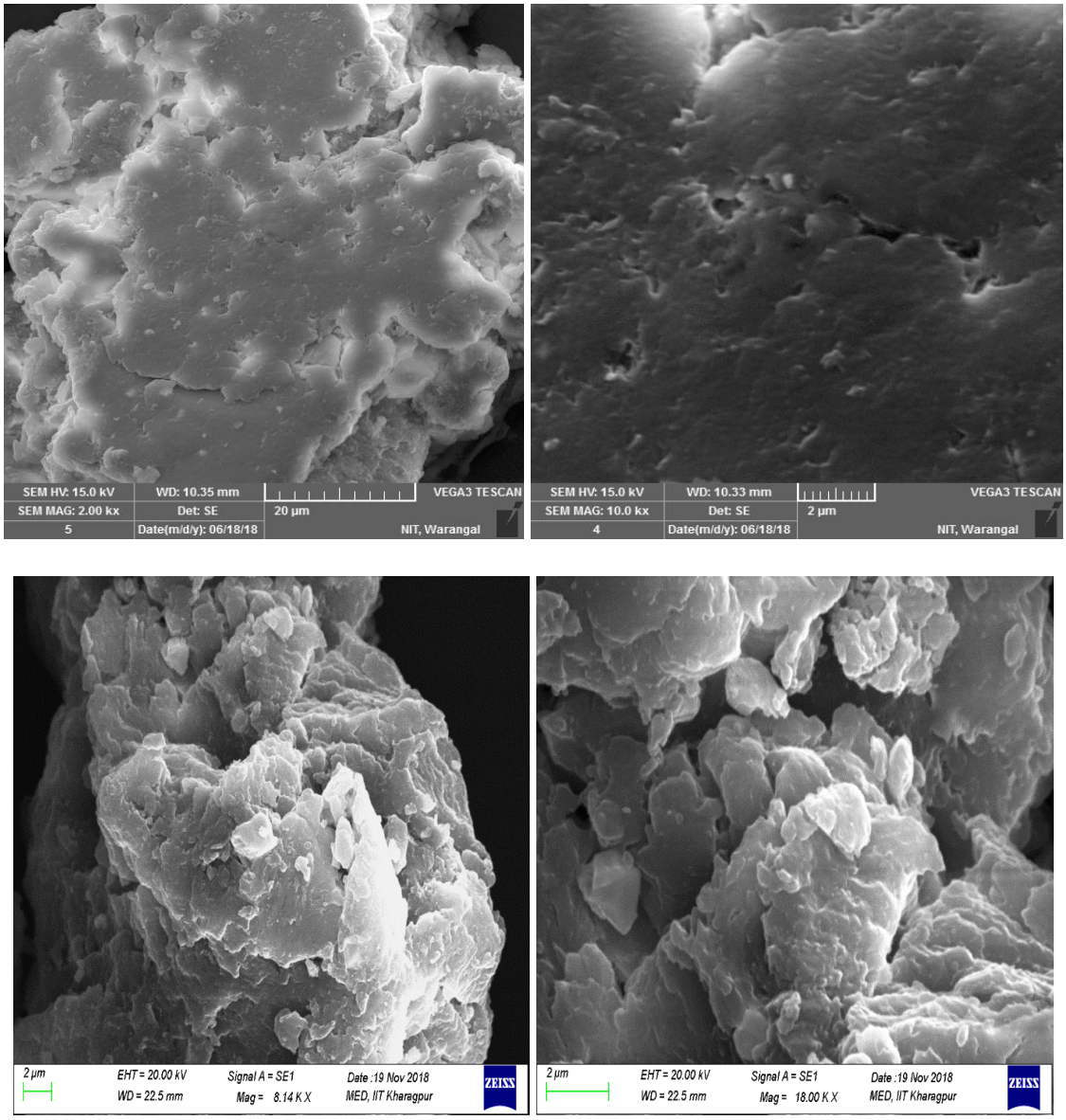

Fig 3.33 Scanning electron microscopy images of chitosan microparticles

The TEM image in figure 3.34 presents the nature of chitosan nanoparticles where the particles accumulate to form a solid lump with a coarse surface. The coarse nature of chitosan surface is influenced by the level of de-acetylation. [138].

TEM images also reveal that the nanoparticles are also in the layered structure form like microparticles. The molecular structure as shown in figure 3.35 can also be observed from TEM images. It shows the fibrous and crystalline structure with molecules aligned in antiparallel fashion[136]. A noteworthy point here is that the particles never lose their layered structured orientation irrespective of size.

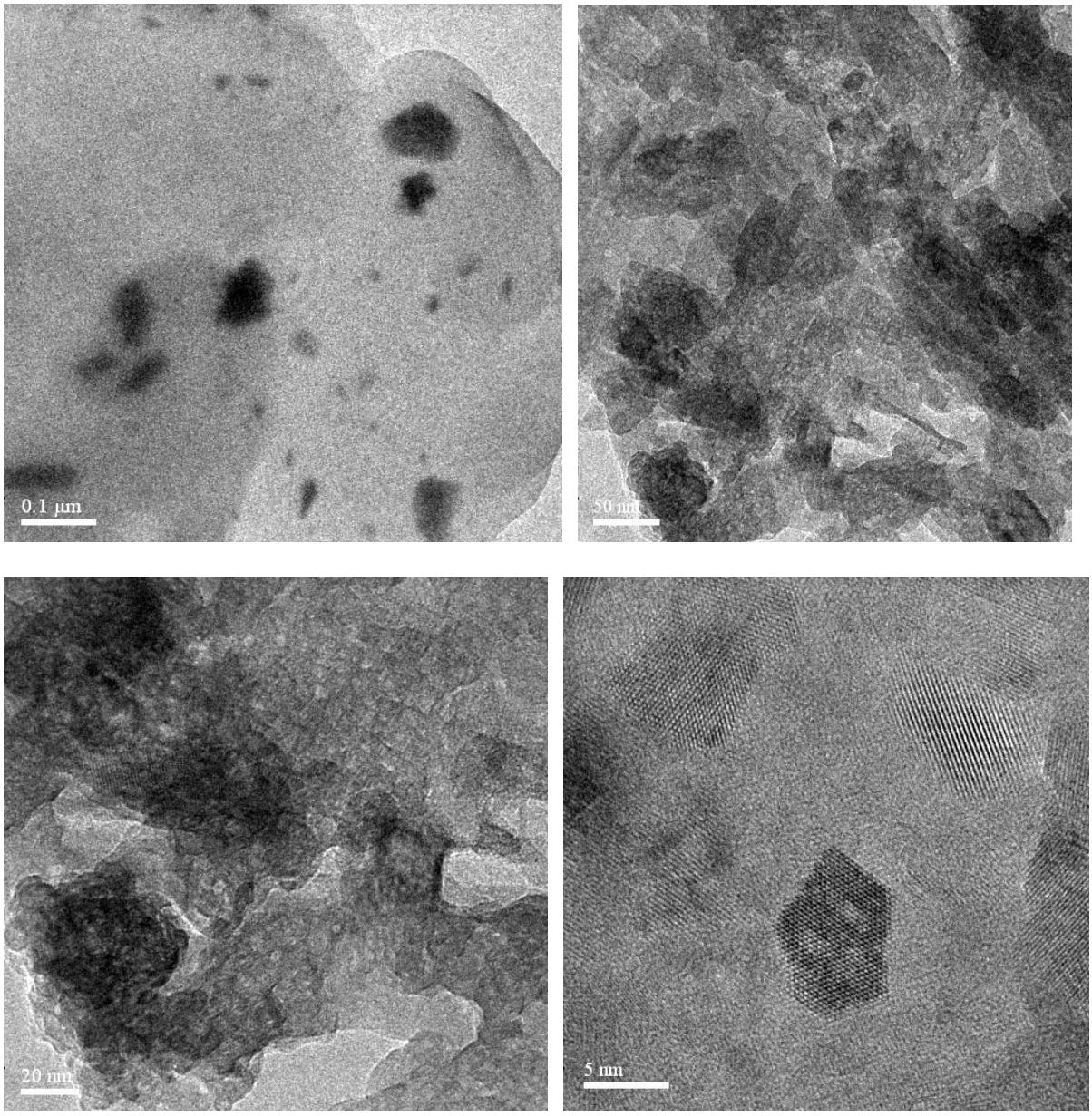

Fig 3.34 Transmission electron microscopy images of chitosan nanoparticles

SEM and TEM results indicate that ball milling does not alter the basic layered structure of prepared chitosan, which has an advantage over other nanoparticle preparation methods reported in the literature. The layered structure enables the use of produced chitosan for filtration process, which could be more efficient than spherical particles prepared by other methods.

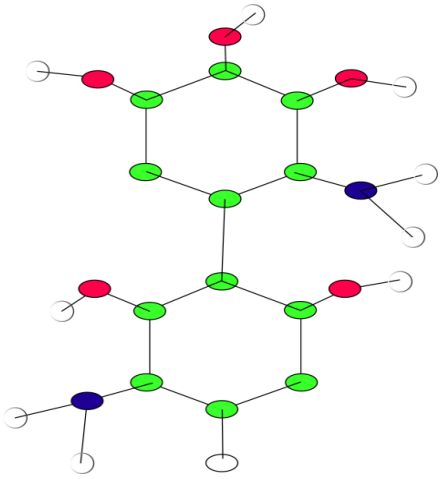

Fig 3.35 Molecular structure of chitosan

3.4.3.5 Thermogravimetric analysis

Figure 3.36 represents the thermogravimetric analysis of chitosan nanoparticles. The initial downward trend (mass loss) in curve from 100% to 87% at around 100°C is due to moisture loss. A drastic loss in weight was detected as a temperature increase from 200 to 350°C. Chitosan loses close to 50% of its mass in this temperature range. Further reduction in mass after 350°C might be from depolymerization and decomposition of CH_2OH and NH_2 moieties [107,137]. This analysis suggests that chitosan nanoparticles could be applied in waste water treatment at temperature up to 200°C, without drastic effect on its structure. The residual mass left after TG analysis of chitosan may be carbon and nitrogen.

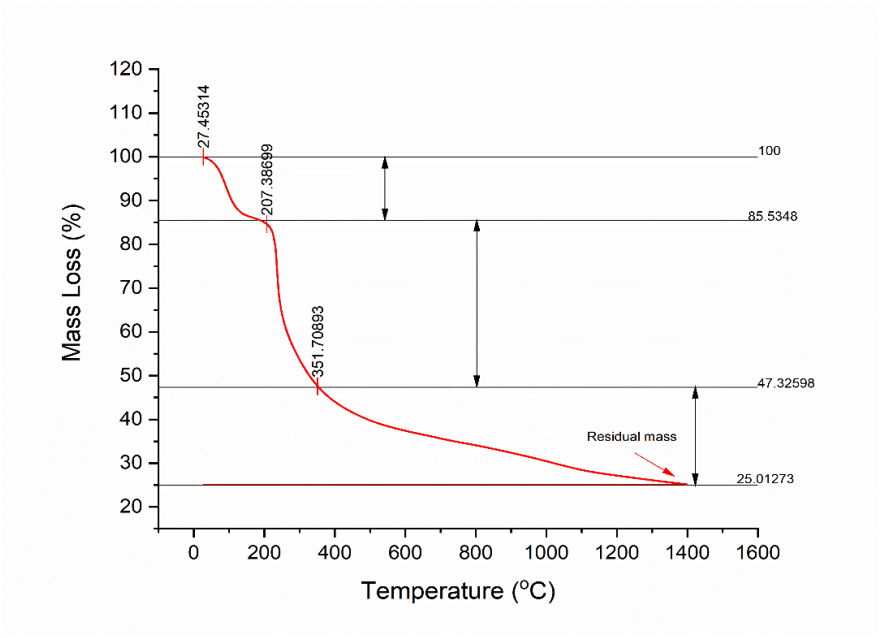

Fig 3.36 Thermal decomposition of chitosan nanoparticles

3.4.3.6 Adsorption studies

A 100 ml of dye solution was prepared with various initial concentrations (50mg/L-500mg/L) of methylene blue dye. An adsorbent (chitosan) dose of 0.2 gram was added in 100ml solution. Solution then stirred at 200 rpm for 6 hours to attain the equilibrium. Uptake at equilibrium by chitosan particles was calculated using equation 3.9.

Figure 3.37 represents the adsorption experimental data fitted with Langmuir [127] and Freundlich [128] isotherms calculated from following formula given by equation 3.11 and 3.12

Langmuir isotherms provide the best fit with R^2 value of 0.9808 suggesting, the monolayer adsorption of methylene blue onto chitosan nanoparticles as noticed from figure 3.37. the values for Langmuir and Freundlich parameters are given in table 3.7. Value of The R_L is found from equations to be 0.0243 ($0<R_L<1$, favorable) which suggest the favorable condition for dye adsorption.

Table 3.7 Langmuir and Freundlich isotherms parameters for methylene blue adsorption by chitosan nanoparticles

q_m	R_L	R^2	K_L	K_F	n	R^2
187.76	0.0243	0.9808	0.08029	49.85	4.177	0.94635

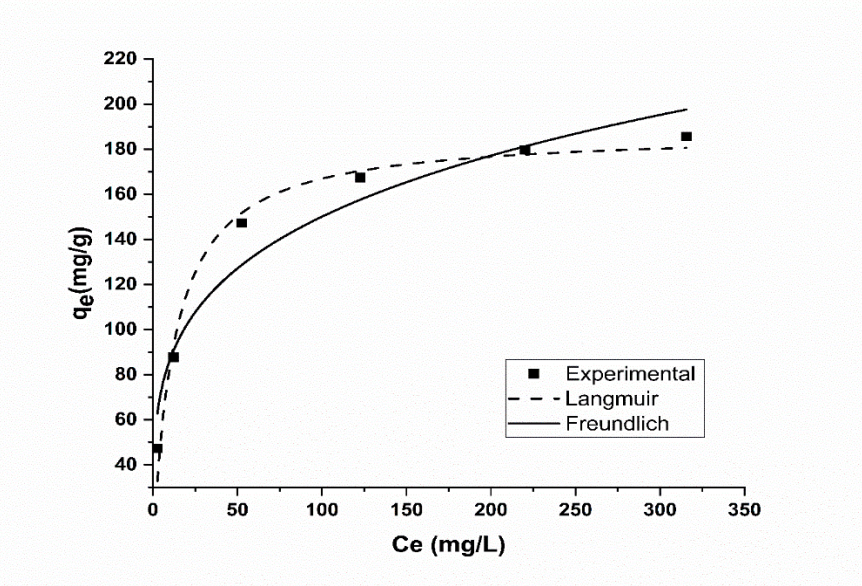

Figure 3.37 Adsorption isotherms of methylene blue dye by chitosan nanoparticles

3.5 Conclusions

- X-ray diffraction showed that the calcium carbonate ($CaCO_3$) is the major constituents in eggshell powder. It was confirmed through XRD that between unboiled and boiled eggshell, boiled eggshell has more amount of calcium carbonate. SEM analysis confirmed that outer layer (cuticle layer) is not present in boiled eggshell.
- SEM, TEM results showed that unboiled eggshell particles are well within nano range. TEM analysis also suggests that particles are crystalline in nature and hexagonal structure. The FTIR analysis reveals that the eggshells particle has amine salt as surface functional. TGA results indicate that the eggshells decompose between 650ºC and 800ºC due to the decomposition of calcium carbonate into CO_2 and CaO.
- A novel method was used to synthesize ordered porous carbon (activated carbon) from natural biowaste. Hierarchical (ordered) porous carbon was successfully produced using coconut shell as the precursor and eggshell as template as well as activating agent.
- 1:1 ratio of eggshells powder and coconut shells is optimum ratio and 800ºC temperature is optimum temperature. XRD and Raman spectroscopy analysis confirms the partially crystalline graphite.
- TGA, XRD and FTIR results confirm that the optimum temperature for the pyrolysis of eggshells and coconut mixture was 800ºC for ordered activated carbon preparation. The mesopores and micropores pore formation in the ordered activated carbon sample is confirmed through SEM, TEM and BET analysis.
- BET analysis results show that the surface area for 1:1 ratio of eggshells and coconut shell is 375.4 m^2/g while the micropores volume is 0.2478 cm^3/g with around 73% micropores. The average pore size is found to be 2.64nm though BJH analysis.
- For 1:1 sample of activated carbon highest methylene blue adsorption capacity of 305.76 mg/g was found for 1 g/L of ordered activated carbon addition and 4.5 h contact time. Adsorption isotherms was best fitted with Langmuir isotherms.
- Nano chitosan has been successfully synthesized from crab shells and converted into nanoparticle using ball milling method.
- Formation of layered structure on chitosan surface was observed in SEM analysis.

- X-ray diffraction analysis confirms successful extraction of chitosan from crab shells.
- Ball milling process results in the formation of layered nano chitosan which was observed in TEM images.
- This layered chitosan can be utilized further as filtration media due to the formation of layered structure with pores.
- FTIR analysis showed the presence of amine and amide functional group, which show good adsorbent properties.
- Chitosan nanoparticles showed a good capacity of dye adsorption with highest methylene blue adsorption capacity of 187.76 mg/g was found for 2 g/L of chitosan nanoparticle addition. Adsorption isotherms was best fitted with Langmuir isotherms. The good adsorption property of chitosan is due to the presence of amine and amide functional as well as the presence of porosity at surface.
- Comparing the adsorption capacity of activated carbon and chitosan, the activated carbon provides better adsorption capacity compared to chitosan, with adsorption capacity of 305.76 mg/g.

Chapter 4

Environmental, tribological and mechanical properties of eggshell epoxy composite

4.1 Introduction

As polymer composite is a combination of more than one material, the properties of composites are affected by numerous elements, for example, filler attributes, filler content, and interfacial adhesion.

Epoxy composites are one of most widely used polymer composites. Epoxy based composite materials have a wide area of applications in automobile, aerospace, marine and oil and gas industries, owing to the composite economy, good mechanical properties, high specific properties, good adhesive property, good heat resistance etc.[139]. For the aforementioned reason, it has become necessary to study and predict the mechanical and tribological behavior of epoxy-based composite materials. Several materials have been used as reinforcement and as filler material in epoxy resin. Glass fiber [140–143] and carbon fiber [144,145] are most widely used synthetic fibers as reinforcement material while jute fiber [146] and bamboo fiber [147,148] are some of the most widely used natural fibers. In addition to fiber reinforcement, filler materials are added to composite to provide additional attributes. In some cases, filler materials act as reinforcing materials. In the present scenario, owing to critical climatic condition, research is oriented towards the development of biocomposite. A biocomposite utilizes biowaste as reinforcement thereby reducing the burden on the environment and is economical. There are a number of biowastes which find use as reinforcement with epoxy resin such as jute [146], bamboo [147,148], rice husk [149], coconut shell [150], coir fiber [151], eggshells [152,153] etc. Eggshells have been used for numerous purposes [4].

Various composites were made by using eggshell as a filler material and its effect on composite properties have been investigated by numerous researchers. The eggshell filler addition was found to increase thermal resistance [154], moisture absorption resistance [155], eggshells particulate addition also found to increase the mechanical properties of polymer composites when added to resins such as, HDPE [156], wheat protein isolate [157], soy protein [158], elastomers [159] etc. eggshell particulate addition reduces the mechanical properties when added to certain polymer resins such as polypropylene [160]; however, the properties of polypropylene composite could be improved by modifying eggshell surface [161]. There are only few examples found in literature, where eggshell particles have been used as filler material in epoxy resin [51,162,163]. Limited study has been conducted on using eggshell nanoparticles as filler material in epoxy resin.

4.2 Raw materials

Raw materials used for composite preparation of egg shell particulate reinforced epoxy polymer composite are as follows:

1. Eggshell particles (unboiled and boiled)
2. Epoxy resin, LY 556.
3. Hardener, HY 951

4.2.1 Eggshells filler

Method of preparation of unboiled eggshells and boiled eggshell micro and unboiled eggshell nanoparticles were discussed chapter 3 article 3.3.1 and 3.3.2.

4.2.2 Epoxy and Hardener

Epoxy is widely used in the composite industry due to its good mechanical, thermal, and electrical properties. Also, its ability to cure at room temperature and low shrinkage during curing are added advantages over other polymers. Araldite LY-556 grade epoxy resin used as matrix material for composite fabrication. The term epoxy resin encompasses both pre-polymer and cured resin. Epoxy resins are designated by 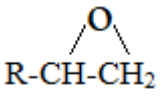 epoxy group. An epoxy resin is generally developed by the reaction of bisphenol-A with epichlorohydrin. Epoxy resin is also known by the name of Diglycidyl-Ether of Bisphenol-A (DGEBA). DGEBA is extensively used in industries owing to its low viscosity, easy processability, good mechanical properties. LY-556 grade epoxy resin is pale yellow colored resin with a density of 1.2 g/cm^3 and viscosity of 10000-12000 mPa.s at 25°C. [164]

Hardening agent or cross-linking agent used for curing of epoxy resin was HY-951 [N, N`-(bis (2-aminoethyl) ethane-1, 2]. Both epoxy resin and hardener were purchased from Sri polymers Pvt. Ltd. Hyderabad, India.

4.3 Composite fabrication

The composite samples were fabricated using hand lay-up technique. A wooden mold was prepared with dimension (180× 280× 4) mm^3. A sheet of non-sticky material (Cellulose acetate) was put on the mold for easy removal of final cast composite sheet. The weight of epoxy, and hardener was calculated for different weight fractions of filler material and then

filler material was thoroughly mixed in a glass container. Then the quantities of boiled and unboiled eggshell fillers were calculated and added to the epoxy resin and hardener mixtures respectively and mixed properly. Finally, the mixture was poured into the molds. Composites with of 4, 8, and 12wt.% fractions of unboiled and boiled eggshell microparticulate were made using the similar procedure as mentioned above. After curing the samples very taken out of the mold and cut into required sizes as per ASTM standards for testing using jig saw cutter. Table 4.1 shows nomenclature for eggshell microparticulate epoxy composite samples.

Table 4.1 Nomenclature for eggshell microparticulate epoxy composite

Symbols	Filler content wt. %	Filler condition
4UB	4	Unboiled
8UB	8	Unboiled
12UB	12	Unboiled
4B	4	Boiled
8B	8	Boiled
12B	12	Boiled

The nanocomposite with 1wt.%, 2wt.%, 3wt.% and 4wt.%, percentage of unboiled eggshell nanoparticulate addition was made using the similar procedure used for fabrication of micro composite.

4.4 Characterization of Composite

4.4.1 Moisture absorption

With increasing use of composite materials in outdoor applications; the component is subjected to severe environmental conditions. It has become an area of extreme importance to predict the environmental behavior of composite material, as composites are prominently used in oil and gas and chemical industry to carry the environmentally hazardous gases and liquids, even a small leakage in the pipeline is dangerous for nature, animal kingdom as well as human being. Even though natural fiber composites such as jute, rice husk, bamboo, coconut shell, and oil palm shell however natural fiber composites can be severely affected by extreme environmental conditions due to the presence of the hydroxyl group. Hence it has become very important to find the effect of environmental condition on biocomposites. Several researchers

have studied environmental behavior of biocomposite. However, the focus here is on either calcium carbonate filled or eggshell particulate filled composite.

Leong, Y. W., et al. [165]compared mechanical and environmental stability of polypropylene (PP) composites reinforced with talc powder or calcium carbonate and compared with the polypropylene/talc/$CaCO_3$ hybrid composites samples exposed to tropical climate condition for 6 months. It was found that after 6 months of exposure, severe deterioration in mechanical properties of single-filler PP was recorded while no significant deterioration in mechanical properties of the hybrid-filler composites was noticed. It was therefore concluded that 'hybridization' significantly improves resistance to severe environmental degradation.

Guermazi, Noamen, et al. [166] studied the influence of calcium carbonate ($CaCO_3$) fillers on the hygrothermal performance of polyvinylchloride (PVC). The properties of PVC/$CaCO_3$ composite were examined in water up to 3 months at various temperatures. It was found that the addition of fillers in PVC demonstrated an increment in both T_g value and storage modulus.

Li, X. H., et al. [167] found that incorporation of calcium carbonate into polypropylene carbonate (PPC) resulted in an increase in its thermo oxidative stability. Adeosun, S. O., et al.[168] found that water absorption of polypropylene- $CaCO_3$ composite increased by 400% at 10%-$CaCO_3$ addition.

Hussein, Abdullah A. et al. [169] investigated water absorption behavior of eggshell–High density polyethylene (HDPE) composite as a function of exposure time. Increase in water absorption with an increase in the exposure time was recorded. It was found that the amount of water absorbed increases by increasing the wt.% of egg shell while keeping the time period constant.

Shuhadah, Siti, and A. G. Supri [170] investigated mechanical properties, morphology and water absorption behavior of chemically modified low density polyethylene/egg shell powder composites. It was found that the chemical treatment of eggshell powder had a positive effect on mechanical properties, water absorption and morphology of composite.

The aim of this test is to investigate the effect of filler on moisture absorption under different environmental (sub-zero temperature, salt water, mineral water, kerosene) conditions. The amount of weight gain by composites under different environmental conditions is calculated from following formula. To study the effect of subzero temperature, the composite samples were kept in the freezer compartment of refrigerator. There is no fixed temperature but a majority of the refrigerator goes below -20ºC in the freezer compartment. To do the mineral

water test, the drinking water is used, while for the saline water test, edible salt is dissolved in water till it reaches saturation.

$$amountofweightgain = \frac{M_a - M_b}{M_b} \ldots\ldots (4.1)$$

Where M_a is mass of composite after being subjected to the various environmental conditions, M_b is the mass of composite before being subjected to environmental conditions.

The same methodology is used for calculation of moisture absorption under different environmental (salt water, mineral water, moist soil) conditions for nanocomposites.

4.4.2 Erosion test

The tremendous use of polymer composites where the component surface is impacted by solid particulate has led to their extensive applications in manufacturing of aircraft wings [171], aircraft rotor blades [171], spacecraft body parts [172], advanced aircraft engine parts [172], outer body structure of fighter jets [173], wings and rotor blades of ultra-sonic fighter air jets [173], automobile body structure [174], steam turbine blades [175], wind turbine blades [175], pipelines carrying solid particulate material etc. Hence the study of erosion wear behavior of polymer composites has become an area of extreme importance, particularly in the selection of alternative materials.

The progressive permanent damage caused to of material surface due to the impact of solid particles on material surface of a material is defined as erosion wear. Erosion wear results in loss of material, abrasive nature of surface, surface deterioration, and reduction in the reliability of the structure as well as an increase in maintenance and repair cost. Hence, solid particle erosion has become an area of major attention as it is accountable for permanent component damage in lots of dynamic applications. The rate of erosion wear rate is influenced by many parameters such as impingement angle, impact velocity, erodent type, size, shape and hardness of erodent, the mechanical properties of the specimen and percentage of reinforcement improvised.

Researchers have characterized the erosion behavior of composite material based upon the maximum and minimum erosion rates at a certain angle. If the maximum erosion rate occurs at normal incidence (90°) it is characterized as Brittle behavior, while the ductile behavior is characterized by the maximum erosion wear rate at lower angles i.e. ~15-30° impingement angle. For maximum erosion at 60^o of impact the material said to have shown semi brittle behavior [176,177].

A comprehensive review has been presented on the effect of the aforementioned parameters on the erosion behavior of polymer and polymer-based composites by Barkoula and Karger-Kocsis [176]. Various models and empirical relations have been analyzed and suggested to relate the erosion rate with some of the influencing parameters. Another review has been presented by Patnaik, Amar, et al. [177] focusing on erosion behavior with respect to various modes and processes of polymer matrix composites. The evolution in experimental erosion studies has also been reviewed. There are a number of fillers which have been used to increase erosion resistance of composite material such as Al_2O_3, SiO_2, TiO_2, SiC, $CaCO_3$ etc.

However, no one has worked on using eggshell particle as filler material to enhance erosion wear resistance.

Erosion tests were conducted on air jet erosion test rig as depicted in figure 4.1. The erosion test rig consists of a rotor which controls the flow of sand particle, a mixing chamber where sand particles are accelerated. A compressed air provides the required pressure to the silica sand which is fed constantly by rotor into the mixing chamber. This pressurized sand particle then passes through a convergent nozzle of 3 mm internal diameter. The specimen impacted upon the erodent sand particles at different angles (i.e. 30°, 45°, 60° and 90°) which can be adjusted using a swivel head and an adjustable sample holder. Table 4.2 shows the process parameters for erosion test. Square shaped specimens of dimensions (20×20×4) mm^3 were prepared for erosion test. After every experimental run the samples were cleaned with acetone and dried. And then weighed before and after the erosion test. The weight loss was calculated for subsequent calculation of erosion rate.

The effect of different environmental (sub-zero temperature, salt water, mineral water, kerosene) conditions on erosion rate of unboiled and boiled eggshells epoxy composite was studied; this was to compare the erosion rate in dry condition with erosion rate after exposure to different environmental conditions. For micro composite the erosion rate was calculated for 5 mins.

For nanocomposite same procedure was followed as for micro composites. The erosion rates were measured at various impact angles (i.e.30º, 45º, 60º and 90º) at different velocities 101 m/s, 119 m/s, 148 m/s. for nano composite the erosion rate was calculated for 15 mins.

To study the effect of different environmental (salt water, mineral water, moist soil) conditions on the erosion rate of the nanocomposite erosion test was conducted for 10 mins for composite samples, which gives best results for erosion resistance.

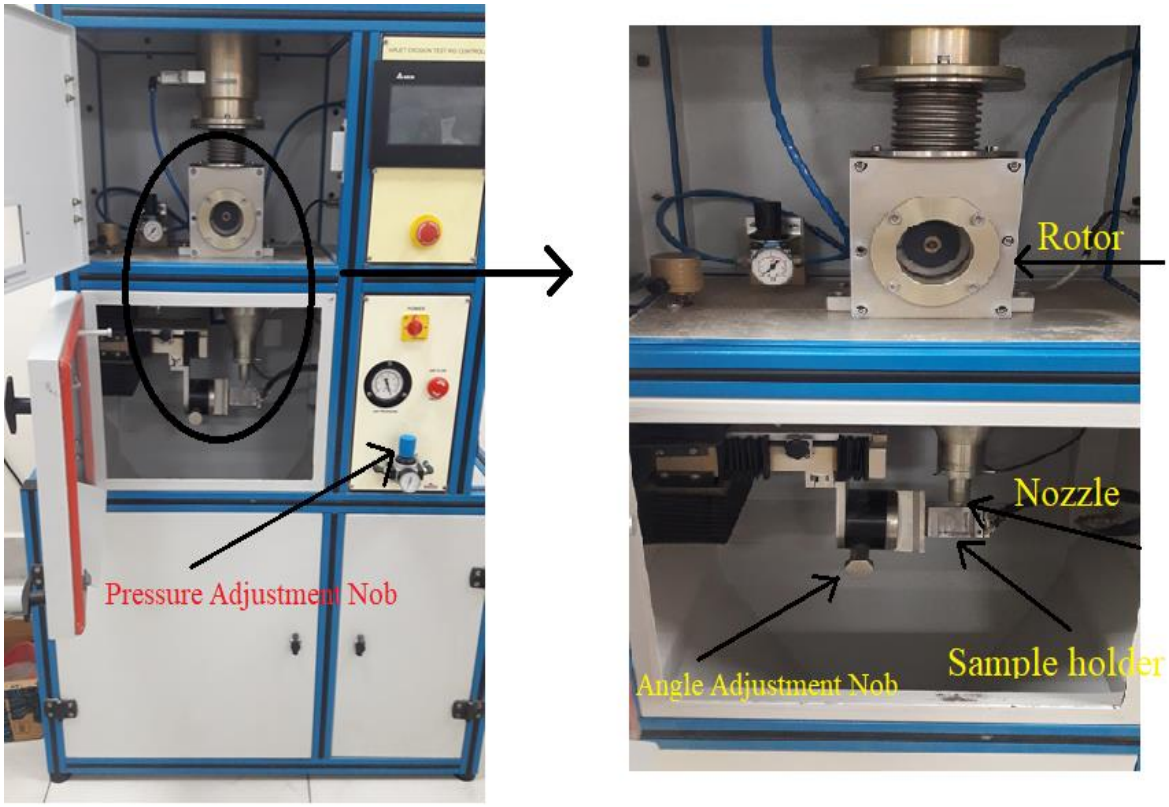

Figure 4.1 Erosion test rig

The wear rate was expressed in terms of $\Delta w_1 / \Delta w_2$

Where Δw_1 - is the loss in weight of the composite and Δw_2 - is the total weight of the erodent used

Table 4.2 Parameters for erosion test

Test parameters	
Erodent	Silica sand
Erodent size (μm)	200±50
Erodent shape	Angular
Hardness of silica particles (HV)	1420±50
Impingement angle (α°)	30, 45, 60 and 90
Impact velocity (m/s)	86,101,119,148
Erodent feed rate (gm/min)	1.467±0.02
Test temperature:	RT
Nozzle to sample distance (mm)	10

4.4.3 Tensile test

Tensile test was performed on HIECO electro mechanical UTM. ASTM (American Society for Testing and Materials). D 3039-76 standards were used for the preparation of a flat dog bone shaped specimen for tensile testing of nano composite is shown in figure 4.2. Load rate of 2 mm/min was used for testing. The dimensions of tensile samples were as follows: length -140mm, width at centre-10mm and thickness -4mm.

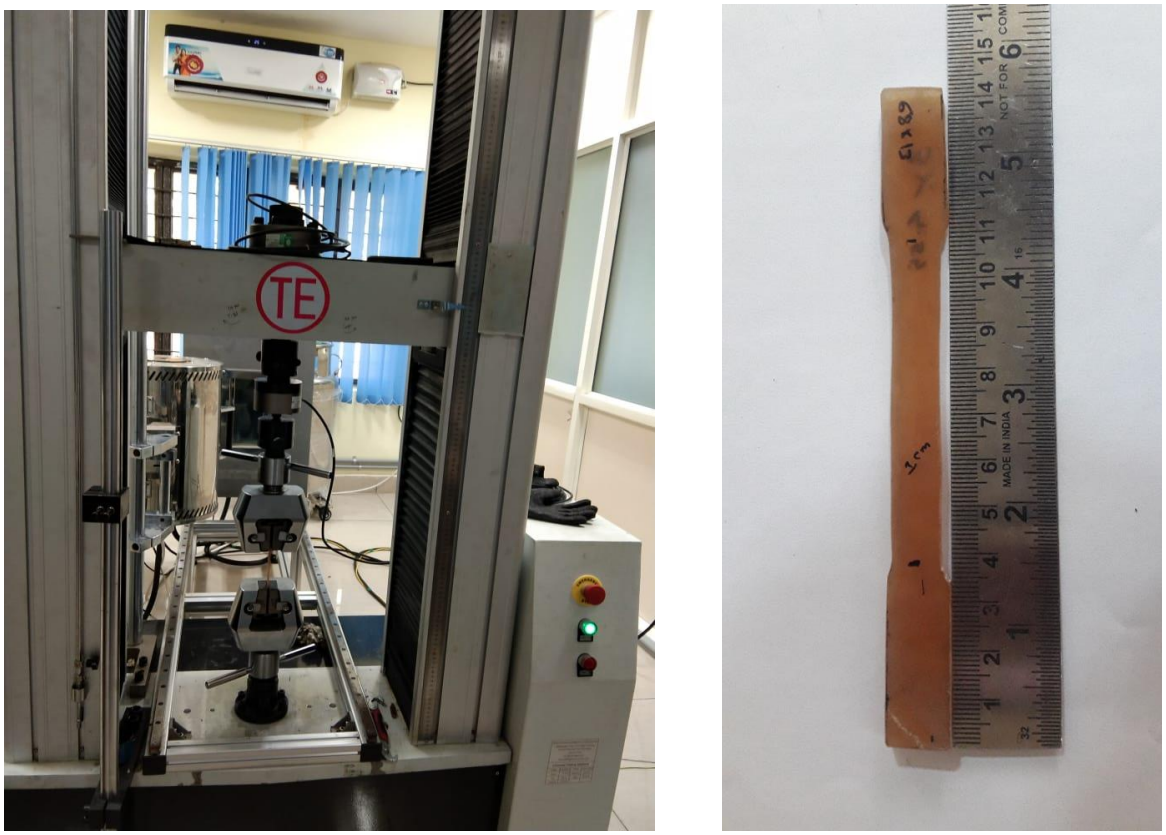

Figure 4.2 (a) HIECO universal testing machine (b) Sample for Tensile Test

4.4.4 Three-point bending test

Samples for bending test were prepared according to ASTM D2344-84 standards. A rectangular shaped specimen of dimensions length-140 mm, width -20 mm and thickness- 4 mm was prepared for bending tests of nanocomposite is shown in figure 4.3. Three-point bending test was also conducted on HEICO digital Universal testing Machine (UTM) using 3-point bending fixture. The parameters for bending test were: load rate 2 mm/min and load cell of 5kN was used for applying the load.

Figure 4.3 Flexural test sample

4.4.5 Hardness test

The hardness test was conducted on the Vickers micro Hardness tester. Square shaped specimens of dimensions (20×20×4) mm^3 were prepared for the hardness test. Hardness test was conducted on the Vickers micro hardness tester. A load of 0.25 N was applied onto the sample for about 10 seconds and then the load was removed. The hardness was calculated using the shape of the indentation obtained.

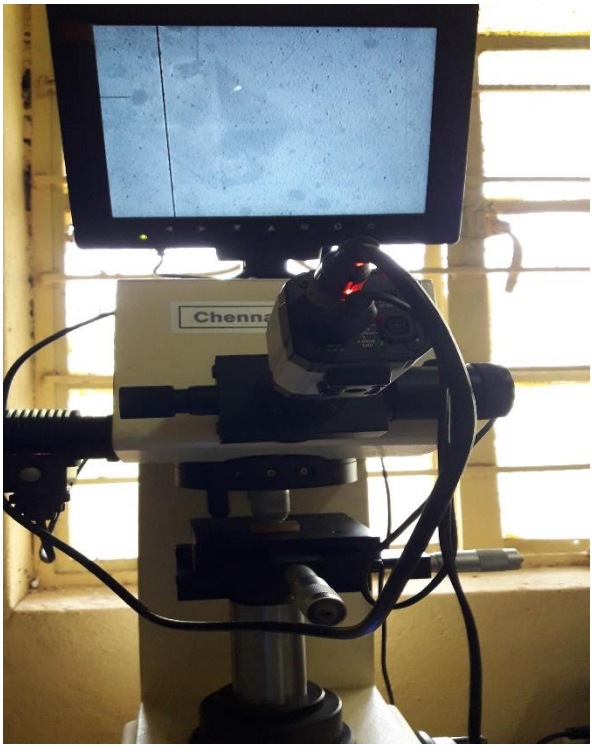

Figure 4.4 Vickers hardness tester

4.5 Results and discussion

4.5.1 Eggshell microparticulate epoxy composite

4.5.1.1 Moisture absorption

Figure 4.5 (a-d) shows the weight gains by unboiled egg shells filler reinforced (4wt.%, 8wt.% and 12wt.%) epoxy composites in different environments (saline, mineral, subzero and kerosene).

For different environmental conditions i.e. saline water, mineral water, and sub-zero temperature as shown in Fig. 4.5 (a–c) respectively, an increment in moisture absorption with increase in filler addition is clearly observed.

Similar kinds of results were obtained by Hussein A.A. et al. [169]. The figure also demonstrates significant moisture absorption in the initial days and then the gradual decrease in moisture absorption day by day and finally it comes to saturation condition after a certain period of time. The amount of moisture absorption is more in saline water compared to mineral and subzero environment. This may be due to the presence of many surface functional groups, such as amines, amides and carboxylic groups in the eggshell particles as observed in FTIR analysis of eggshell in chapter 3 article 3.4.1.5, which are highly reactive in the salt environment. Similar kind of behavior was notice by Raghavendra G. et al. [146] in the salt environment.

From the graphs was also been noticed that the 12wt.% unboiled eggshell epoxy composite samples show highest moisture absorption in sub-zero temperature, saline water, and mineral water. This proves that as the filler percentage increases, the weight of samples in saline, mineral and the subzero temperature condition also increases due to moisture intake. The increase in the amount of $CaCO_3$ with an increase in percentage of reinforcement could be the reason for this behavior. The very same effect of $CaCO_3$ on polymer composite was observed by Adeosun SO et al. [168].

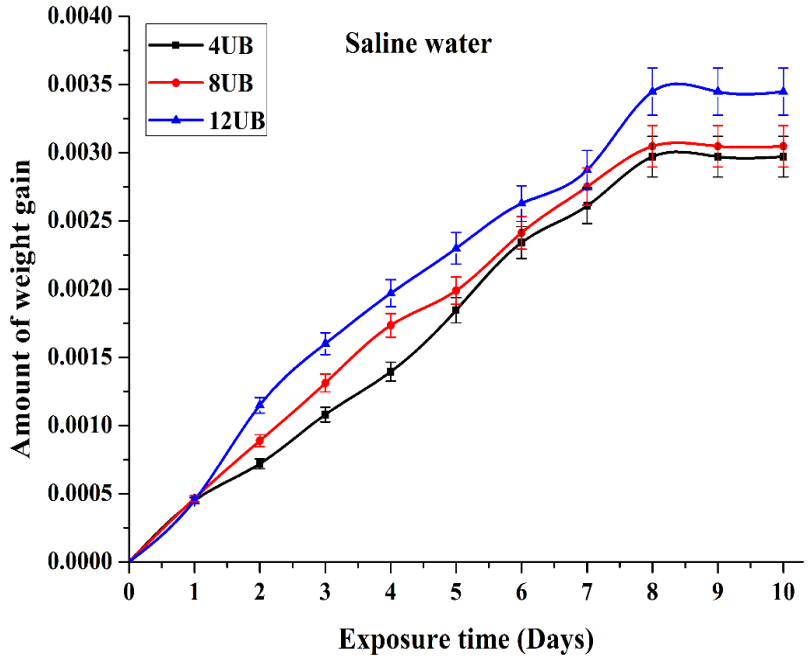
Saline water
4UB
8UB
12UB
Amount of weight gain
Exposure time (Days)
0.0040
0.0035
0.0030
0.0025
0.0020
0.0015
0.0010
0.0005
0.0000
0
1
2
3
4
5
6
7
8
9
10

(a)

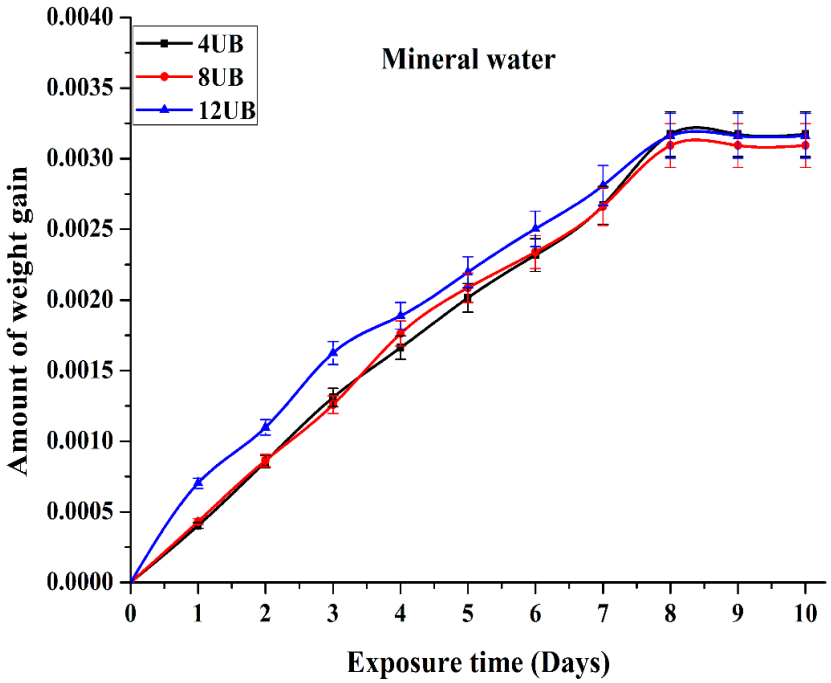
Mineral water
4UB
8UB
12UB
Amount of weight gain
Exposure time (Days)
0.0040
0.0035
0.0030
0.0025
0.0020
0.0015
0.0010
0.0005
0.0000
0
1
2
3
4
5
6
7
8
9
10

(b)

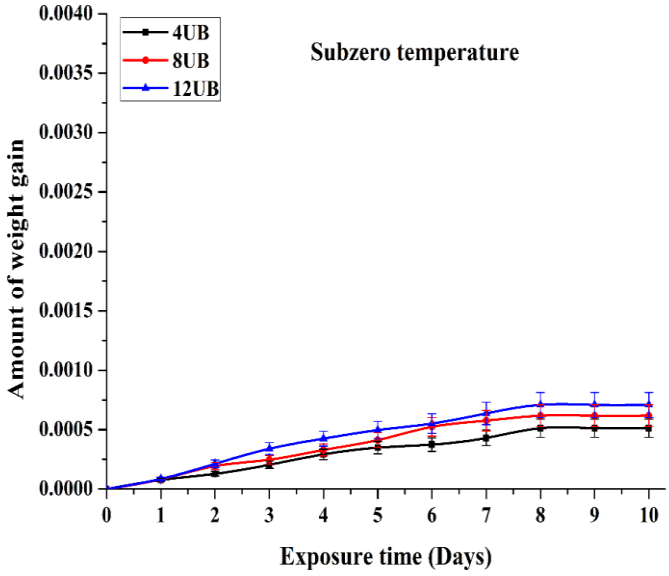

(c)

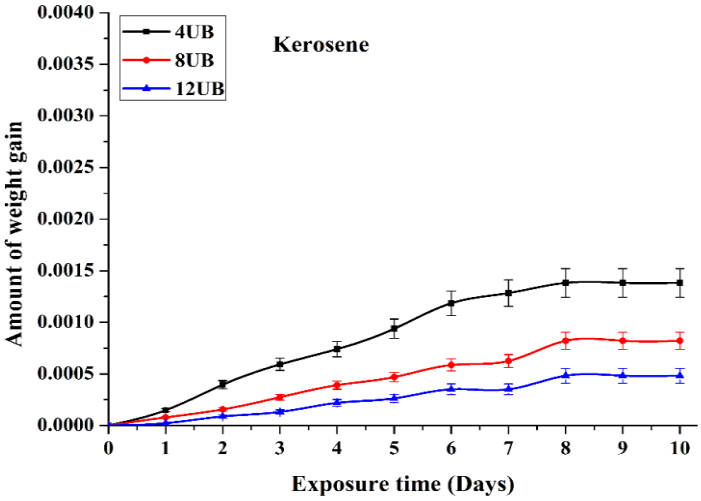

(d)

Figure 4.5 Weight gains by unboiled eggshells filler composites exposed to (a) saline (b) mineral water (c) subzero (d) kerosene environment.

The trend observed in water absorption is subzero<kerosene<mineral< saline. The immersion of samples in kerosene shows the opposite behavior to other environments. From figure 4.5(d) it is evident that with an increase in filler percentage of unboiled eggshells particles, kerosene absorption rate decreases. Moreover, the absorption rate is also less when compared to saline and mineral water condition. This implies that $CaCO_3$ is not reactive to kerosene and no chemical reaction therefore occurs. The exposure to the subzero environment

results in the least absorption, since in the subzero environment once the outer layer is covered with ice, the moisture cannot diffuse inside the sample; which is not the case in mineral water or saline water environment, where the sample were immersed the sample into the water.

Figure 4.6(a-d) shows the weight gain by boiled egg shells filler reinforced (4wt.%, 8wt.% and 12wt.%) epoxy composites in different environments (saline, mineral, subzero and kerosene). The trend in the absorption is the same as in unboiled eggshell filler composites but the initial absorption is more as compared to unboiled egg shell filler composites; this may be due to removal of the outer layer of egg shell and pore formation during boiling.

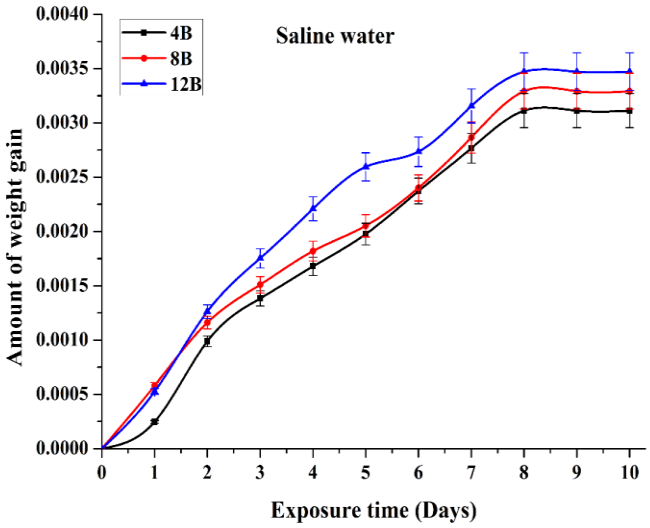

(a)

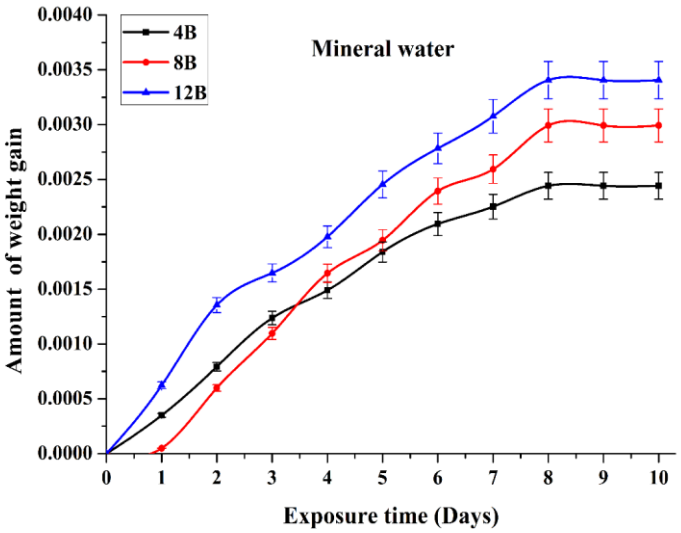

(b)

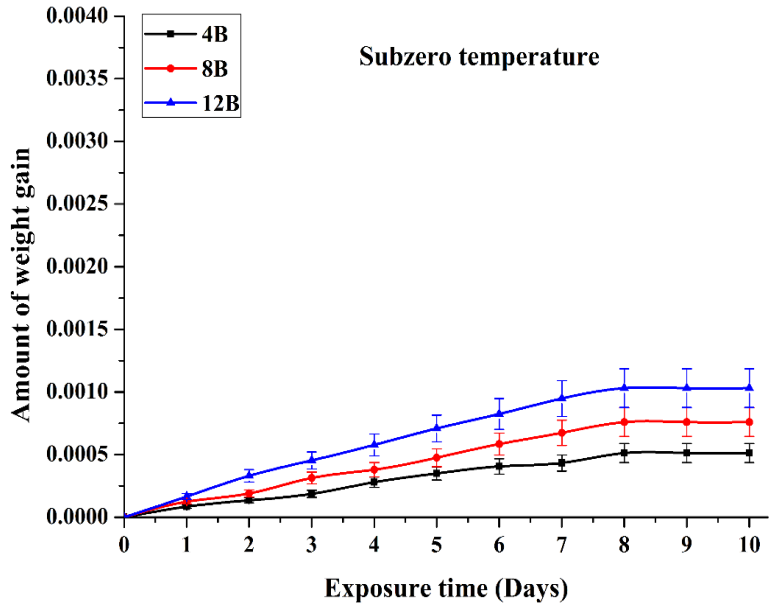

(c)

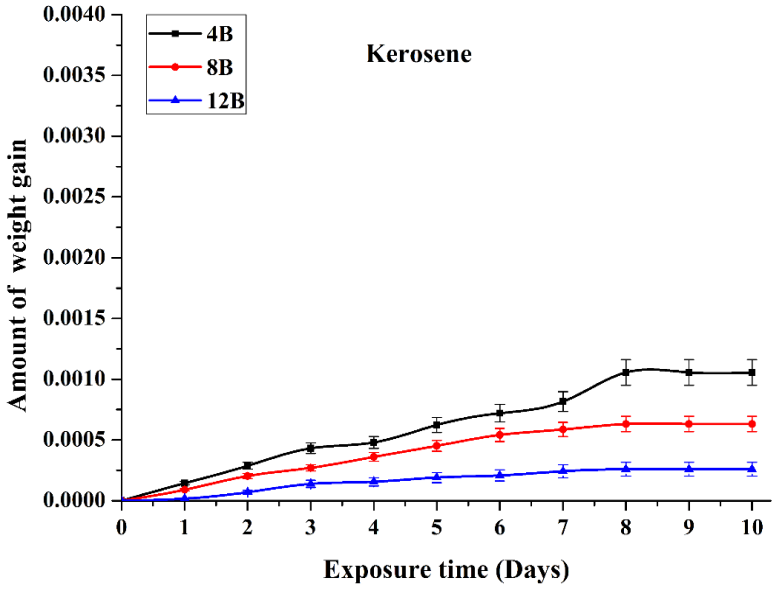

(d)

Figure 4.6 Weight gains by boiled eggshells filler composites exposed to (a) saline (b) mineral water (c) subzero (d) kerosene environment

Figures 4.7 (a-b) show weight gains of 4 and 12 wt.% unboiled egg shells filler composites after being exposed to different environments. From the figure it is evident that the absorption rate is more in saline and mineral environment when compared to kerosene and subzero in both 4wt.% and 12wt.% fillers. It is also found that at higher filler percentage, the least absorption is in kerosene environment, which may be due to the reduction in epoxy, which is responsible for liquid absorption in kerosene.

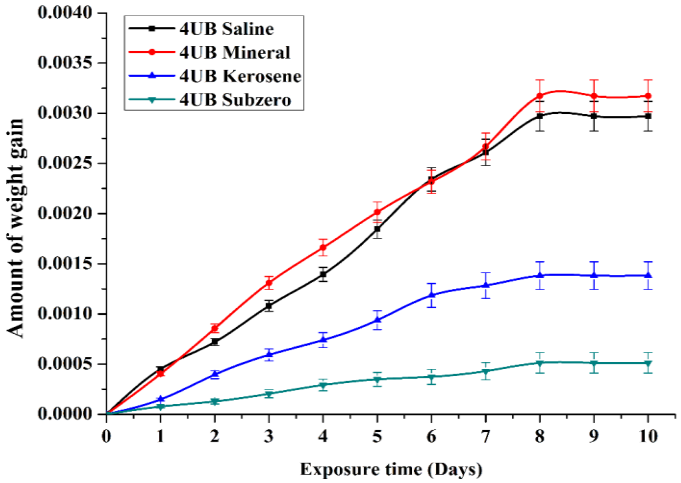

(a)

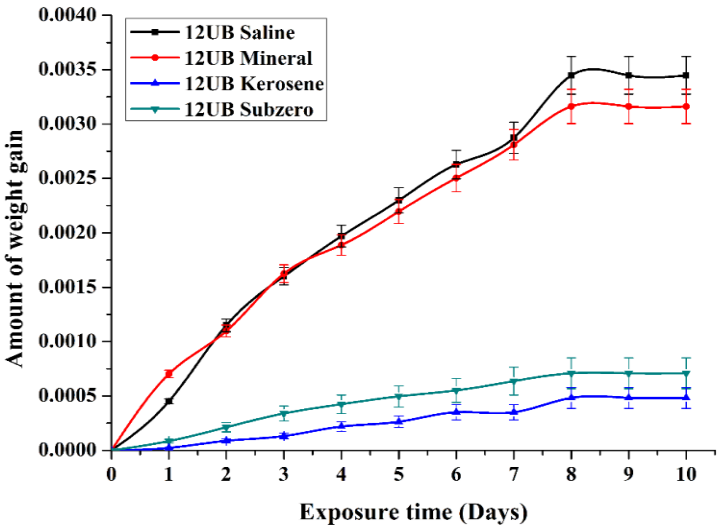

(b)

Figure 4.7 Weight gains for (a) 4wt.% filler (b) 12wt.% unboiled eggshells filler composites under different environments.

Figures 4.8 (a-b) show weight gains of 4wt.% and 12wt.% boiled egg shell filler composites after exposure to different environments. From figure 4.7, similar type of behavior is observed in unboiled egg shell fillers. At higher filler percentage, subzero shows least absorption when compared to kerosene, which may be due to absorption of kerosene by the pores formed during boiling.

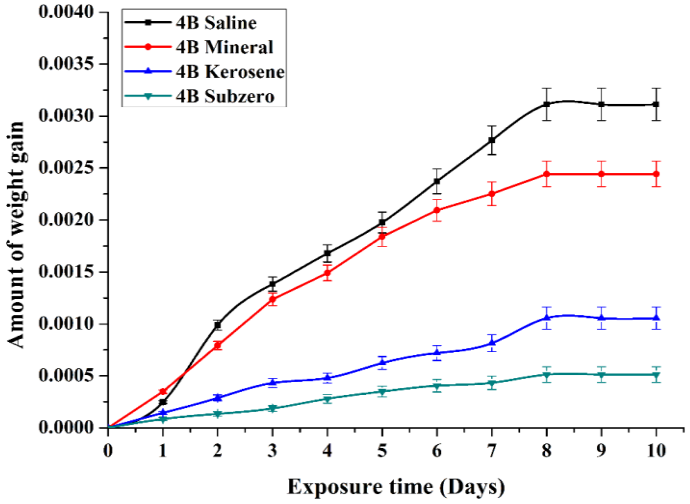

(a)

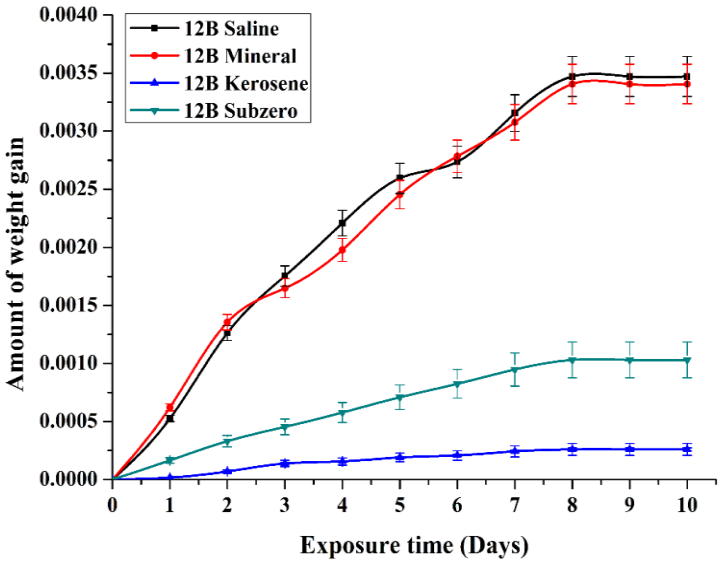

(b)

Figure 4.8 Weight gains for (a) 4wt.% filler (b) 12wt.% unboiled eggshells filler composites under different environments.

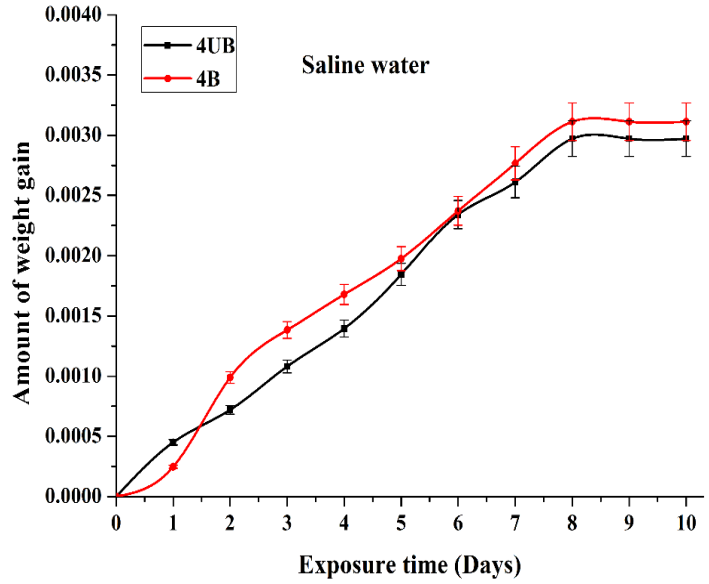

4.9 (a)

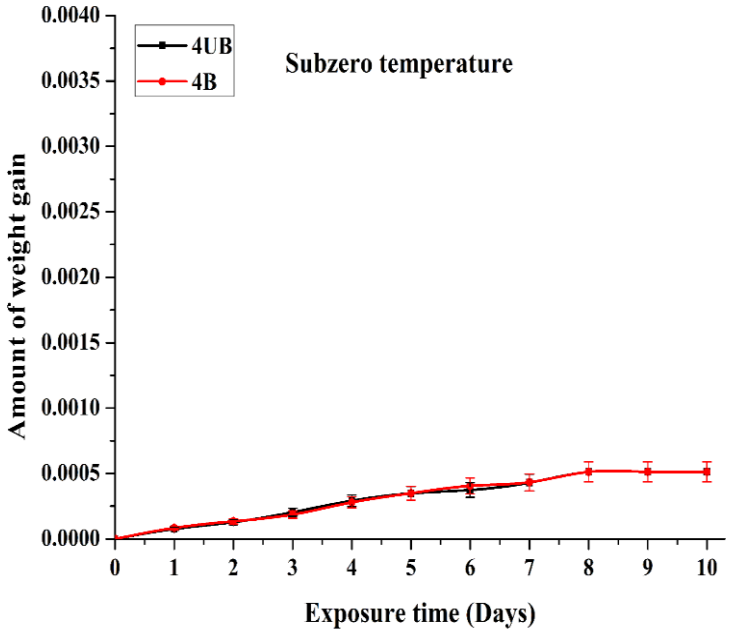

4.9 (b)

Figure 4.9 Weight gains by unboiled and boiled eggshells filler composites under (a) saline (b) subzero environment

Figure 4.9 (a-b) shows the comparison between boiled and unboiled egg shells filler composites. From figure 4.9 (a) it is clearly observed that the initial absorption is more in unboiled egg shell filler composites and later it reduces. In boiled eggshell filler composite, initial moisture absorption is less but after some time the absorption is more as compared to boiled eggshell filler composite. From figure 4.9 (b) it can be observed that in subzero condition, the absorption in unboiled and boiled are almost same. From moisture absorption it is observed that unboiled eggshell microparticulate epoxy composite has a lesser moisture absorption compared to boiled eggshell microparticulate epoxy composite. One further observation is kerosene does not have any effect of moisture absorption, therefore moisture absorption analysis of nanocomposite kerosene environment was chosen for analysis

4.5.1.2 Erosion test

Figure 4.10 shows the comparative analysis between the erosion rate of unboiled and boiled eggshells filled epoxy composite and pure epoxy. From figure 4.10 it is observed that the erosion wear resistance of pure epoxy increases when added with eggshell filler.

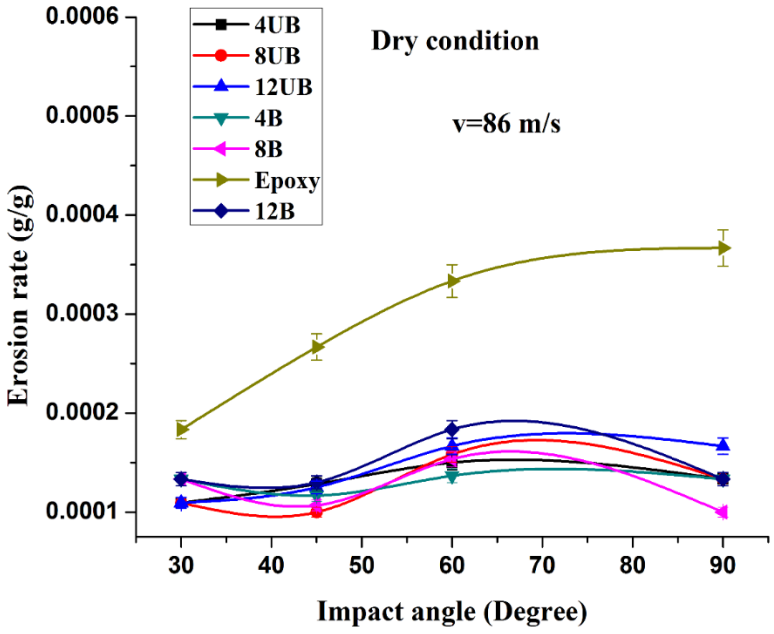

Figure 4.10 Erosion rate for 4,8 and 12wt.% of unboiled and boiled eggshells epoxy composite with epoxy

Further examination of figure reveals that the erosion wear rate increases with increment in filler addition for both unboiled and boiled eggshell filler composites, however the erosion

wear rate is still lower when compared to pure epoxy. The maximum erosion rate for the composite is observed for 12wt.% boiled eggshell filled epoxy composite. Erosion wear behavior of the composite greatly is influenced by the impingement angle of the erodent. For maximum erosion at 60^{o} of impact, the material said to have shown semi brittle behavior. As closer observation of figure 4.10 shows eggshell epoxy composite samples show the maximum erosion wear rate around 60-75 degree; it could have been of semi brittle nature. This behavior is due to incorporation of eggshell particles. At low angle the erosion is lower because the ductile failure is prominent at low angle. The opposite behavior is due to fact that material property has been changed from brittle to semi brittle

Figure 4.11 (a-d) illustrates the erosion wear behaviour of composite after exposure to mineral water, kerosene, subzero temperature and saline water respectively.

Figures 4.11 (a,b and d) show similar nature of erosion behavoiur. The maximum erosion rate was observed in all three conditions at 60°, while the composite samples which were exposed to subzero temperature showed different behaviour with maximum erosion occurring at 90° as shown in figure 4.11 (c).

Another observation that can be seen in figure 4.11 (a-d) is that maximum erosion occurs at 12wt.% of boiled eggshell filler composite which is same as observed in figure 4.10. The agglomeration of eggshell microparticles could be the reason for the increase in erosion rate with an increase in filler content for composites.

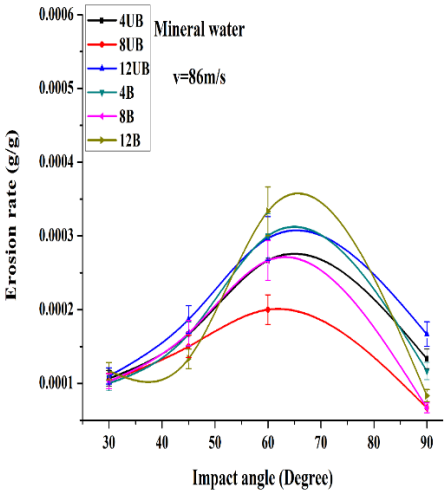

(a) mineral water

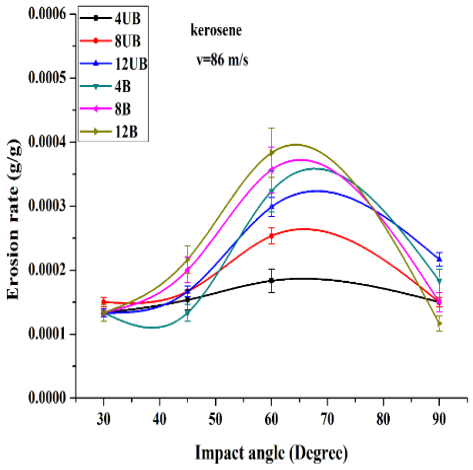

(b) kerosene

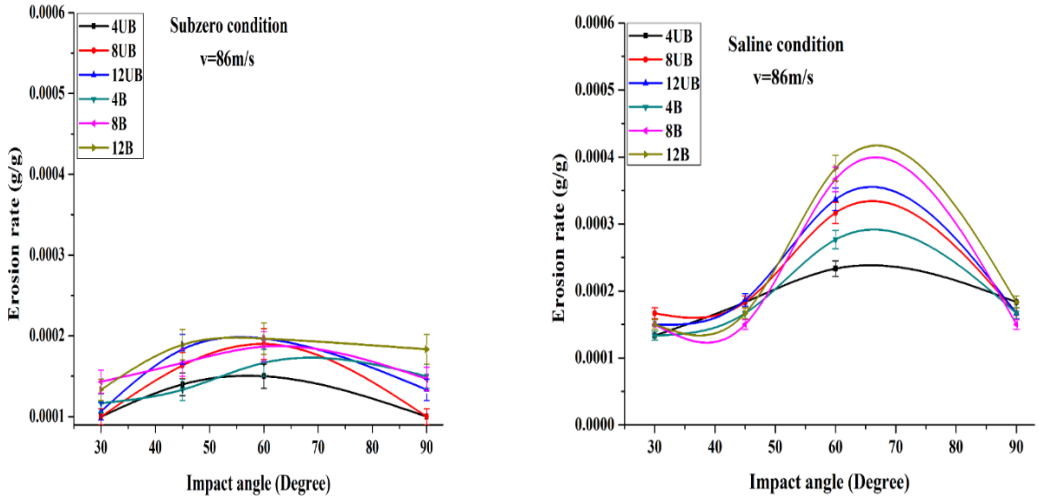

(c) subzero temperature (d) saline water

Figure 4.11 erosion wear for eggshell epoxy composite after exposure to (a) mineral water (b) kerosene (c) subzero temperature (d) saline water.

Figure 4.12 shows the erosion wear behavior of 4wt.% unboiled and boiled eggshells filler epoxy composites under dry condition. Figure 4.12 illustrates that the wear rate of boiled eggshells filler composite is higher than the unboiled eggshells filler composite. One other observation can be made from figure 4.12 is that the increase in impact velocity results in deterioration of erosion resistance.

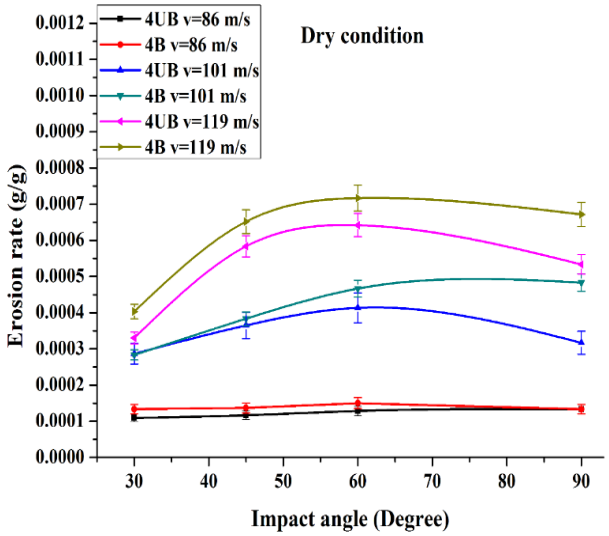

Figure 4.12 Erosion wear for 4wt.% boiled and unboiled eggshell epoxy composite in dry condition at different impact velocity(86 m/s, 101 m/s, 119 m/s).

Variation of erosion wear rate with impact velocity and comparative analysis between 4wt.% unboiled and boiled eggshell filler composites after exposure to different environmental condition is shown in figure 4.13. From figure 4.13 it can be clearly observed the for every environmental condition the increase in impact velocity results in increased erosion rate increment; the boiled eggshell filled composite shows less wear resistance compared to unboiled eggshells epoxy composite as is evident from figure 4.12; this may be due to more moisture absorption by boiled eggshell filler composite through pore formation during the heating of eggshells.

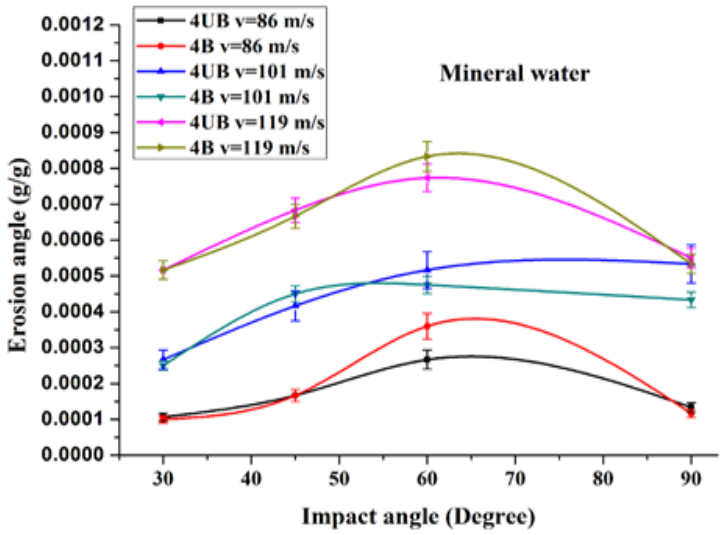

(a) mineral water

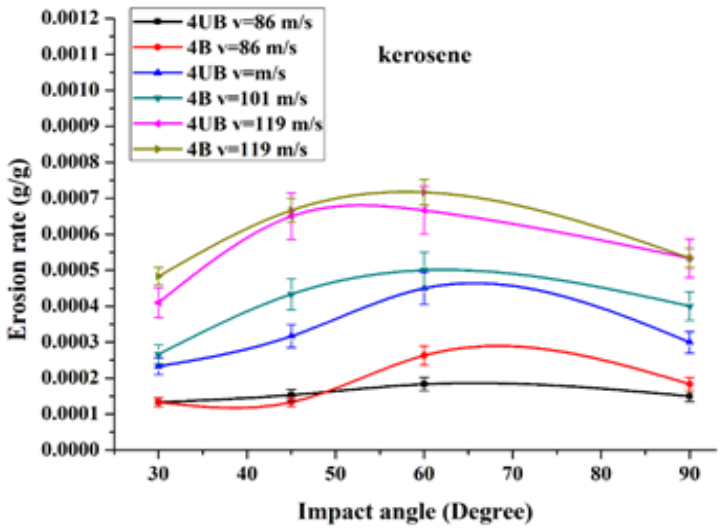

(b) kerosene

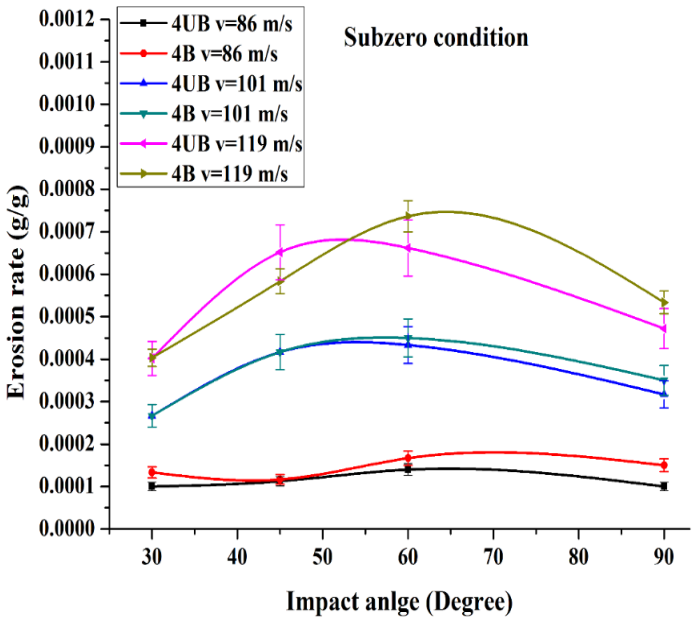

(c) subzero temperature

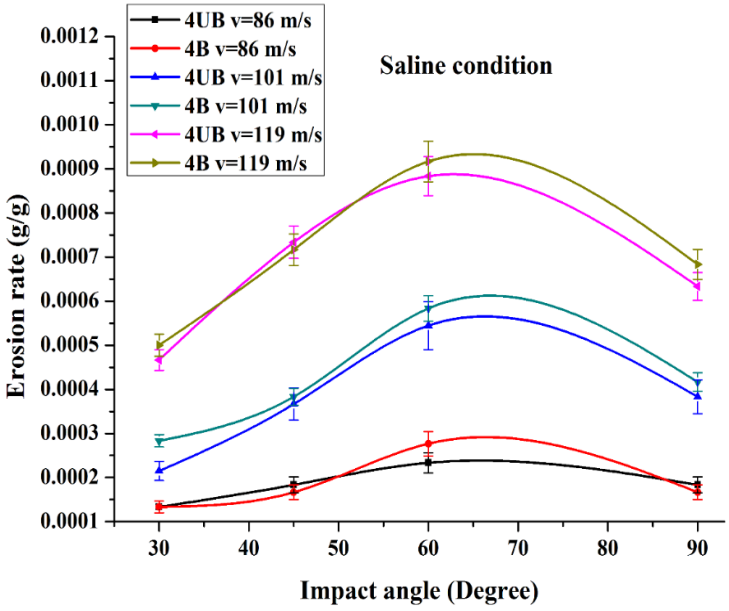

(d) saline water.

Figure 4.13 Erosion wear for 4wt.% boiled and unboiled eggshell epoxy composite after exposure to (a) mineral water (b) kerosene (c) subzero temperature (d) saline water at different impact velocity(86 m/s, 101 m/s, 119 m/s).

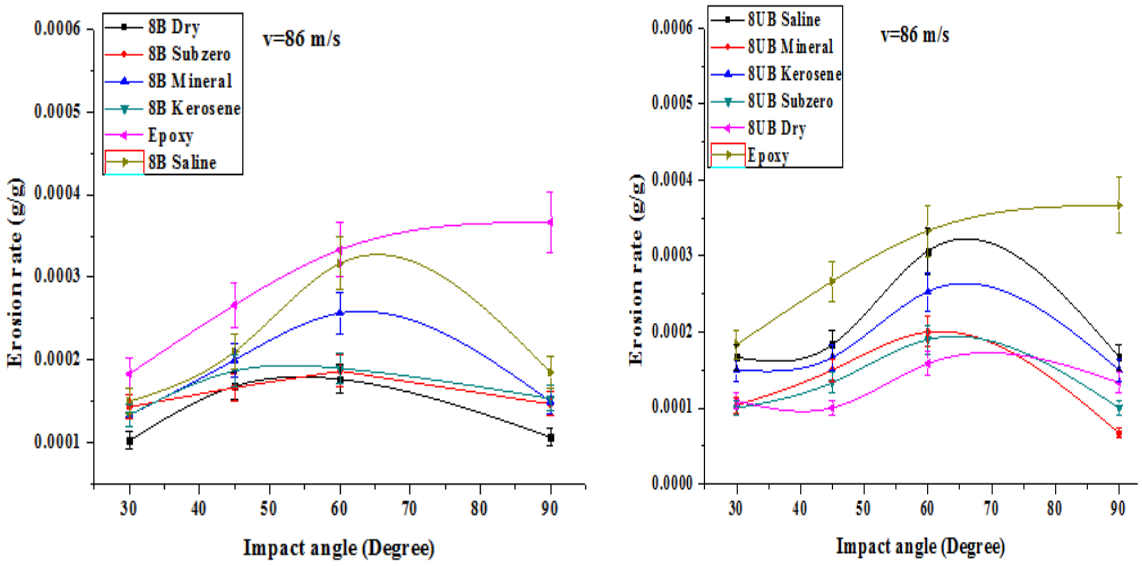

4.14 (a) 4.14 (b)

Figure 4.14 Erosion wear for (a) 8wt.% boiled and (b) 8wt.% unboiled eggshell epoxy composite after exposure to different environments.

Figure 4.14 showed that the wear rate of composite is least in dry condition while it increased when exposed to saline, mineral, kerosene and subzero condition. Moisture may be the reason that composite for saline condition shows the highest wear rate when compared to other environmental conditions.

From both the test (moisture absorption test and erosion wear test) it was observed that unboiled eggshell particulate epoxy composite gives better results compared boiled eggshell epoxy composite, therefore unboiled eggshell nanoparticles were further used for fabrication of nanocomposites and their environmental, tribological and mechanical properties were tested.

4.5.2 Nano unboiled eggshell-epoxy composite

4.5.2.1 Moisture absorption test

Figures 4.15 (a)-(c) show the weight gain due to moisture uptake by eggshell nanoparticulate (1wt.%, 2wt.%, 3wt.%, and 4 wt.%) reinforced epoxy composites in different environments (saline water, Mineral water, moist soil). It is noticed from figures 4 (a)-(c) that, as the particulate filler addition increases, moisture absorption increases. Figures 4 (a)-(b) reveal that, significant absorption is observed for mineral water and saline water, during the initial days and then it becomes stagnant. From figure 4 (c) it is recognized, that water

absorption keeps on increasing in the moist soil environment, which may be due to the presence of minerals in moist soil; which are adsorbed by eggshell particles.

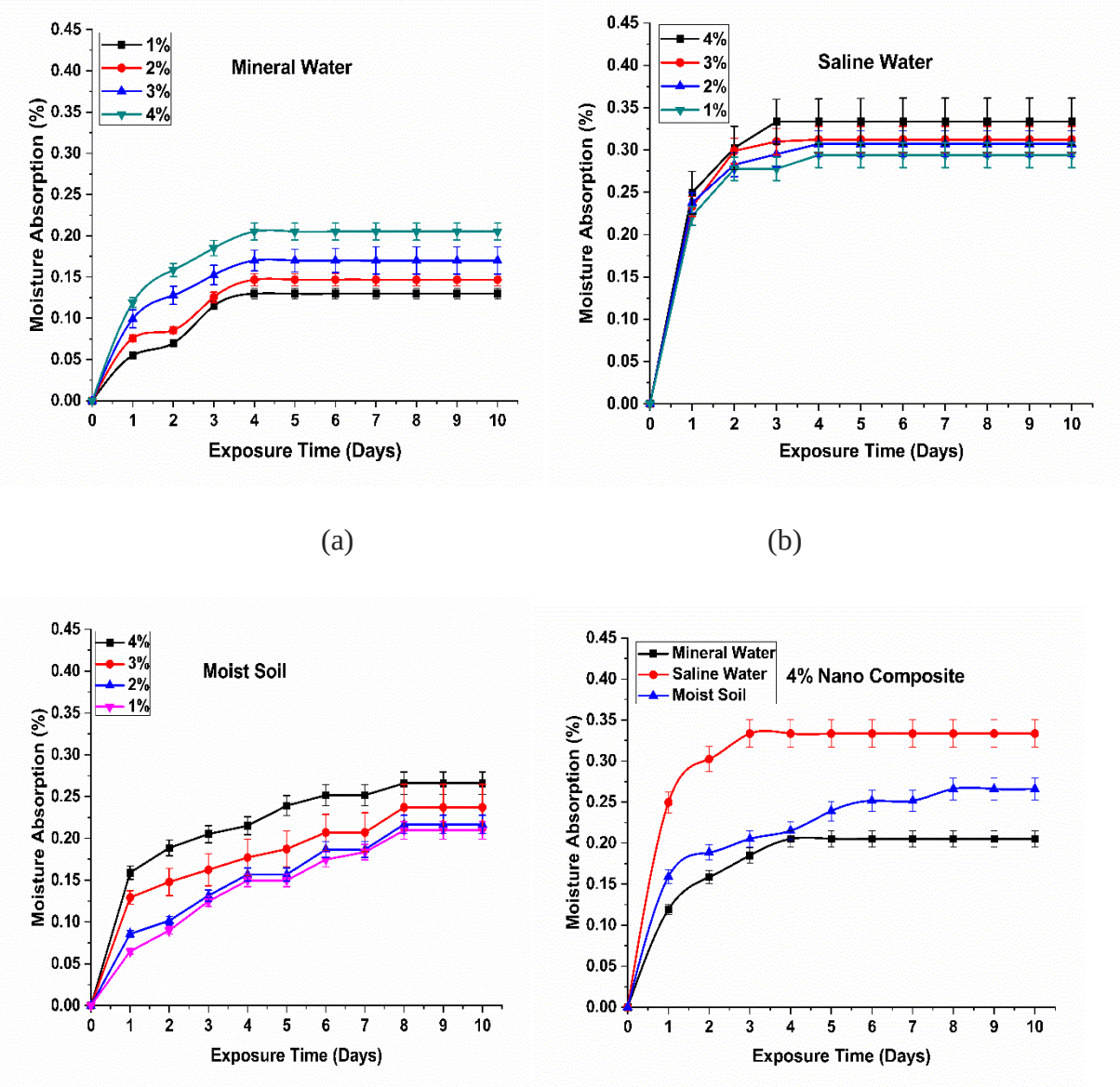

Fig. 4.15 Moisture Absorption of eggshell nanoparticulate epoxy composite under different environments

Figure 4 (d) illustrates moisture absorption in different environments for 4wt.% eggshell nanoparticulate epoxy composites. From a comparison of moisture absorption in different environments, it is observed that moisture absorption is higher in salt water compared to other environmental conditions i.e. mineral water and moist soil, owing to the existence of amines and carboxylic functional group in eggshell particles. It is noticed that there is a significant increase in moisture absorption with the incorporation of eggshell nanoparticles, which may be

due to an increase in the percentage of eggshell particles incorporated. Compared to results for moisture absorption analysis of micro composite; nano composites are very much active during initial days, which may be due to the reactive nature of nanoparticles. The nano composites saturated within 4 days which was not the case in micro composites.

4.5.2.2 Erosion test

Figure 4.16 shows the variation of erosion rate with the impact angle of nano composite at an impact velocity of 101 m/s for various percentages of eggshell nanoparticulate epoxy composite. From figure 4.16, it is noticed that the erosion resistance of eggshells epoxy is far better than that of epoxy irrespective of percentage of nanoparticulate addition. This may be due to the presence of $CaCO_3$, as observed in XRD analysis may be the reason behind astounding enhancement in erosion wear resistance, a similar observation was made by Yilmaz, M. G et al. [178] for erosion wear behavior of $CaCO_3$/ glass fiber polyester composites.

One further observation is that the maximum erosion rate is found at 60º impact angle depicts showing semi brittle behavior of nano composite same was observed in case micro composites. 2wt.% nano eggshell particulate composite shows maximum erosion wear resistance. Further increase in particulate addition resulted in decrease in erosion resistance. This may be due to proper distribution of particles in epoxy and the bonding between epoxy and eggshells nanoparticles which may be inferred from SEM image shown in figure 4.18.

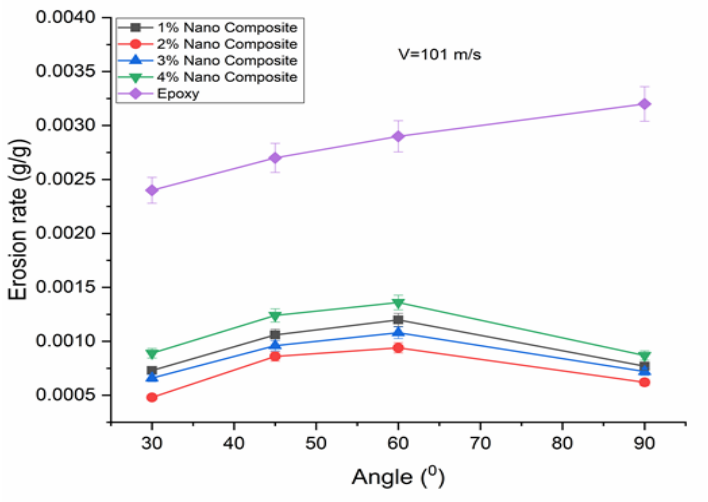

Figure 4.16. Erosion rate for different percentage of eggshell nanoparticulate epoxy composite at V=101 m/s.

The reason behind improved erosion resistance is attributed to particle size, which is very minute compared to erodent particle size. Another important observation one can notice is that

for the same area of interest, the number of particles resisting the impact is more when compared with microparticles.

From figure 4.17 show variation of erosion wear rate with change in sand velocity. it is apparent from figure 4.17 that as the impact velocity increases erosion resistance decreases.

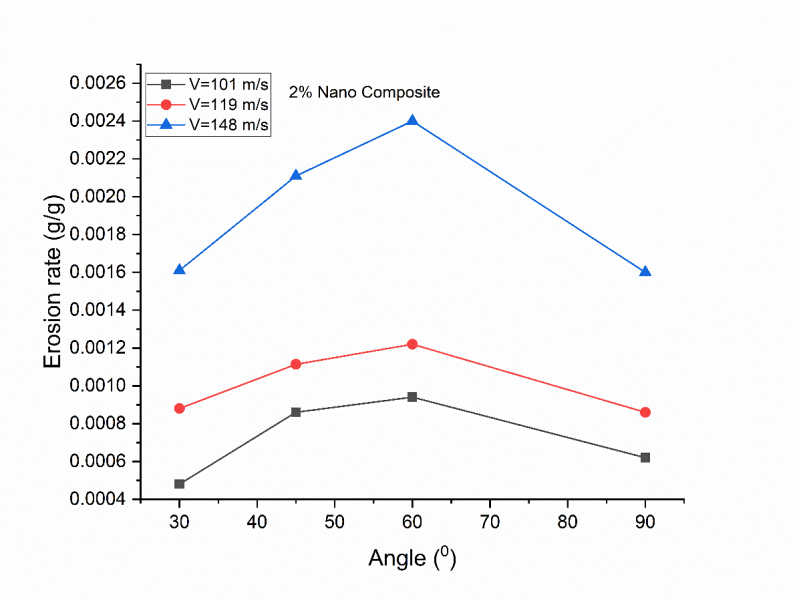

Figure 4.17. Erosion wear rate of 2wt.% eggshell nanoparticulate composite at different velocities.

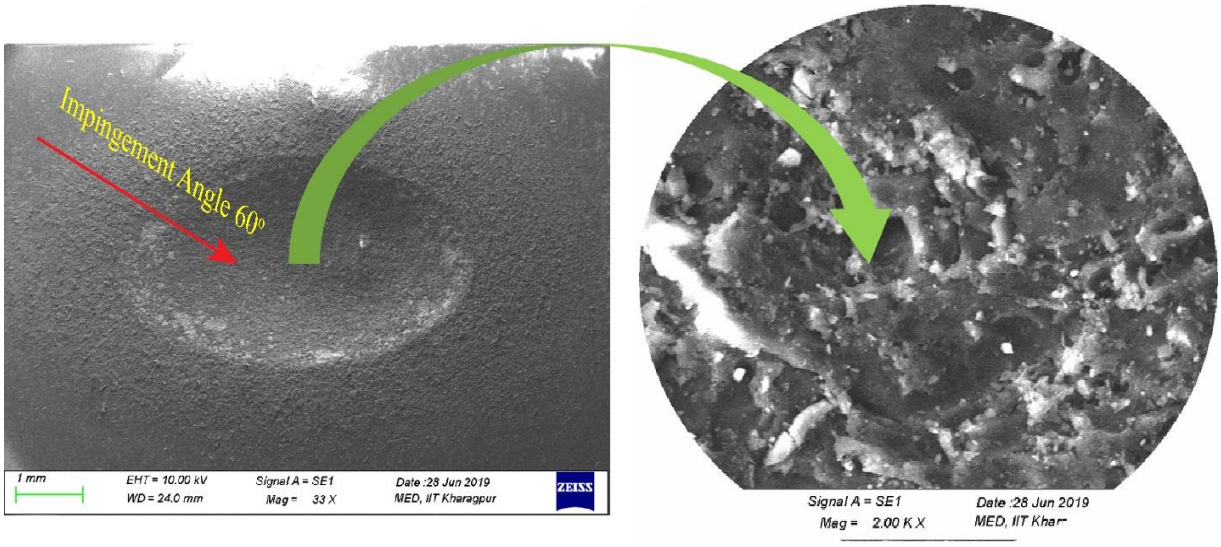

Figure 4.18 Eroded surface of 2wt.% eggshells nanoparticulate epoxy composite at 60º impact angle

The SEM image shown in figure 4.20 for 4wt.% nanoparticulate eggshells epoxy composite shows the sites of agglomeration, which hampers erosion resistance.

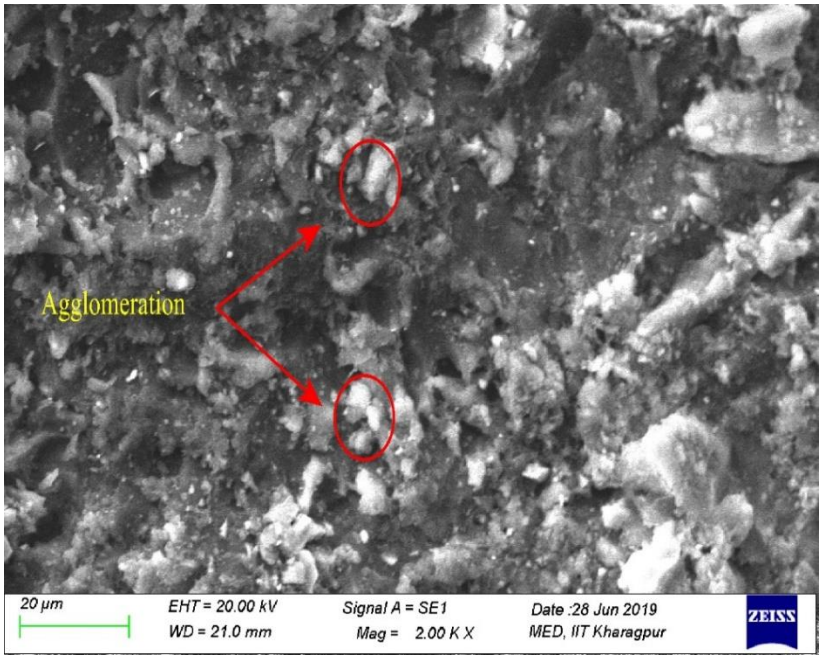

Figure 4.19 Eroded surface of 4wt.% eggshells nanoparticulate epoxy composite at 60º impact angle

Figure 4.20 shows the variation of wear rate in the different environment for 2wt.% nanoparticulate epoxy composites. It is evident from figure 4.20 that erosion wear is highest for sample, which were put in saline water compared to other environments (mineral water and moist soil). same observation was made in case of micro composites. The least erosion wear rate was found in case of dry samples.

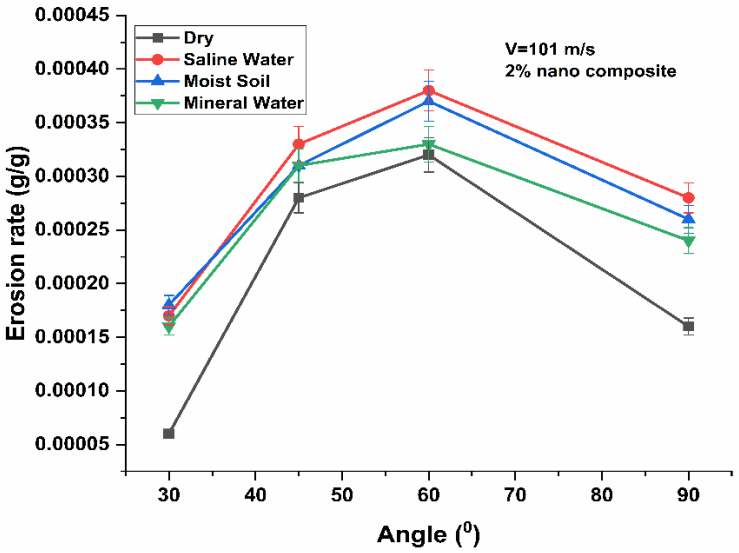

Figure 4.20 Erosion wear rate of 2wt.% eggshell nanoparticulate composite after exposure in different environments

4.5.2.3 Tensile Test

The stress strain curve of eggshell nanoparticulate epoxy composites for the tensile test is shown in figure 4.21. Figure 4.21 shows that there is an elastic zone followed by total fracture of the sample which indicates brittle failure of sample. Figure 4.21 shows that tensile strength improves with the eggshell nanoparticulate addition.

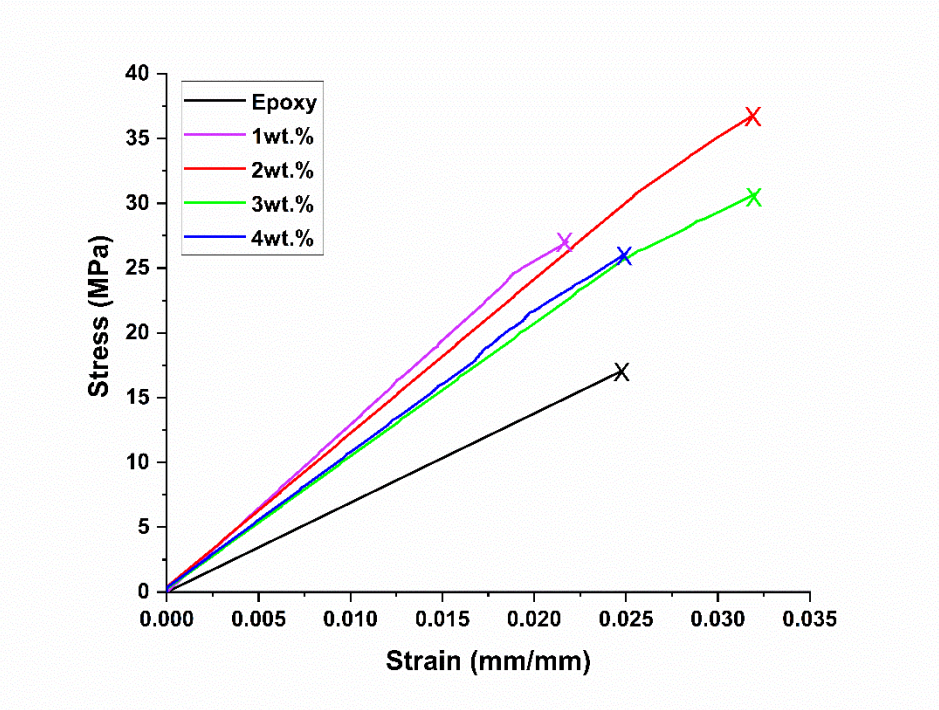

Figure 4.21 Stress-Strain curve for uniaxial tensile test

Figure 4.22 shows that the tensile strength increased to 27 MPa with 1wt.% eggshell nanoparticulate concentration as compared to bare epoxy, which has a tensile strength of 17MPa. Further increase in eggshell nanoparticulate concentration up to 2wt.% resulted in the improvement of tensile strength. For 2wt.% concentration of eggshell nanoparticles in eggshell nanoparticulate epoxy biocomposite, tensile strength was enhanced by 117% compared to bare epoxy. However, with further increase particulate addition, tensile strength was found to decrease when compared to 2wt.% of particulate addition, although the tensile strength was still more than bare epoxy. Positive enhancement in tensile strength may be due to the incorporation of high stiffness nanoparticles than the matrix material. The addition of high moduli nanoparticles could have enhanced the yield limit of matrix material under tensile loading as reported in the literature [156,161,179]. The bonding also plays a significant role in the enhancement of the mechanical properties of nanocomposites. The presence of amine group and organic protein [112] as observed in FTIR analysis of eggshell nanoparticles, ensure good

chemical bonding with the epoxy resin, a similar kind of observation was by G. Ji et al. [51] for interaction between the epoxy resin and eggshell microparticles. The physical bonding between matrix material and nanoparticles depends on various parameters such as particle size, particle shape, surface area, etc. [180,181]. In this case, the shape of the particles is irregular which helps in adhesion between the particles and epoxy resin. As nanoparticles have a high surface area which turns results in more area of contact between polymer matrix and nanoparticles. The good physical bonding ensures effective load transfer between matrix and between matrix and fillers. The reduction in tensile strength after 2wt.% of nanoparticle incorporation may be due to an excess amount of filler addition which leads to agglomeration. The agglomeration reduces the surface area as particles are joined together and behave as microparticles.

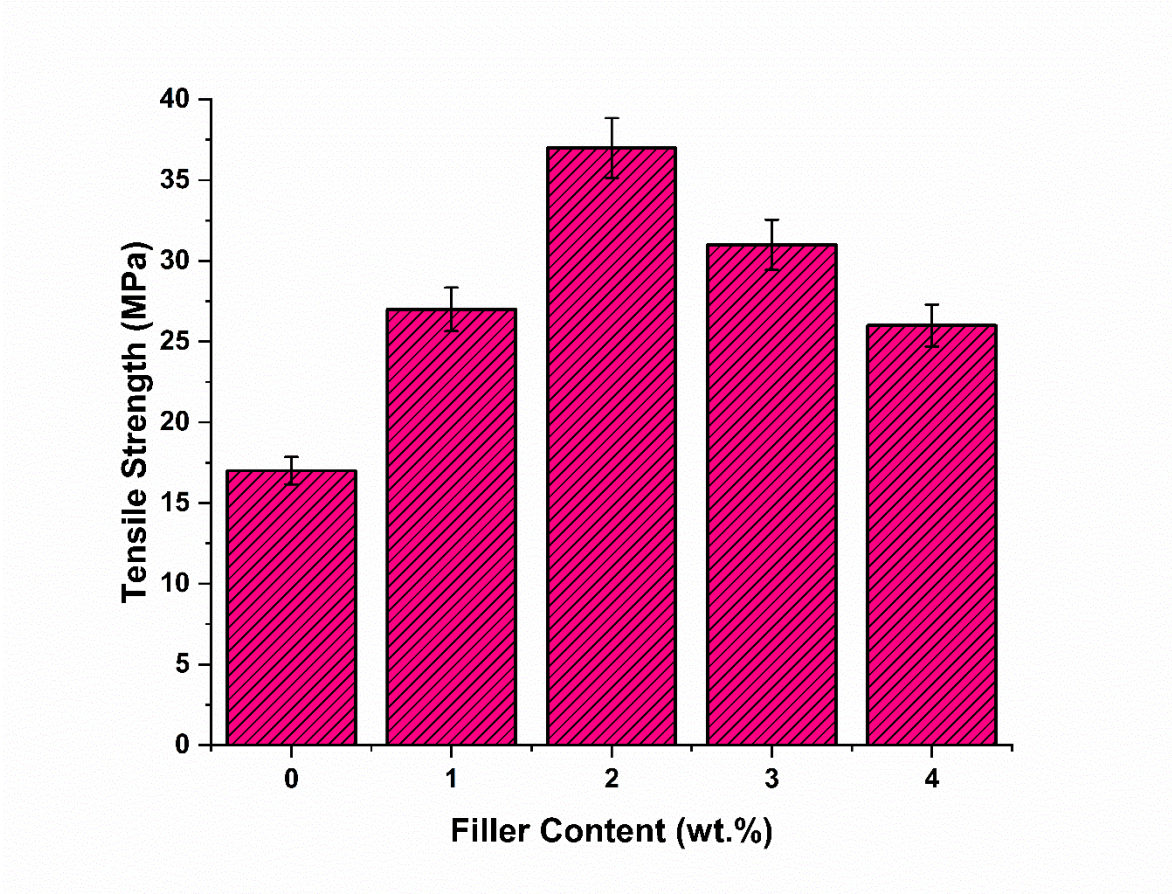

Figure 4.22 Variation of tensile strength with filler content.

From figure 4.21 it is evident that the slope of the curve decreases from 1wt.% to 3wt %, eggshell particles concentration in epoxy but again increased for 4wt.% nanoparticulate incorporation. The slope was highest for the 1wt.% particulate nanoparticulate addition which indicates that the tensile modulus was highest for the 1wt.% particulate nanoparticulate

addition. Variation of tensile modulus can be observed from figure 4.23. The tensile modulus of bare epoxy increased from 0.59 GPa to 1.28 GPa.

Figure 4.23 demonstrates that tensile modulus was reduced to 1.144 GPa for 2wt.% of nanoparticulate addition. Further increase in the eggshell nanoparticle incorporation resulted in decreased tensile modulus. The increase in tensile modulus owing to the presence of eggshell nanoparticles, which has a very high tensile modulus (47.4 to 53 GPa) [48]. Tensile modulus is also affected by particle size it increases suddenly for particle size below a certain critical value (30nm) [180]. As in this case particle size is below 20nm the positive change in tensile strength was observed, the tensile modulus was almost doubled with the addition of eggshell nanoparticles, a similar study was reported elsewhere for $CaCO_3$/PP composites [183].It is noted from figure 4.24 that the load bearing capacity for 2wt. % eggshell concentration in epoxy is highest followed by 3wt.% and 4wt.% respectively. Of all the concentrations, 1wt.% had the lowest load carrying capacity. In this graph linearity was also observed at the beginning. The results revealed that eggshell nanoparticle addition increases tensile strength and tensile modulus. 2wt.% particulate addition found to be optimum for tensile strength while the tensile modulus was maximum for 1wt.% nanoparticulate addition.

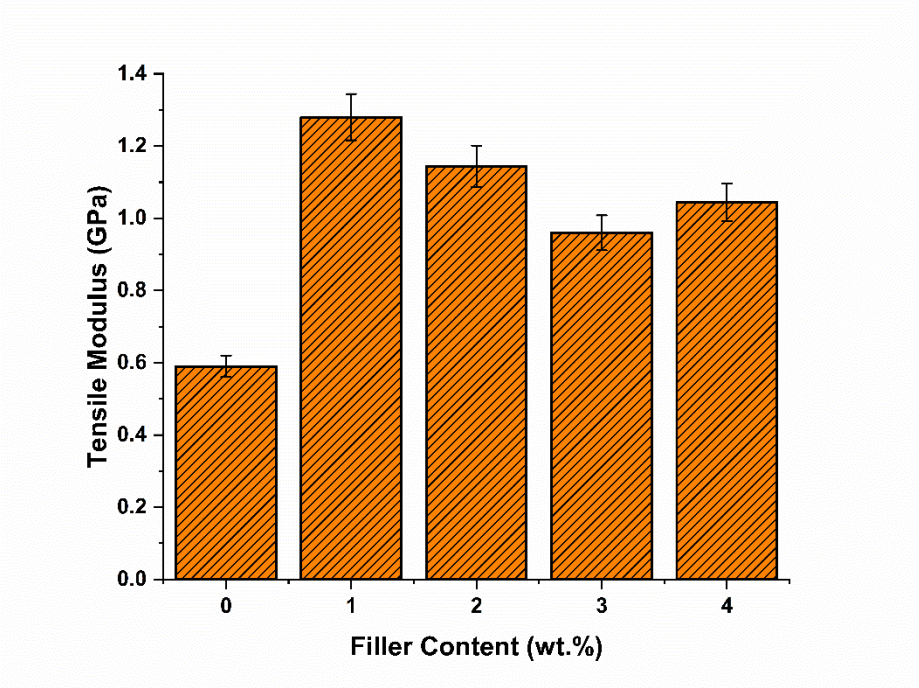

Figure 4.23 Variation of tensile modulus with filler content.

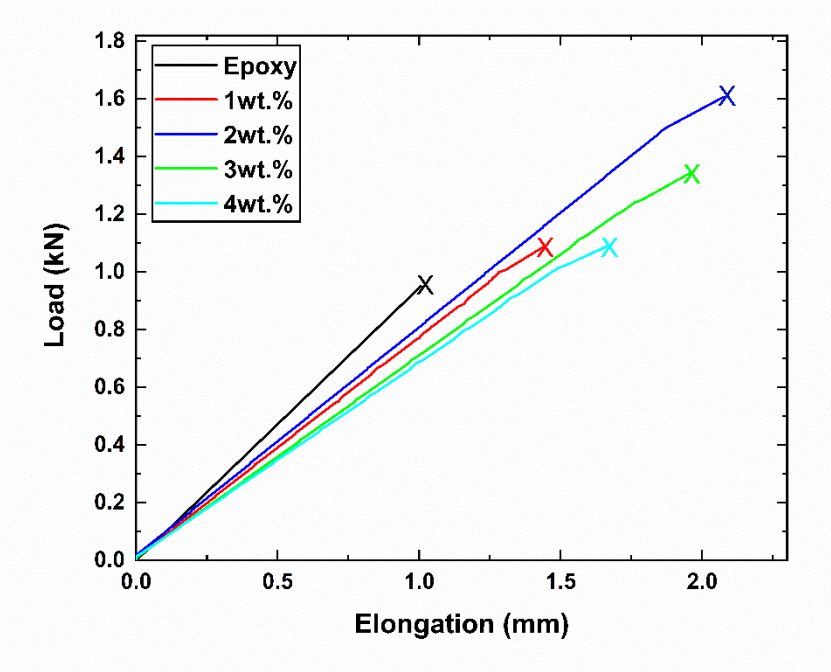

Figure 4.24 load vs elongation curve for uniaxial tensile test

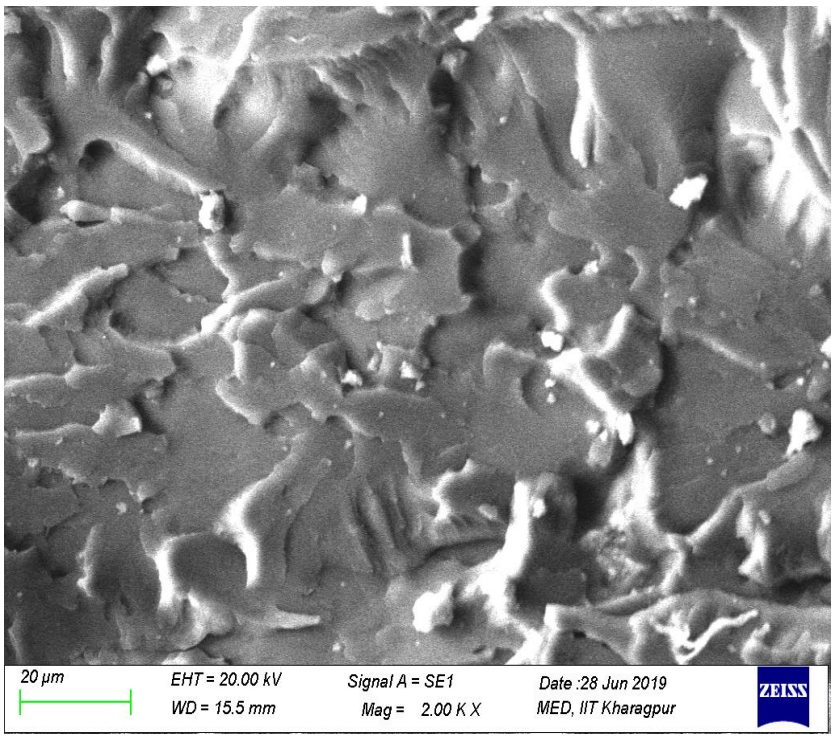

Figure 4.25 Fractured surface of 2wt.% eggshell particulate epoxy composite tensile sample

The fractured surface of 2wt.% eggshell particulate epoxy sample can be seen from SEM image shown in figure 4.25. The SEM image 4.25 shows a brittle failure, the fractured surface shows minor cracks. The cracks are coming out of the surface during crack propagation

suggesting inhibition of crack propagation by nanoparticles thereby enhancing the load-bearing capacity and tensile strength of composites.

4.5.2.4 Three-point bending test

The stress-strain curve of the eggshell epoxy composites for three-point bending test is shown in figure 4.26. It is noticed from figure 4.26 that with eggshell nanoparticulate addition, flexural strength increases just like tensile strength. It was observed from figure 4.27 that flexural strength increased from 41.6 MPa to 49.73 for 1wt.% eggshell particulate inclusion. Further addition of eggshell nanoparticulate resulted in an increased flexural modulus up to 3wt. %, and then there was a decrease in flexural strength.

The maximum flexural strength was found for 3wt.% nanoparticulate addition. The flexural strength increased from 41.6 MPa to 67.1 MPa for 3wt.% eggshell particulate inclusion. One other observation here is that for 2wt.% and 3wt.% nanoparticulate addition, the flexural strength was almost same; although the flexural modulus was maximum for 2wt.% nanoparticulate addition. The flexural strength of 3% concentration of eggshell epoxy was highest followed by 2wt.% and 1wt.% respectively. It is noted from the bar graph in figure 4.28 that the flexural modulus is notably higher for 2wt.% eggshell concentration in epoxy followed by 4wt.% and 1wt.% respectively; flexural modulus is lowest for 3wt.% eggshell concentration in epoxy.

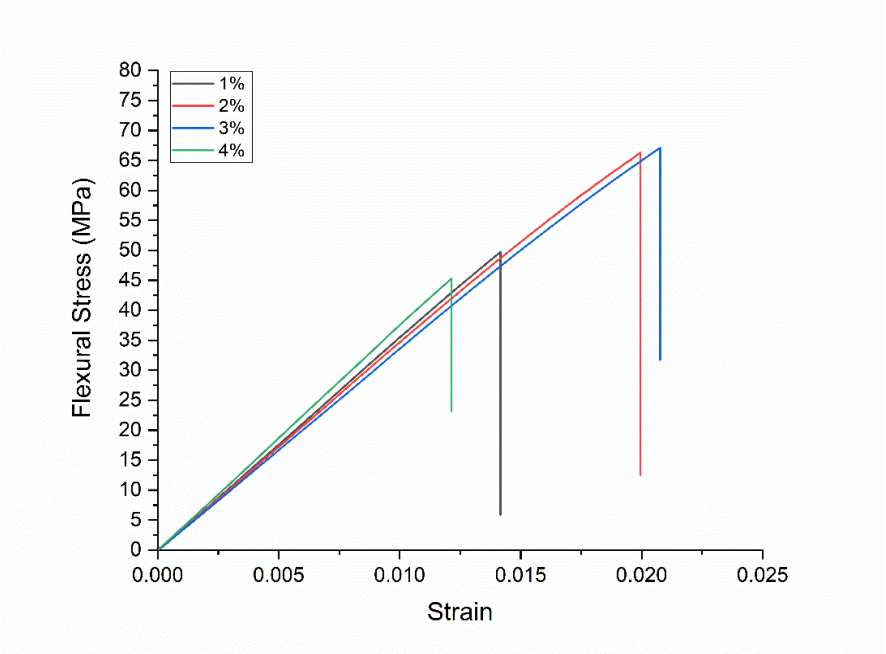

Figure 4.26 Stress- Strain curve for three-point bending test

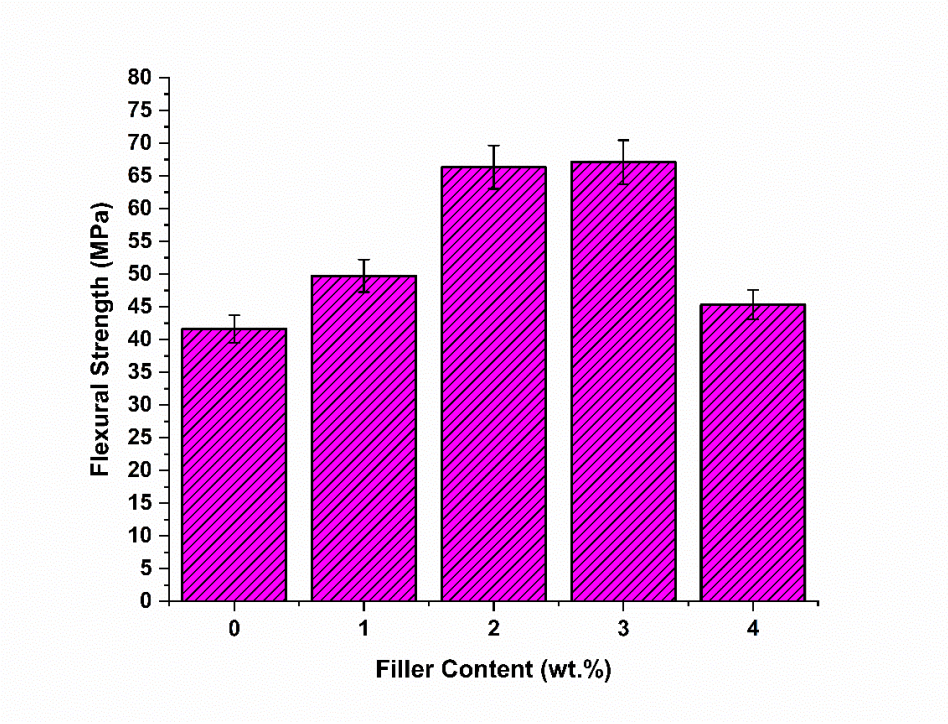

Figure 4.27 Variation of flexural strength with filler content

The load deflection curve shown in figure 4.29 shows that the deflection is highest for 3wt.% eggshell particulate epoxy, which can be appreciated from the fact that 3wt.% eggshell particulate epoxy has highest flexural strength.

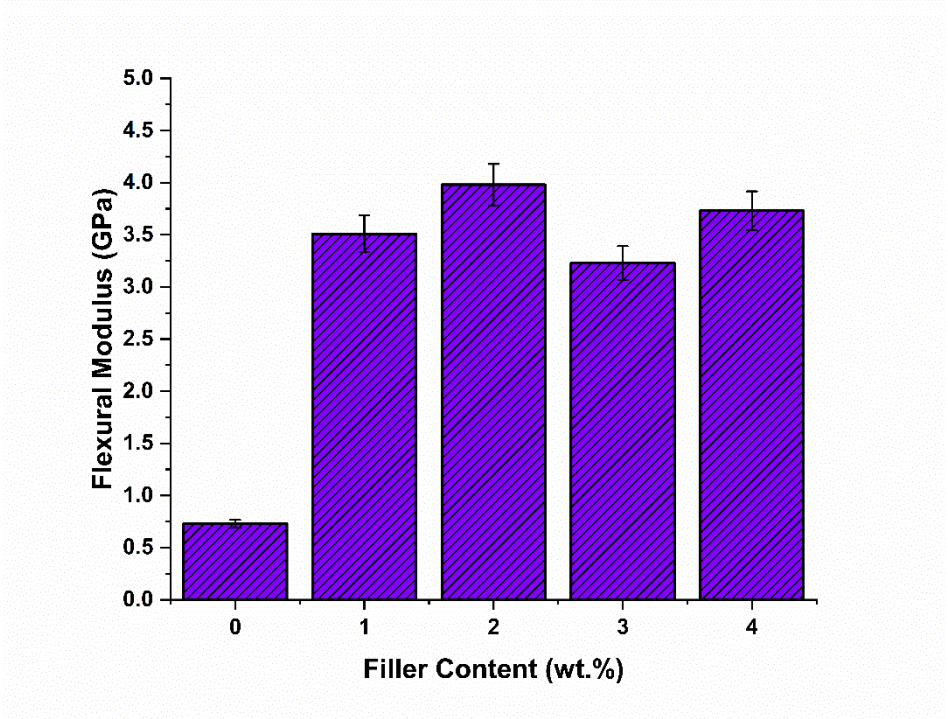

Figure 4.28 Variation of flexural Modulus with filler content

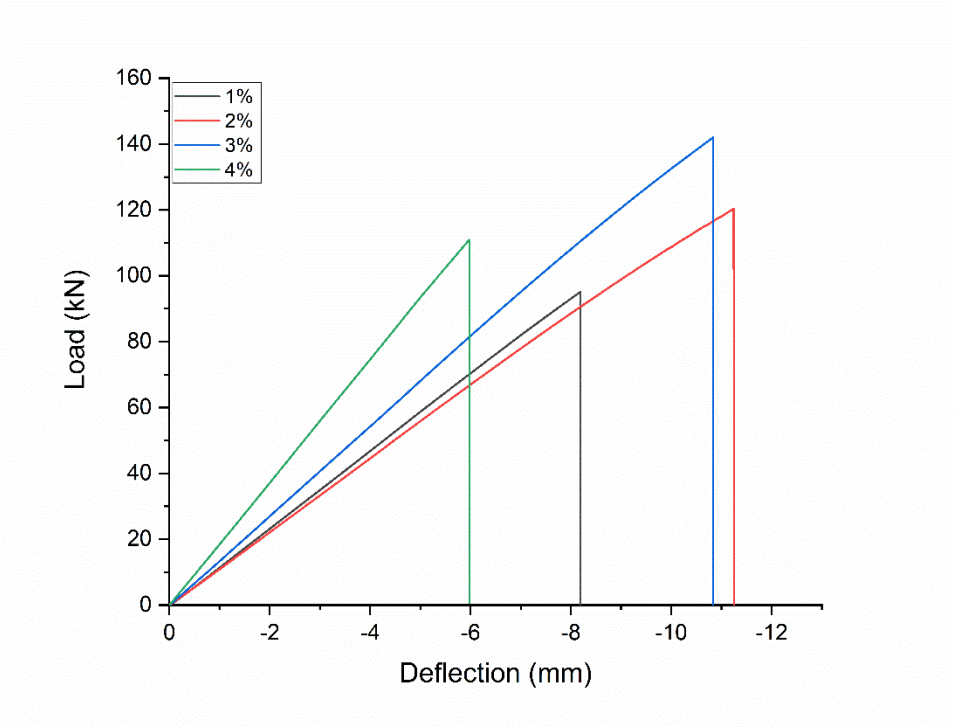

Figure 4.29 load vs Deflection curve for three-point bending test

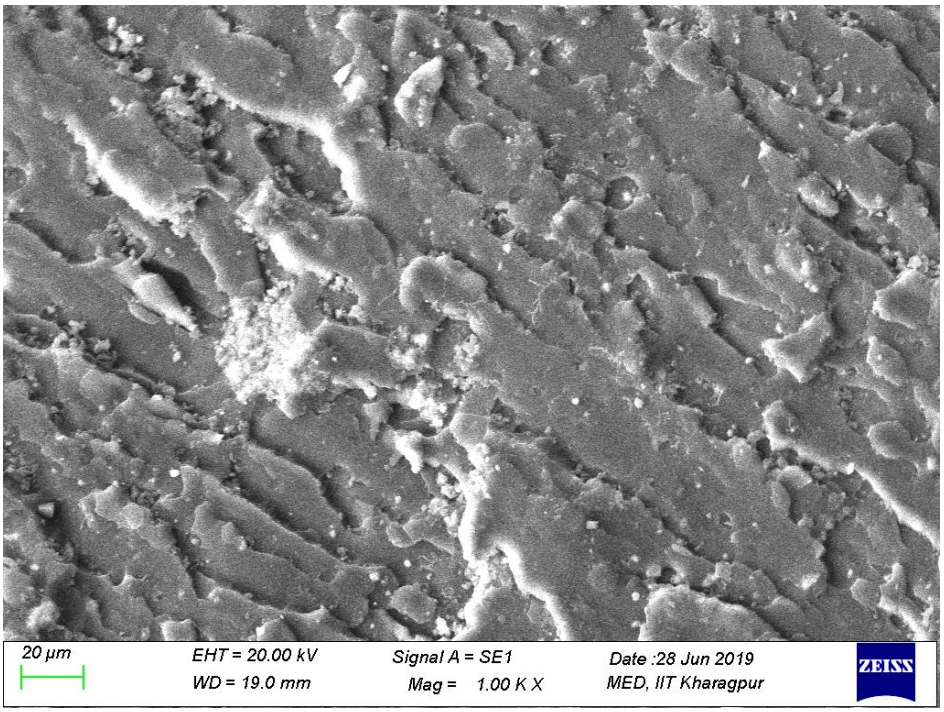

Figure 4.30 Fractured surface of 3wt.% eggshell particulate epoxy composite sample flexural test

The fractured surface can be seen from SEM image of fracture surface for flexural test of 3wt. % eggshell particulate epoxy composite sample shown in figure 4.30. it is inferred from SEM

image in figure, there a are number of blowholes, which might be generated from branching out of particles during the application of load. Eggshell nanoparticles may be a reason behind the restriction of crack propagation thereby enhancing the flexural strength.

4.5.2.5 Micro hardness test

The bar graph for micro hardness is shown in figure 4.31. The hardness of epoxy was found to increase with the addition of eggshell nanoparticles. With 1wt.% of eggshell nanoparticles addition the hardness value increased to 18.4 which compared to bare epoxy is almost double; this has a hardness value of 9.4. Further increase in eggshell nanoparticles increases hardness value. The maximum hardness value was found for 2wt.% of eggshell nanoparticles. The hardness value of epoxy is increased by 127% with addition of 2wt.% of eggshells nanoparticles. It was noted from figure 4.31 that for nanoparticulate addition 3wt.% the hardness value decreased compared maximum value; however, it is still higher than bare epoxy. For nanoparticulate addition of 4wt.%, hardness value further decreased compared to maximum value. It was observed that 2wt.% of nanoparticulate addition provide the best result for hardness.

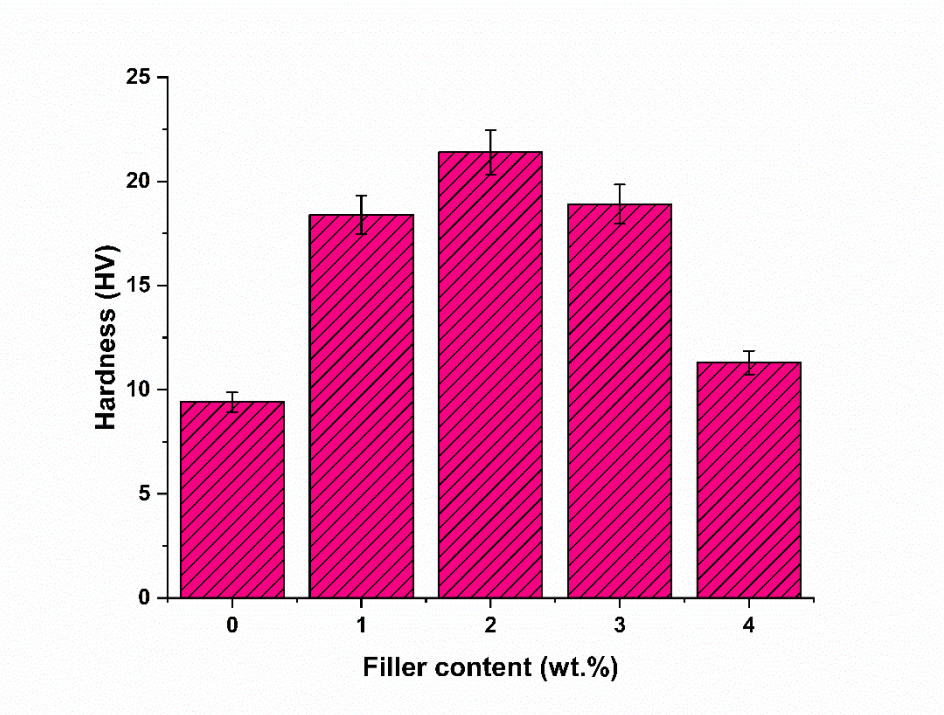

Figure 4.31 Variation of hardness with filler content

4.6 Conclusions

The following conclusions may be drawn based from the study

1. Exposure to different environmental conditions had a negative effect on erosion resistance. The erosion rate was maximum for composite samples exposed to saline environment.
2. Least erosion rate was observed in dry condition and subzero condtion. The erosion rate for composite samples exposed to subzero temperature was almost equal to erosion rates for the composite in dry condition.
3. In comparison between mositure absorption results of unboiled eggshell microparticulate composite and boiled eggshell microparticulate composite, the unboiled eggshell microparticulate composite has a lesser moisture absorption.
4. The incorporation of eggshell filler increases the wear resistance compared to pure epoxy.
5. In comparasion of erosion rate of unboiled eggshell composite to boiled eggshell epoxy composite, the composite samples with unboiled eggshell fillers showed better wear resistance than boiled eggshell filler composites. However, the addition of filler content by more than 4wt% of unboiled eggshells increases the wear rate.
6. The inclusion of eggshell nanoparticles has a positive influence on mechanical properties. The eggshells nanoparticle addition enhanced tensile strength and tensile modulus. 2wt.% particulate addition was observed to be optimum for tensile strength. the tensile strength was increased by 117%. Tensile modulus was enhanced by 116% with 1wt.% particulate nanoparticulate addition.
7. The flexural strength and modulus also increased owing to the addition of eggshell nanoparticles. The flexural strength was enhanced by 61% while flexural modulus was multiplied by more than four times owing to eggshell nanoparticles incorporation.
8. 3wt.% nanoparticulate addition was found to be optimum for flexural strength while flexural modulus was maximum for 2wt.% particulate nanoparticulate addition.
9. The hardness value improved by incorporation of eggshell nanoparticles. The 2wt.% particulate addition was observed to be optimum for enhancement of hardness value. The hardness value was increased by 117% with 2wt.% particulate addition.

10. The addition of nanoparticles results in a drastic increase in erosion resistance; the erosion resistance of eggshells nanoparticulate composite has far better erosion resistance compared to bare epoxy.
11. The maximum erosion wear rate was observed at 60º of impact angle, which showed that the erosion behavior of eggshell nanoparticulate composite was semi brittle. The maximum erosion resistance was observed for 2wt.% nanoparticulate addition. The erosion wear rate was decreased by 68%.

Chapter 5

Environmental, and tribological properties of activated carbon epoxy composite

5.1 Introduction

Activated carbons have a wide variety of applications as already described in chapter 2. There are some examples in literature, where activated carbon was used in composite applications. There are a number of fillers used to enhance erosion wear resistance of polymer composite as described in chapter 4. However, these fillers are costly and are an environmental hazard. Carbon is one of those materials which have the ability to greatly increase erosion resistance. Here we have used activated carbon in epoxy resin to enhance the erosion wear behavior of composite in different environments (Saline water, mineral water, Moist soil). To do this moisture absorption test was performed and then erosion test was performed on those samples.

5.2 Raw Materials

Raw materials used for the preparation of activated carbon particulate reinforced epoxy polymer composite material are given below

1. Activated Carbon.
2. Epoxy resin.
3. Hardener.

5.2.1 Activated Carbon

Activated carbon used for composite fabrication was derived from biowaste using the method described in the chapter 3 article 3.3.3.

5.2.2 Epoxy Resin and hardener

Resin and hardener properties have already been described in the chapter 4 article 4.2.2.

5.3 Composite Preparation

Nanocomposites with 1, 2, and 3 weight fraction of activated carbon particulate addition were made using the method described in the chapter 4 article 4.3. Composite samples are shown in figure 5.1.

Figure 5.1 Composite samples

5.4 Characterization of composite

5.4.1 Moisture absorption test

The amount of moisture soaked up by composites in different environmental conditions (Mineral water, Saline water, Moist soil) was calculated from the formula as described in the chapter 4 equation 4.1.

5.4.2 Erosion Test

The erosion wear tests of activated carbon epoxy composite were carried out on the erosion test rig described in the chapter 4 article 4.4.2. The schematic diagram of the erosion test rig is shown in Fig.4.1. Parameters for erosion test are given in the table 4.2. The erosion test was conducted for 15 mins as in the case of eggshell nanocomposite. The reading was taken every 5 mins to see the variation in erosion rate with depth. The total erosion rate for 15 mins was calculated using the formula given in article 4.4.2.

5.4.3 Hardness test

The hardness test was conducted as described in the chapter 4 article 4.4.5.

5.5 Results and discussion

5.5.1 Moisture absorption test

Figures 5.2 (a)-(c) show the weight gain due to the moisture absorbed by activated carbon (1wt.%, 2wt.%, and 3wt.%) particulate reinforced epoxy composites in different

environments (saline water, Mineral water, moist soil). It is evident from figures 5 (a)-(c) that, as the particulate filler addition increases, moisture absorption increases.

Figures 5 (a)-(b) reveal that significant absorption is observed for mineral water and saline water, during the initial days and then it becomes stagnant. From figure 5 (c) it is noticed that water absorption keeps on increasing in the moist soil environment, which may be due to the presence of minerals in moist soil, which are adsorbed by activated carbon particles. Figure 5.3 illustrates moisture absorption in different environments for 3wt.% activated carbon composites. From a comparison of moisture absorption in different environments, it is observed that moisture absorption is more in saline water, compared to other environmental conditions i.e. normal water and moist soil. The presence of many functional groups in activated carbon such as amines, amides and carboxylic groups which are observed in FTIR analysis of activated carbon in chapter 3 article 3.4.2.3. Activated carbon is more reactive in salt water, resulting in a higher amount of moisture absorption. From the figure it is evident that 3wt.% activated carbon filled composite showed the maximum weight gain in saline water condition and as the filler content is increasing, we can see there is a significant increase in moisture absorption and the same was observed by H.Almari et.al [184] This may be due to an increase in the percentage of activated carbon incorporated.

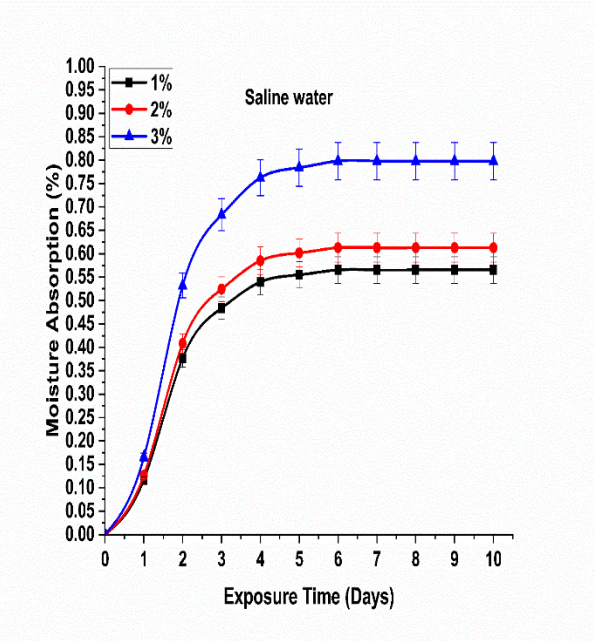

(a)

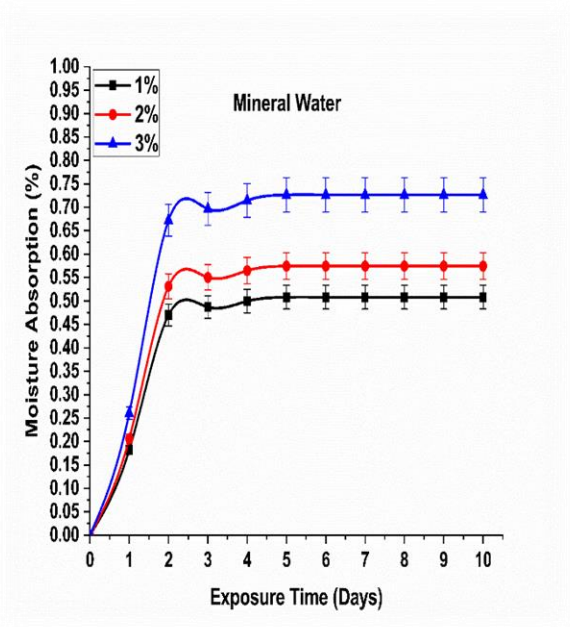

(b)

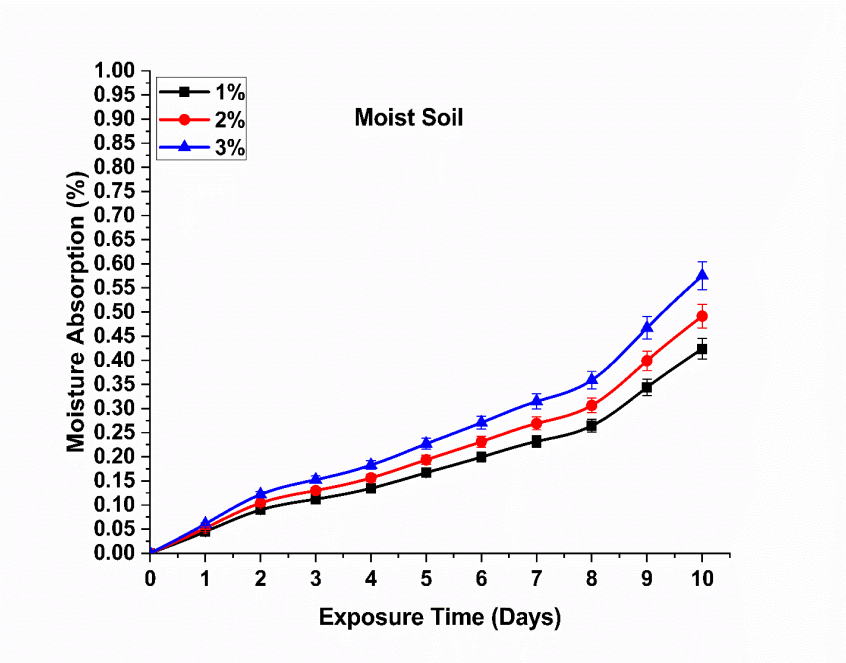

Figure 5.2 Moisture absorption in different environments (a) Saline water (b) mineral water (c) moist soil

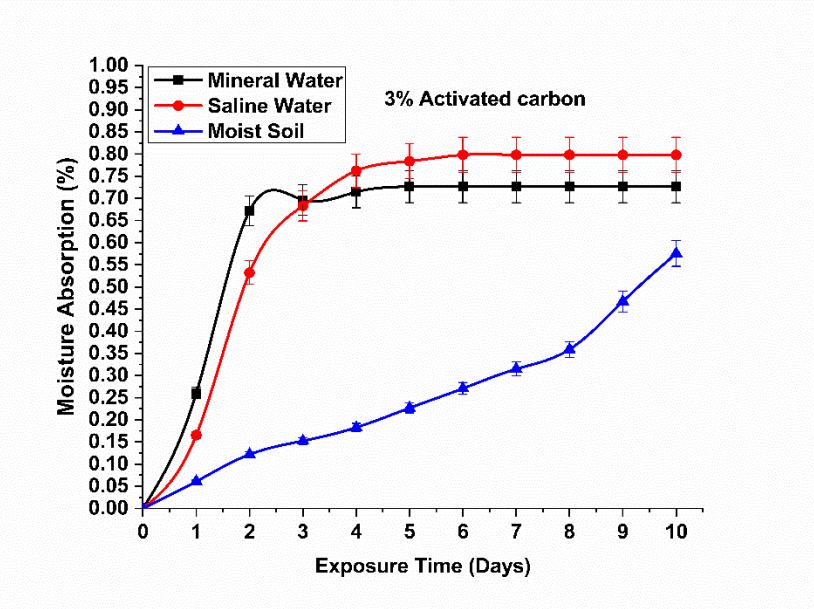

Figure 5.3 Moisture absorption in different environments for 3wt.% activated carbon composites

5.5.2 Erosion test

Figure 5.4 shows the variation of erosion rate with the impact angle at an impact velocity of 101 m/s. It is observed that the erosion resistance of nanocomposite is quite higher than bare

epoxy. 2wt.% activated carbon particulate composite shows maximum erosion wear resistance. Further increase in particulate addition resulted in a decrease in erosion resistance.

From figure 5.4 it is noticeable that the maximum erosion rate is found at 45º impact angle, which exhibits the semi ductile behavior of composite, this may be due to the presence of graphite in activated carbon, which provide the shear effect. Another important observation one can appreciate is that the surface area of a particle is very high as observed in the BET analysis (chapter 3 article 3.4.2.6), which results a greater number of sites for interfacial adhesion. Moreover, the presence of the amine functional group was observed in the FTIR analysis of activated carbon, as described in chapter 3 article 3.4.2.3. improves the interfacial bonding between activated carbon and epoxy polymer.

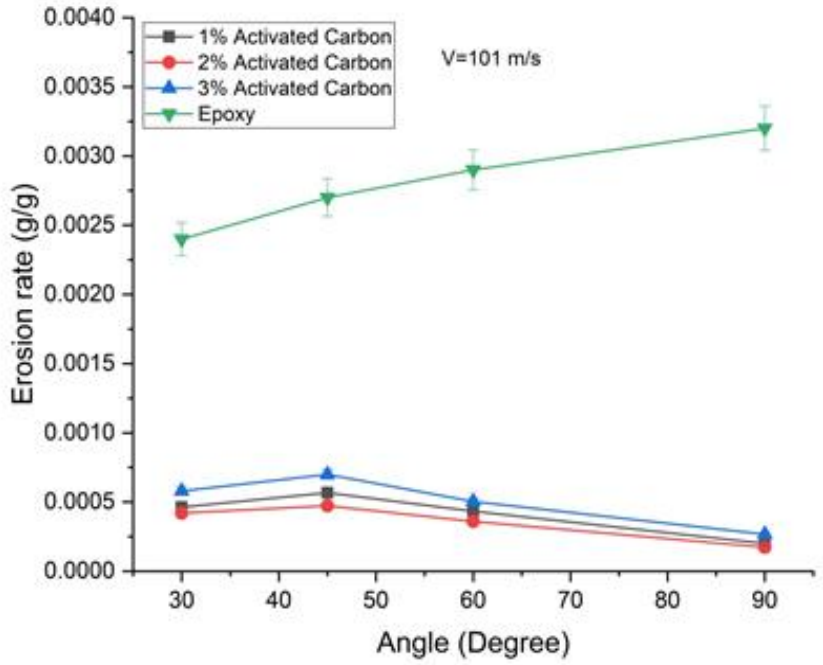

Figure 5.4. Erosion rate for different percentage of activated carbon particulate epoxy composite at V=101 m/s

Distribution of activated carbon particles in epoxy resin and the bonding between epoxy and activated carbon particles may be inferred from SEM image shown in figure 5.5. It is recognized from figure 5.5 that 2wt.% activated carbon epoxy composites sample has a proper distribution of activated carbon particles and good dispersion between activated carbon particles and epoxy resin. The SEM image shown in figure 5.6 shows the fractured surface of erosion wear tested sample of 3wt.% activated carbon particulate epoxy composite. Figure 5.6 shows the sites of agglomeration, which hampers erosion resistance.

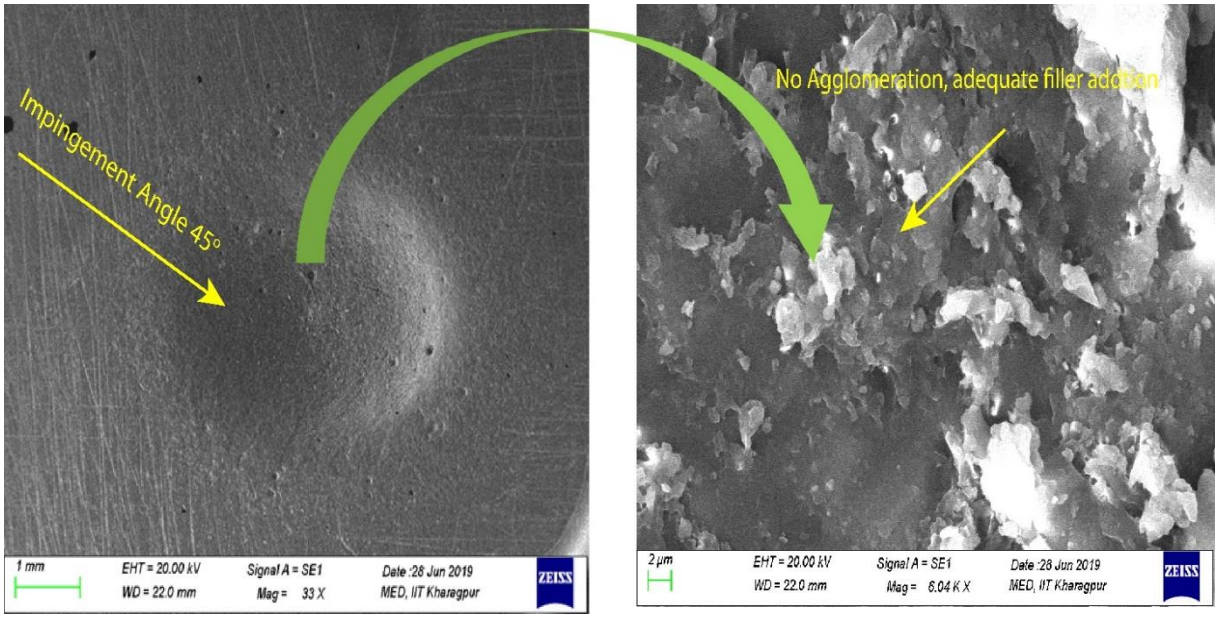

Figure 5.5 Eroded surface of 2wt.% activated carbon particulate epoxy composite at 45º impact angle

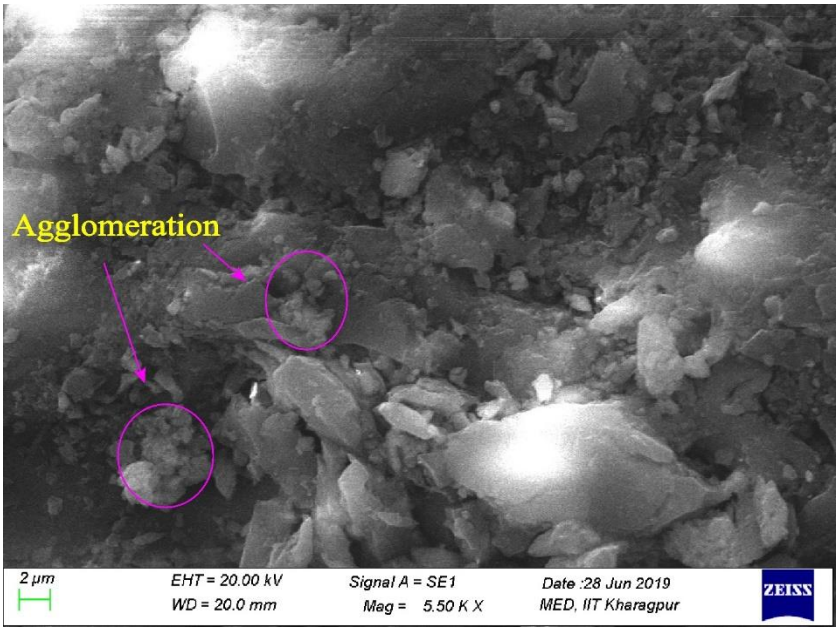

Figure 5.6 Eroded surface of 3wt.% activated carbon particulate epoxy composite at 45º impact angle

Figure 5.7 and 5.8 shows variation of erosion wear rate with velocity. It is inferred from figure 5.7 and 5.8 that as the impact velocity increases erosion resistance decreases.

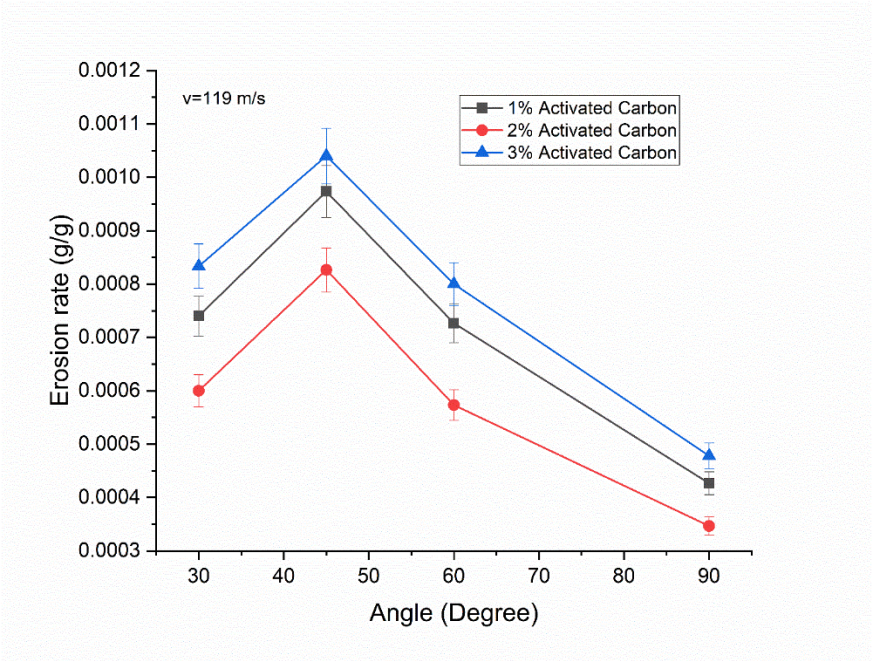

Figure 5.7 Erosion wear rate of activated carbon particulate composite at V=119 m/s

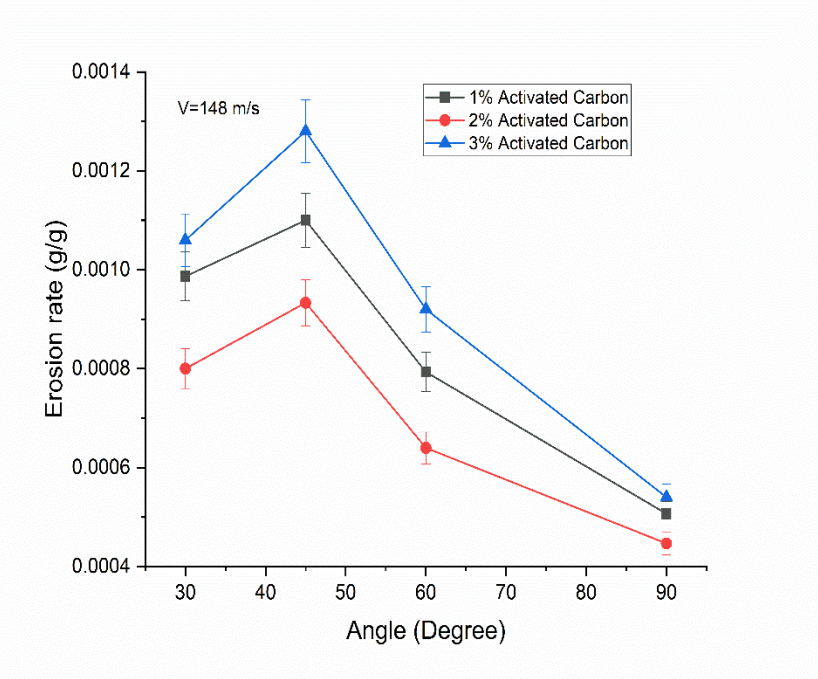

Figure 5.8 Erosion wear rate of activated carbon particulate composite at V=148 m/s

Figure 5.9 shows that erosion test was also conducted after keeping the samples in different environmental conditions (salt water, normal water and moist soil). It was found that the erosion wear is higher in case of saline water compared to other conditions. Samples immersed in saline water exhibited more wear rate than the erosion rate for samples in other

environments, this is due to saline water being corrosive in nature. When immersed in different environments mineral, saline and moist soil samples show semi ductile erosive wear behavior.

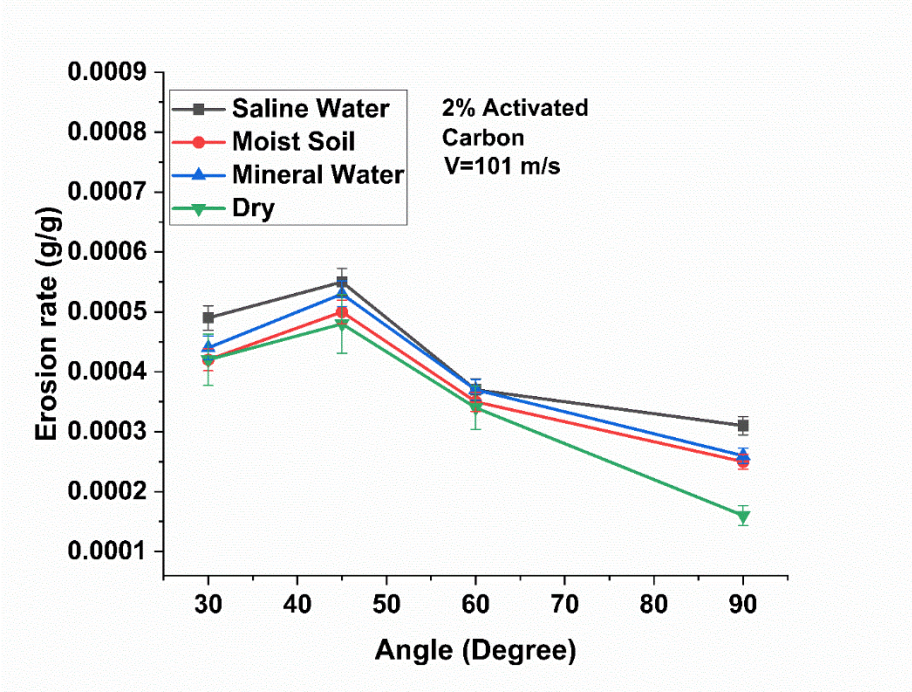

Figure 5.9 Erosion wear rate of 2wt.% activated carbon particulate composite exposed to different environments

5.5.3 Hardness test

The bar graph for micro hardness is shown in figure 5.10. Hardness value of epoxy was found to increase with the incorporation of activated carbon particles. With incorporation of 1% of activated carbon particles, hardness value increased to 12.8 from the original hardness value of 9.4. Further increase in activated carbon particles increases hardness value. The maximum value of hardness was found for 2 wt. % of activated carbon particulate addition. The hardness value of epoxy increased by 72% with the addition of 2 wt. % of activated carbon particulate addition. It may be noted from figure 5.10 that for activated carbon particulate addition of 3 wt. %, the hardness value decreased compared to the maximum value; however, it was still higher than bare epoxy. It was observed that 2 wt.% of activated carbon particulate addition provide the optimum result for hardness.

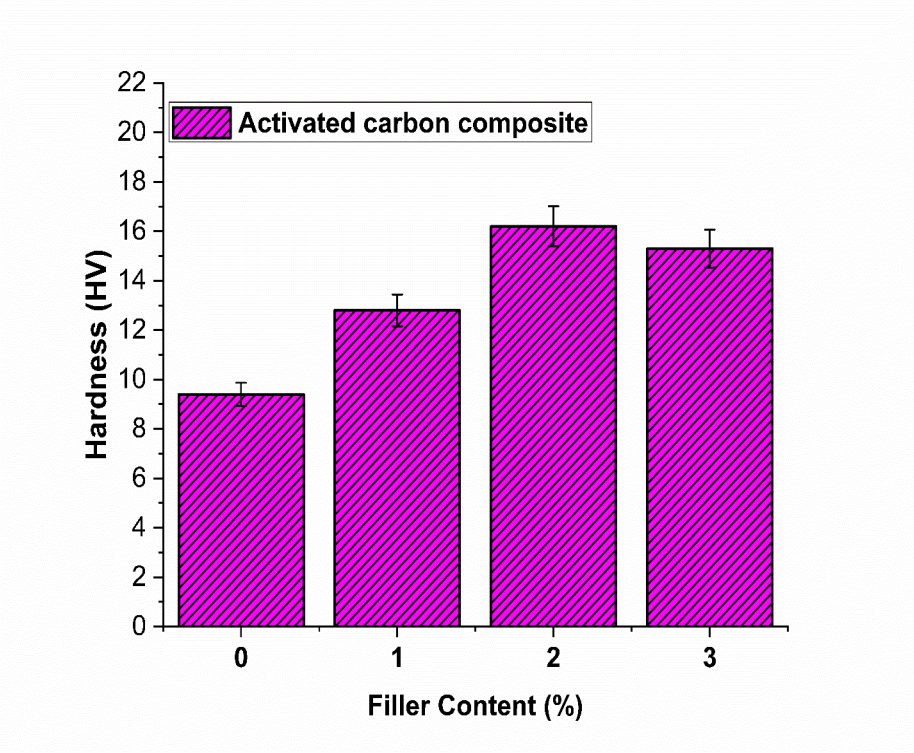

Figure 5.10 Variation of hardness with filler content of activated carbon epoxy composite

5.6 Comparison of both the composites

This section discusses the comparison between moisture absorption, erosion wear behavior and change in hardness of two composites viz. eggshell nanoparticulate epoxy composites and activated carbon epoxy composite.

5.6.1 Comparison of moisture absorption rate

when comparing moisture absorption behavior of eggshell-epoxy composite and eggshell epoxy composite in both the composites the increase in particulate addition leads to increase in moisture absorption. in the both type of composites the moisture absorption is more in saline water compared mineral water and moist soil environment. Further observation reveal that the activated carbon epoxy composites sample have more moisture absorption than the eggshell nanoparticulate epoxy composite samples. This may be due to the more number pores which leads to more absorption. These more entraps the impurities such as salts and minerals.

5.6.2 Comparison of erosion wear rate

In both the composites i.e. eggshell nanoparticulate epoxy composite and activated carbon epoxy composite the erosion resistance increases with increases particulate addition up to certain limits. Both cases the optimum weight percentage of particulate was found to be

2wt%. In comparing the erosion resistance of both the composites, the activated carbon epoxy composites provide better erosion resistance than the eggshell nanoparticulate epoxy composites. eggshell nanoparticulate epoxy composites showed semi brittle erosion wear behavior while activated carbon epoxy composites showed semi ductile erosion wear behavior.

5.6.3 Comparison of hardness

The hardness value of both the composites increases with increase particulate addition up to 2wt. %. When comparing both the composites the eggshell particulate composite provides better results compared with activated carbon epoxy composites.

5.7 Conclusions

1. 3wt.% of activated particulate reinforced epoxy composites showed the highest weight gains when exposed to different environments. Least absorption rate observed for 1wt.% activated carbon composite in normal water
2. Amount of moisture absorption was more in saline environment when compared to moist soil and normal water. This may be due to the presence of many surface functional groups, such as amines, amides in activated carbon.
3. The filler addition has a positive effect on erosion resistance, the 2wt.% particulate reinforcement was found to be the optimum percentage of reinforcement. The erosion wear rate was decreased by 82.4%
4. erosion rate was found to be highest at 45° impact angle. The analysis suggests that the activated carbon epoxy composite generally semi ductile in nature.
5. The 2wt.% filler content composite shows the highest wear resistance in dry condition. The exposure of composite in different environmental condition had a detrimental effect on erosion rate.
6. When comparing both the composites, it was found that the eggshell nanoparticulate epoxy composites provides better water absorption resistance and has more hardness than activated carbon epoxy composite, while the activated carbon epoxy composites provide better erosion wear resistance than the eggshell epoxy composites.

Chapter 6

Preparation and Characterization of silica, activated carbon, eggshell nanoparticulate ceramic composite

6.1 Introduction

There are a number of pollutants, which adversely affect water purity such as heavy metals, organic dyes, chemicals, agricultural waste, etc., which originate from industries, residential area and from agricultural runoff. A number of methods are used for waste water treatment as described in chapter 1. Using nano materials and composites for water purification is one technique and use of nanomaterials for water treatment is mentioned in literature. nanoparticles of noble metals such as Ag, Au, Pd, Pt, etc. [185] are found to be useful for water treatment; however, these nanomaterials are very costly and production of these nanoparticles is tedious. Some other nanomaterials such as TiO_2 nanoparticles, Graphene Oxide nanosheets, carbon nanotubes etc. are also used for water treatment. Besides nanomaterials, composites have also been used for water treatment.

Jahanshahi, M.et al.[186] prepared a thin film composite membrane through interfacial polymerization between piperazine (PIP) with trimesoylchloride (TMC) for nanofiltration.

Xu, Chao, et al.[187] studied dye adsorption capacities of graphene oxide- TiO2 composite films. Bao, Q et al.[188] synthesized silver nanoparticulate- graphene oxide composite films and characterized them for bacterial activity of bacteria such as Escherichia coli and Staphylococcus aureus.

Taha, Ahmed A. et al. [189] fabricated cellulose acetate (CA)/silica composite membranes sol-gel technique and tested adsorption capacity for removal of Chromium ion.

Baojun Li et al. [190] investigated the adsorption capacity of ZnO/graphene composite for removal of rhodamine B (RhB) dye. the dye removal capacity was also compared with ZnO and graphene particles. It was observed that composite displays improved performance for adsorption of rhodamine B (RhB) dye.

Upadhyay, R. K et al. [191]presented a review of water treatment capabilities of graphene/metal oxide composites as a photocatalyst, adsorbent and disinfectant.

Tesh, S. J., & Scott, T. B [192]comprehensively reviewed water remediation capabilities of nanocomposites.

Much of the previous work involves using either costly nanoparticles or nano composites which are difficult to produce. Here we have prepared a novel silica-activated

carbon-eggshell nano particulate composite pellet to be used in conjunction with chitosan pellet for dye removal.

6.2 Raw materials

Table 6.1 shows the list of raw materials used for fabrication of composite.

Table 6.1 List of raw materials used

S. No.	Material	Role	Provider
1	Fused silica powder (SiO_2)	Ceramic Powder	M/S Ants Ceramics Pvt Ltd, Thane- India
2	Methacrylamide CH_2-C(CH_3) $CONH_2$	Monomer	Sigma Aldrich Chemicals-Germany
3	N N'-Methabisacrylamide (MBAM) ($C_7H_{10}N_2O_2$)	Cross linker	Sigma Aldrich Chemicals, Germany
4	Darvan 821A	Dispersant	Vanderbilt Minerals LLC-USA
5	Polyethelene glycol 400 (PEG-400)	Surfactant	Sigma Aldrich Chemicals-Germany
6	Tetramethylethylenediamine-(TEMED) $C_6H_{16}N_2$	Catalyst	Sigma Aldrich Chemicals-Germany
7	Ammonium persulfate (APS) $H_8N_2O_8S_2$	Initiator	Alfa Aesar- USA
8	Activated Carbon	Filler	Prepared as per method described in chapter 3
9	Eggshell nanoparticles	Filler	Prepared as per method described in chapter 3

6.3 Composite preparation

Composite was prepared using the gel-casting method. Fused silica was used as base material, while eggshell nanoparticles and activated carbon particles acted as filler material. The process flow chart for the preparation of composite filter specimen is shown in figure 6.1.

For a solid loading of 48 wt.% of silica powder the amount of water and silica required for the process was calculated.

A fixed amount of water was taken in a 100 ml beaker and continuously stirred on a magnetic plate heater. Then dispersant-Darvan 821A (1 wt.% of MAM+MBAM), PEG, monomer (10 wt.% of SiO_2) and ceramic powder was added to water respectively. After stirring for some time, once the silica powder is totally dispersed; 10 wt.% of activated carbon and 10 wt.% of eggshell nanoparticles were added to the solution. The solution was stirred on a magnetic heating plate for seven hours. After that, some drops of APS and TEMED were added to slurry initiate the reaction. Once, TEMED was added to slurry, it began to solidify and become gel; then this semi solid slurry was poured into glass molds of required shape. After casting was done, the green molds were dried in an oven for 12 hrs. at a temperature of 50 ºC-60 ºC. Later the molds were heated in a furnace for binder burnout and sintering. The binder burnout was carried out in a horizontal tube furnace at a temperature of 650 ºC for 1 hour. The sintering was done by keeping the green body at a temperature of 1250 ºC for 1 hour. The prepared composite samples are shown in figure 6.2.

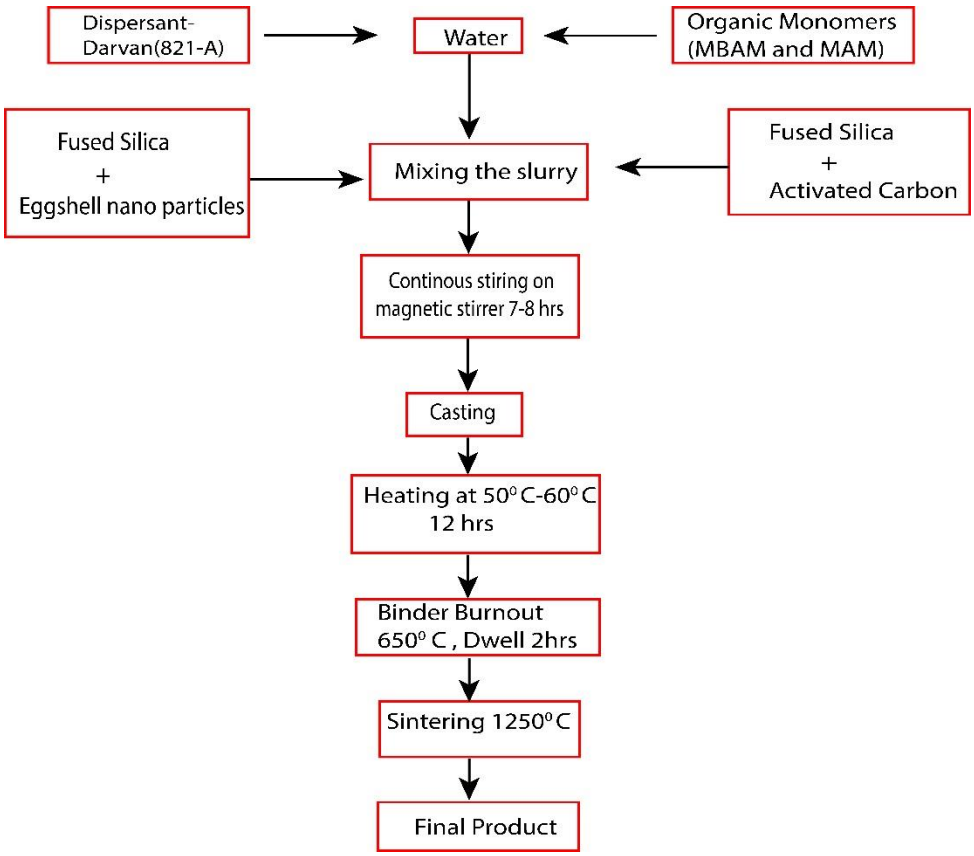

Figure 6.1 Flow chart of method of preparation of silica-activated carbon-eggshell nanoparticulate composite sample.

(a) (b)

(c)

Figure 6.2 Composite samples of (a) Silica (b) Silica-activated carbon composite (c) Silica-activated carbon-eggshell nanoparticulate composite

6.4 Preparation of chitosan pellet

Chitosan pellet was prepared using compression molding. Polyvinyl alcohol (PVA) was used as a binding material. Polyvinyl alcohol solution prepared from 4 grams of PVA in 100 grams of water. Chitosan powder was mixed with PVA solution and then compression molded. the green pellets then taken out and sintered in a horizontal tube furnace at temperature of 150ºC. Figure 6.3. shows the prepared chitosan pellet.

Figure 6.3 Chitosan pellet

6.5 Methods

6.5.1 X-ray diffraction

The quantification of compound present in composite samples were characterized with Malvern X-pert Pro X-ray diffraction machine. Samples were scanned with 2θ angle which varies from 6^{o}-60^{o} with a step size of 0.008 degrees per second.

6.5.2 SEM-EDX analysis

Textural analysis composite sample and chitosan pellet was carried out on Vega 3 Tescan scanning electron microscope. EDX analysis of composite sample was also carried out with SEM analysis for identification of the element present on the surface.

6.5.3 UV-vis Spectroscopy

Composite sample (silica-activated-eggshell nanoparticulate composite) and chitosan pellet were used in combination for adsorption of methylene blue dye. Dye adsorption capacity for adsorption of methylene blue dye of composite sample (silica-activated-eggshell nanoparticulate composite) used along with chitosan was tested using the dye adsorption test. The dye adsorption test was conducted using Beckman DU640 UV/Vis spectrophotometer as described in chapter 3. 100 ml of dye solution was prepared with various initial concentrations (500 mg/L-900mg/L) of methylene blue dye. A composite pellet and a chitosan pellet were put in 100ml solution in a beaker. The solution was then stirred at 200 rpm for 5 hours to attain equilibrium.

Adsorption capacity of composite sample used along with chitosan was calculated using equation 3.8 and Langmuir and Freundlich isotherms were calculated using equation 3.10 and 3.11.

6.5.4 Total dissolved solid content and pH

The TDS analysis was carried out using a portable TDS meter shown in figure 6.4.

Figure 6.4 Portable TDS meter

6.6 Results and discussion

6.6.1 XRD analysis

Figure 6.5 shows the X-ray diffraction pattern of silica, eggshell and activated carbon used for composite preparation along with the XRD pattern of composite for comparison. Figure 6.5 shows that silica has a peak around 22º. Activated carbon shows peaks around 23 degrees and around 43 degrees as observed in chapter 3 article 3.4.2.1. Eggshells shows the X-ray diffraction pattern is identical to $CaCO_3$, as observed in chapter 3 article 3.4.1.1

Figure 6.6 shows the X-ray diffraction pattern of composite sample. It was observed from the figure that sample shows the peaks at the 2θ value of around 20.8º, 22º, 26.8º, 31.4º, 36º, 39º, 42.5º and around 50.3º. Out of these major peaks, around 20.8º and around 22º is due to the presence of silica in composite. One major peak, which observed around 26 degree is due to the presence of silica, activated carbon and CaO in composite. Other minor peaks around 31.4º, 36º, 39º and around 50.3º are due to the presence of CaO in composite, while a minor peak around 42.5º is due to the presence of activated carbon in composite.

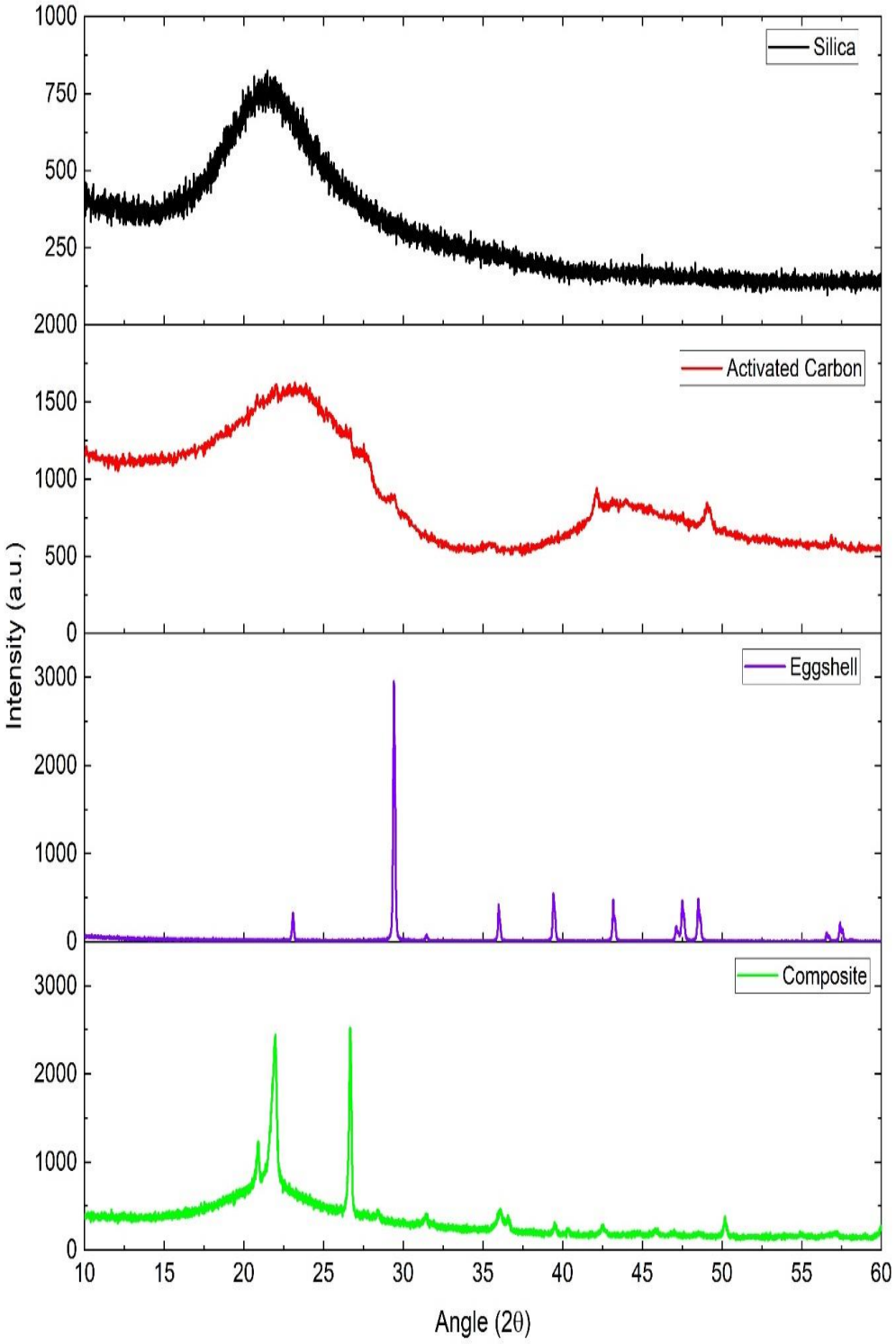

Figure 6.5 Comparison of X-Ray Diffraction patterns of composite sample, eggshell particle, activated carbon, and silica

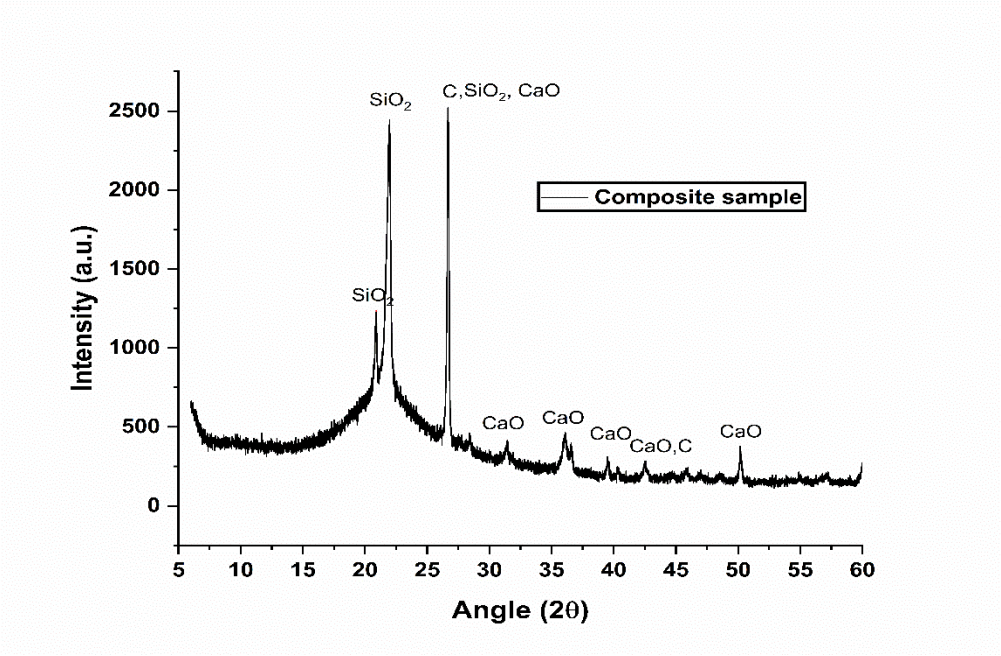

Figure 6.6 X-Ray Diffraction pattern of siilca-activated carbon-eggshell nanoparticulate composite

6.6.2 SEM-EDX analysis of composite sample

Figures 6.7 (a-b) show SEM images of silica-activated carbon composite. The SEM images clearly show the pore formation. It is noticed from the figure that there are plenty of pores all over the surface. The pores are clear, strong and transparent. The pore size varies from a few microns to nanometer.

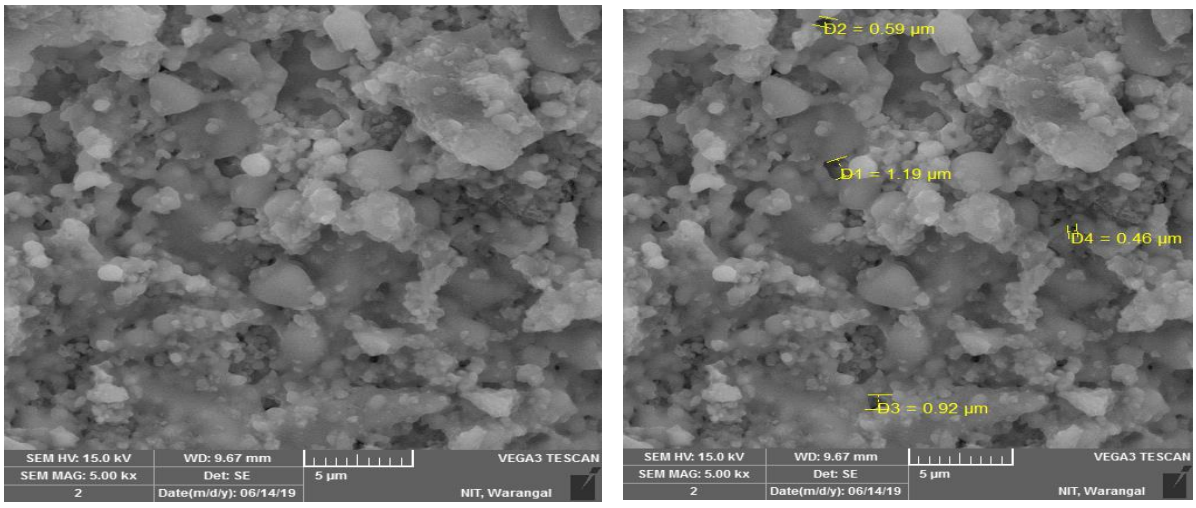

(a) (b)

Figure 6.7 SEM images of silica-activated carbon composite

Figure 6.8 (a-b) shows SEM images of silica-activated carbon-eggshell composite. Figure 6.8 clearly shows pore formation just like figure 6.7.

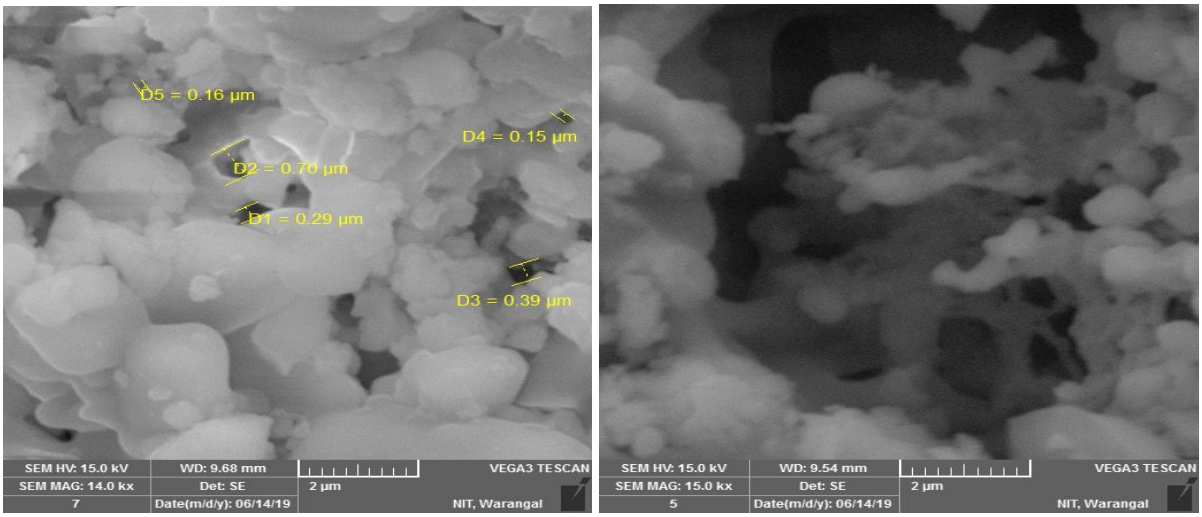

(a) (b)

Figure 6.8 SEM images silica-activated carbon-eggshell nanoparticulate composite

Figure 6.9 shows EDX analysis of silica-activated carbon composite sample. It is observed from figure 6.9 that the sample contains silicon, oxygen and carbon. Table 6.2 shows weight percentage of all the elements presents on the surface. EDX confirms the successful fabrication of composite sample.

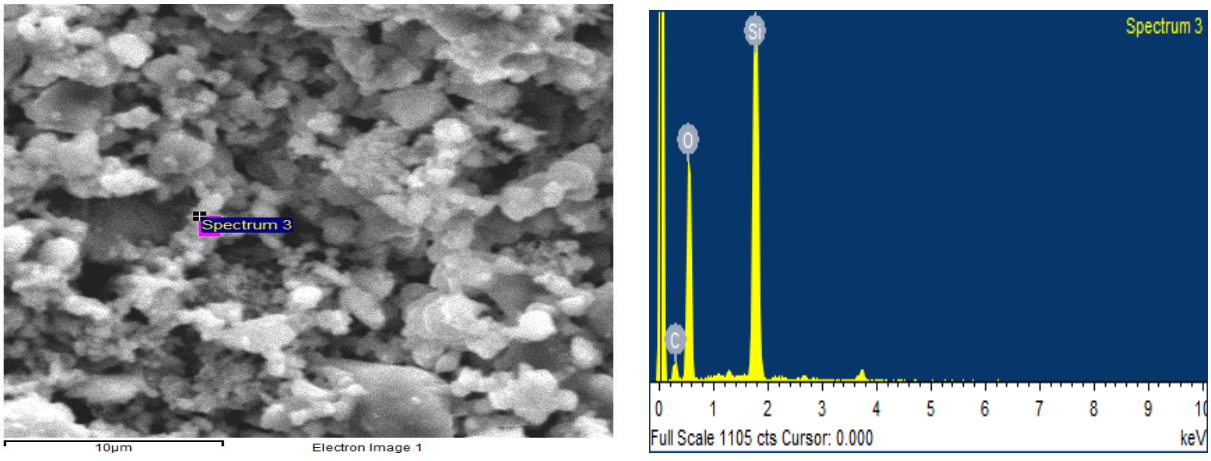

Figure 6.9 EDX analysis of activated carbon-silica composite

EDX analysis of silica-activated carbon-eggshell nanoparticle composite sample is illustrated in figure 6.10. The figure shows the presence of silica, oxygen, carbon and calcium in the sample. Different percentages of elements i.e. silica, oxygen, carbon and calcium in the sample are shown in table 6.3. EDX showed the presence of carbon, calcium, silicon and oxygen which confirms the successful fabrication of the composite. The XRD analysis also supports the claim

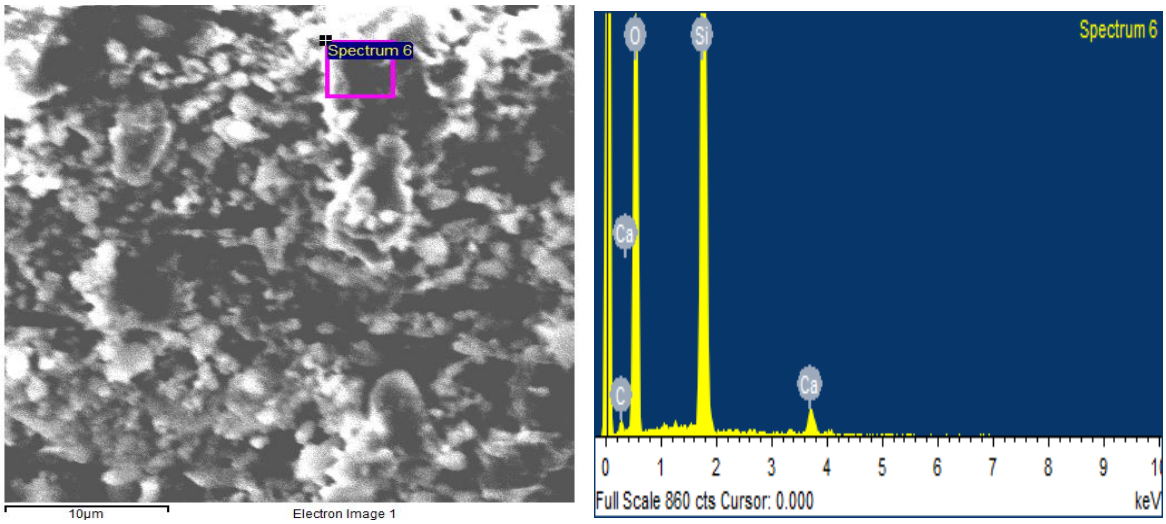

Figure 6.10 EDX analysis of activated carbon silica-eggshell nanoparticulate composite

Table 6.2 Element contents in silica-activated carbon composite

Element	Weight%	Atomic%
C	13.91	20.49
O	53.09	58.72
Si	33.00	20.79
Totals	100.00	

Table 6.3 Element contents in silica-activated carbon-eggshell nanoparticulate composite

Element	Weight%	Atomic%
C	6.64	7.19
O	54.48	70.24
Si	32.32	21.39
Ca	6.56	1.19
Totals	100.00	

6.6.3 Morphology analysis of chitosan pellet

Figures 6.11 (a-c) show SEM images of chitosan pellet. The SEM images clearly show the pore formation. It is noticed from the figure that there are plenty of pores all over the surface. The pores are clear, strong and transparent. The pore size varies from a few microns to nano meter.

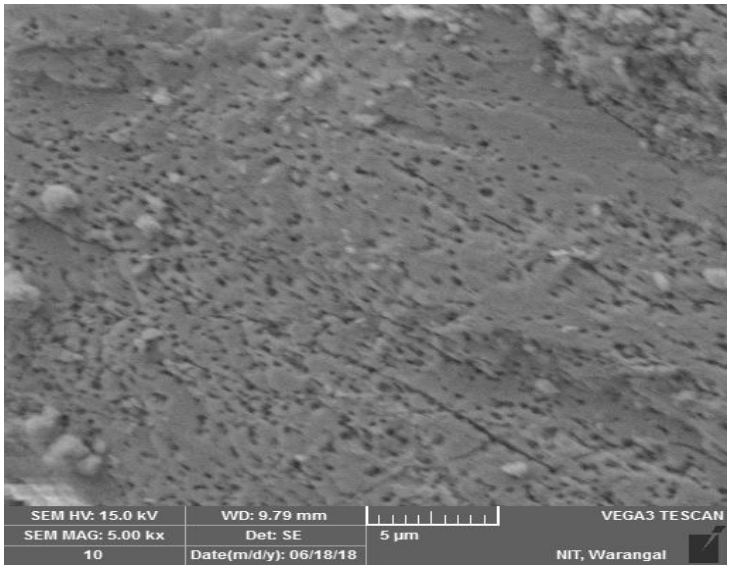

(a)

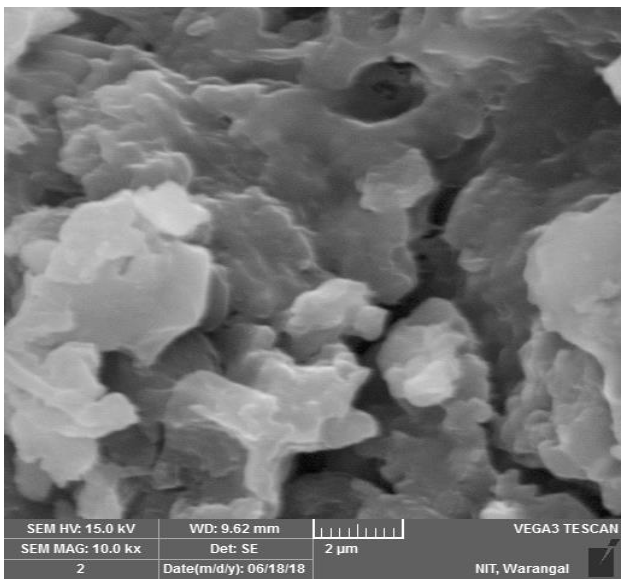

(b)

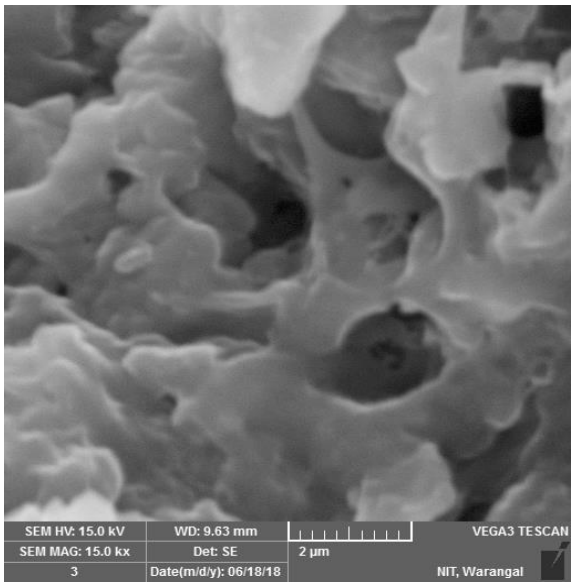

(c)

Figure 6.11 SEM images of chitosan pellet at different magnification

6.6.4 Dye Adsorption Test

Figure 6.12 represents dye adsorption by composite filter (Here the composite filter term used for combination composite sample and chitosan pellet). It is clearly visible from the figure 6.12 that color of the water change from dark blue to light blue and then it shows clear water.

Figure 6.13 illustrates the adsorption rate of composite sample (combination of composite sample and chitosan pellet) used in conjunction with chitosan pellet for various initial concentrations (400-900 mg/L) of the dye solution. The equilibrium was attained after 5 hours of contact time with highest dye adsorption of 635.46 mg/g for 900 mg/L of initial concentration. The figure depicts fast adsorption at initial time periods, which may be due to the availability of unfilled pores with a higher diffusion rate of methylene blue ions into the filter. However, with time, the pores get filled with methylene blue ion and equilibrium is attained.

It is observed from figure 6.13 (a) that Langmuir isotherms provide a better fit with R^2 value of 0.9967 suggesting monolayer adsorption of methylene blue by the filter. The values for Langmuir and Freundlich parameters are given in table 6.4. R_L is found to be 0.00106 ($0<R_L<1$, favorable) which suggest that prepared filter is suitable for dye adsorption.

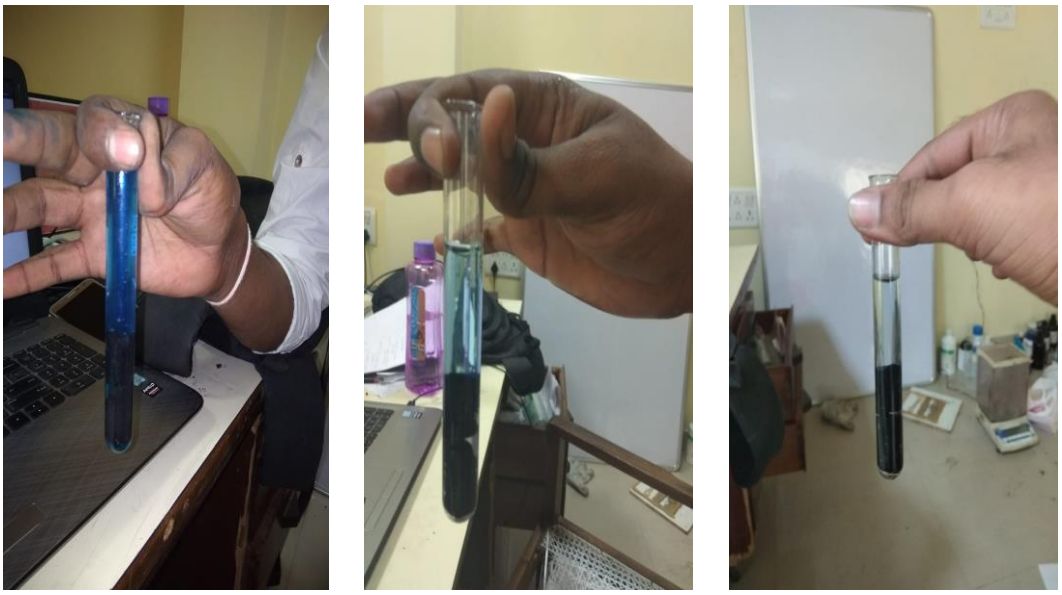

Figure 6.12 Methylene blue dye adosrption by composite filter

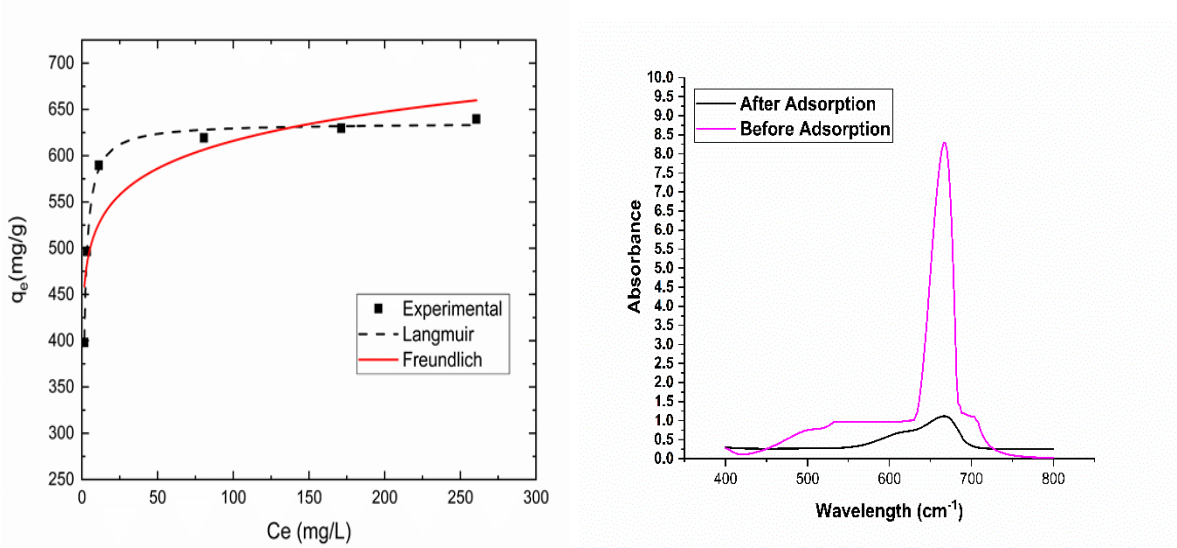

Figure 6.13 (a) Adsorption isotherms of methylene blue dye on composite filter (b) Absorbance before and after dye adsorption by composite filter

Table 6.4 Langmuir and Freundlich isotherms parameters for methylene blue adsorption by composite filter

q_m	R_L	R^2	K_L	K_F	n	R^2
635.46	0.00106	0.9967	1.04517	442.72	13.94	0.813

6.6.5 Total dissolved solid content and pH

From TDS analysis it was found that water had a TDS value of 1100 ppm, before treatment with composite filter and after treatment the TDS value was found to be 284. ppm. The pH analysis results show that the filter makes water basic in nature.

6.7 Conclusions

The following conclusions are drawn based on the study

1. A composite sample is successfully prepared using Silica, activated carbon and eggshells using gel casting method.

2. XRD and EDAX shows the presence of silica, activated carbon and calcium oxide in the composite sample.

3. SEM analysis showed that there are plenty of pores present on the surface of composite sample.

4. The Chitosan pellet was also prepared using compression molding. SEM analysis shows that it has layered structure, which makes it suitable for filtration

5. Composite sample and chitosan pellet were used in combination for adsorption of methylene blue dye. The maximum dye adsorption capacity was found to be 635.46 mg/g for 900 mg/L of initial concentration. The high adsorption of dye makes composite filter a suitable candidate for dye adsorption.

6. Filter decreased TDS concentration significantly also made water from being slightly acidic to basic. This suggests that the filter also can be used for prepared candle for water filtration.

Chapter 7

Conclusions and future scope

7.1 Conclusions

Following conclusions are drawn based on the study

- Biowastes such as eggshell, coconut shell, and crab shell were successfully converted into value added products.
- Eggshell has calcium carbonate ($CaCO_3$) as the major constituents. In comparison between unboiled and boiled eggshell, boiled eggshell, outer layer (cuticle layer) was not present in boiled eggshell.
- Unboiled eggshell nanoparticle has hexagonal structure. Unboiled eggshell nanoparticle has amine salt as surface functional due to the presence of eggshell membrane which was not present in boiled eggshell.
- Activated carbon was successfully synthesized using a novel method. Synthesized activated carbon has a surface area of 375.4 m^2/g and an average pore size of 2.64nm. Activated carbon showed a high absorption capacity for methylene blue dye adsorption with 305.76 mg/g of dye adsorption.
- The chitosan nanopowder was synthesized using planetary ball milling process. FTIR analysis showed the presence of amine and amide functional group, which show a good adsorbent property. Chitosan showed a good adsorption capacity for the dye adsorption with dye capacity of 187.76 mg/g.
- Epoxy polymer composites were successfully fabricated using unboiled eggshell and boiled eggshell microparticulate. Comparative study of environmental behavior and erosion behavior showed that unboiled microparticulate epoxy composite provide better results compared to boiled eggshell microparticulate epoxy composites. 4wt % microparticulate reinforcement was found to be the optimum percentage of reinforcement in case of unboiled eggshell microparticulate epoxy composite.

- Eggshell nanoparticulate epoxy composite was successfully prepared using unboiled eggshell nanoparticles as reinforcement. The erosion wear was synergistically improved by incorporation of eggshell nanoparticles. The composites showed semi brittle behavior. The erosion resistance of nanocomposite is far better than the micro composite. The erosion wear rate was decreased by 68%.

2 wt. % unboiled eggshell nanoparticle addition was found to be the optimum in case of nanocomposite.

- Eggshell nanoparticulate incorporation greatly enhanced mechanical properties. 2wt % eggshell nanoparticulate addition was found to be the optimum percentage for tensile strength and tensile modulus. Tensile strength was increased by 117%. Tensile modulus was enhanced by 116% owing to 1wt.% nanoparticulate addition.

- Flexural strength also found to be increased with filler addition, the maximum bending strength was observed for 3wt% of nanoparticulate addition while flexural modules is maximum for 2wt.% of nanoparticulate addition. The flexural strength was enhanced by 61% while flexural modulus was multiplied by more than four times due to eggshell nanoparticles incorporation.

- Polymer composite with activated carbon particles as reinforcement and epoxy as matrix material; was successfully prepared. The composite showed much higher wear resistance compared to bare epoxy. The composite showed semi ductile erosion behavior. The erosion wear rate was decreased by 82.4%.

- It was observed in environmental tests of composites that different environments have an adverse effect on composite properties.

- When comparing both the composites, it was found that the eggshell nanoparticulate epoxy composites provides better water absorption resistance and has more hardness than activated carbon epoxy composite, while the activated carbon epoxy composites provide better erosion wear resistance than the eggshell epoxy composites. The erosion wear rate was decreased by 82.4% in case activated carbon epoxy composite, while the erosion wear rate was reduced by 68% in case of eggshell nanoparticulate epoxy composite.

- Composite samples in the shape of cylinder were prepared using eggshell nanoparticles and activated carbon and silica as base material was synthesized. Composites sample was used in conjunction with chitosan nanopowder sample for water treatment.

- The filter has high potential of dye adsorption with very high dye adsorption capacity of 635.46 mg/g for initial concentration of 900 mg/L.

- The filter reduced TDS concentration of polluted water and also made water from slight acidic to basic.

7.2 Scope for future work

- Composite manufacturing was done by hand lay-up composite fabrication technique, however there are sophisticated composite manufacturing of composite that can be used composite manufacturing.
- In this work activated carbon was prepared using eggshell as activating agent. The activation was performed in argon environment; however, it can be done nitrogen environment, which might result in a better surface area.
- The activated carbon produced was ordered porous carbon, which was analyzed for its adsorption capacity, it can also be further analyzed for its application to enhance the capacitance.
- A composite sample was prepared which was used along with chitosan for filtration purpose. Two pellets act separately, however there is scope to find out method to join and make one pellet. These pellets can be used to prepare candle and can be utilized for water filtration.
- Few tests were done analyses the filtration capacity, however there exist a number of tests which can be done further analyses the efficiency of composite filter.
- The recovery of activated carbon and chitosan can be a further area of research.

References

1. Hunton, P. Research on eggshell structure and quality: an historical overview. *Revista Brasileira de Ciência Avícola* **2005**, *7*, 67–71.

2. Toro, P.; Quijada, R.; Yazdani-Pedram, M.; Arias, J.L. Eggshell, a new bio-filler for polypropylene composites. *Materials Letters* **2007**, *61*, 4347–4350.

3. Annual Report 2016-17 | Department of Animal Husbandry & Dairying Available online: http://www.dahd.nic.in/reports/annual-report-2016-17 (accessed on Sep 21, 2019).

4. Oliveira, D.A.; Benelli, P.; Amante, E.R. A literature review on adding value to solid residues: egg shells. *Journal of Cleaner Production* **2013**, *46*, 42–47.

5. Moreno-Castilla, C.; Carrasco-Marín, F.; López-Ramón, M.V.; Alvarez-Merino, M.A. Chemical and physical activation of olive-mill waste water to produce activated carbons. *Carbon* **2001**, *39*, 1415–1420.

6. Ioannidou, O.; Zabaniotou, A. Agricultural residues as precursors for activated carbon production—A review. *Renewable and Sustainable Energy Reviews* **2007**, *11*, 1966–2005.

7. Torres-Perez, J.; Gerente, C.; Andres, Y. Conversion of agricultural residues into activated carbons for water purification: Application to arsenate removal. *Journal of Environmental Science and Health, Part A* **2012**, *47*, 1173–1185.

8. Dias, J.M.; Alvim-Ferraz, M.C.M.; Almeida, M.F.; Rivera-Utrilla, J.; Sánchez-Polo, M. Waste materials for activated carbon preparation and its use in aqueous-phase treatment: A review. *Journal of Environmental Management* **2007**, *85*, 833–846.

9. Ahmed, M.J. Adsorption of non-steroidal anti-inflammatory drugs from aqueous solution using activated carbons: Review. *Journal of Environmental Management* **2017**, *190*, 274–282.

10. Sircar, S.; Golden, T.C.; Rao, M.B. Activated carbon for gas separation and storage.

Carbon **1996**, *34*, 1–12.

11. Ao, C.H.; Lee, S.C. Indoor air purification by photocatalyst TiO2 immobilized on an activated carbon filter installed in an air cleaner. *Chemical Engineering Science* **2005**, *60*, 103–109.

12. Yue, L.; Xia, Q.; Wang, L.; Wang, L.; DaCosta, H.; Yang, J.; Hu, X. CO2 adsorption at nitrogen-doped carbons prepared by K2CO3 activation of urea-modified coconut shell. *Journal of Colloid and Interface Science* **2018**, *511*, 259–267.

13. Jain, A.; Aravindan, V.; Jayaraman, S.; Kumar, P.S.; Balasubramanian, R.; Ramakrishna, S.; Madhavi, S.; Srinivasan, M.P. Activated carbons derived from coconut shells as high energy density cathode material for Li-ion capacitors. *Scientific Reports* **2013**, *3*, 3002–3007.

14. Peng, L.; Liang, Y.; Dong, H.; Hu, H.; Zhao, X.; Cai, Y.; Xiao, Y.; Liu, Y.; Zheng, M. Super-hierarchical porous carbons derived from mixed biomass wastes by a stepwise removal strategy for high-performance supercapacitors. *Journal of Power Sources* **2018**, *377*, 151–160.

15. Ojha, S.; Acharya, S.K.; Gujjala, R. Characterization and Wear Behavior of Carbon Black Filled Polymer Composites. *Procedia Materials Science* **2014**, *6*, 468–475.

16. Mohammed, M.H.; Williams, P.A.; Tverezovskaya, O. Extraction of chitin from prawn shells and conversion to low molecular mass chitosan. *Food Hydrocolloids* **2013**, *31*, 166–171.

17. Martínez-Camacho, A.P.; Cortez-Rocha, M.O.; Ezquerra-Brauer, J.M.; Graciano-Verdugo, A.Z.; Rodriguez-Félix, F.; Castillo-Ortega, M.M.; Yépiz-Gómez, M.S.; Plascencia-Jatomea, M. Chitosan composite films: Thermal, structural, mechanical and antifungal properties. *Carbohydrate Polymers* **2010**, *82*, 305–315.

18. Dash, M.; Chiellini, F.; Ottenbrite, R.M.; Chiellini, E. Chitosan—A versatile semi-synthetic polymer in biomedical applications. *Progress in Polymer Science* **2011**, *36*, 981–1014.

19. Kumirska, J.; Czerwicka, M.; Kaczyński, Z.; Bychowska, A.; Brzozowski, K.; Thöming,

J.; Stepnowski, P. Application of Spectroscopic Methods for Structural Analysis of Chitin and Chitosan. *Marine Drugs* 2010, *8*, 1567–1636.

20. Feldman, D. Polymer History. *Designed Monomers and Polymers* **2008**, *11*, 1–15.

21. Sudha, P.N.; Sangeetha, K.; Vijayalakshmi, K. Nanomaterials history, classification, unique properties, production and market. *Emerging Applications of Nanoparticles and Architecture Nanostructures* **2018**, 341–384.

22. Roco, M.C. From Vision to the Implementation of the U.S. National Nanotechnology Initiative. *Journal of Nanoparticle Research* **2001**, *3*, 5–11.

23. Bhatnagar, A.; Sillanpää, M. Utilization of agro-industrial and municipal waste materials as potential adsorbents for water treatment—A review. *Chemical Engineering Journal* **2010**, *157*, 277–296.

24. United Nations Children's Fund (UNICEF), W.H.O. (WHO) Progress on Drinking Water, Sanitation and Hygiene: 2017 Update and SDG Baselines | UNICEF Publications | UNICEF Available online: https://www.unicef.org/publications/index_96611.html (accessed on Sep 21, 2019).

25. Le, N.L.; Nunes, S.P. Materials and membrane technologies for water and energy sustainability. *Sustainable Materials and Technologies* **2016**, *7*, 1–28.

26. Oki, T.; Kanae, S. Global hydrological cycles and world water resources. *Science (New York, N.Y.)* **2006**, *313*, 1068–72.

27. Organization, W.H. *Water quality and health-review of turbidity: information for regulators and water suppliers*; World Health Organization, 2017;

28. Gautam, R.K.; Sharma, S.K.; Mahiya, S.; Chattopadhyaya, M.C. Contamination of Heavy Metals in Aquatic Media: Transport, Toxicity and Technologies for Remediation. In *Heavy Metals In Water*; Royal Society of Chemistry: Cambridge, 2014; pp. 1–24.

29. Cotruvo, J. Hardness in Drinking Water, Background Document for Development of WHO Guidelines for Drinking Water Quality. *Geneva, Switzerland: World Health Organization* **2011**.

30. Boyd, C.E. Microorganisms and Water Quality. In *Water Quality*; Springer International Publishing: Cham, 2015; pp. 233–267.

31. Cabral, J.P.S. Water Microbiology. Bacterial Pathogens and Water. *International Journal of Environmental Research and Public Health* **2010**, *7*, 3657–3703.

32. Cotruvo, J.A. 2017 WHO Guidelines for Drinking Water Quality: First Addendum to the Fourth Edition. *Journal - American Water Works Association* **2017**, *109*, 44–51.

33. Industrial Waste - Chapter 9 - Page 1 Available online: http://www.texascenter.org/almanac/Waste/INDUSTRIALCH9P1.HTML (accessed on Sep 21, 2019).

34. Hanchang, S.H.I. Industrial wastewater-types, amounts and effects. *Point sources of pollution: Local effects and their control* **2009**, *2*, 191–196.

35. Kant, R. Textile dyeing industry an environmental hazard. *Natural Science* **2012**, *04*, 22–26.

36. Lee, S.H.; Wang, S. Biodegradable polymers/bamboo fiber biocomposite with bio-based coupling agent. *Composites Part A: Applied Science and Manufacturing* **2006**, *37*, 80–91.

37. Pirayesh, H.; Khazaeian, A. Using almond (Prunus amygdalus L.) shell as a bio-waste resource in wood based composite. *Composites Part B: Engineering* **2012**, *43*, 1475–1479.

38. Mishra, S.C.; Nadiya Bihari Nayak, N.B.; Satapathy, A. Investigation on Bio-waste Reinforced Epoxy Composites. *Journal of Reinforced Plastics and Composites* **2010**, *29*, 3016–3020.

39. Prithivirajan, R.; Jayabal, S.; Sundaram, S.K.; Kumar, A.P. Hybrid biocomposites from agricultural residues: mechanical and thickness swelling behavior. *Cellulose* **2016**, *35*, 21–27.

40. Khan, M.Z.R.; Srivastava, S.K.; Gupta, M. Hybrid wood particulates composites: mechanical and thermal properties. *Materials Research Express* **2019**, *6*, 105323.

41. Movva, M.; Kommineni, R. Extraction of cellulose from pistachio shell and physical and mechanical characterisation of cellulose-based nanocomposites. *Materials Research Express* **2017**, *4*, 045014.

42. Movva, M.; Kommineni, R. Effect of Green Gram Husk Nanocellulose on Banana Fiber Composite. *Journal of Natural Fibers* **2019**, *16*, 287–299.

43. Venkateswara Rao, T.; Somaiah Chowdary, M.; Siva Sanakara Babu, C.; Mohan Sumanth, C. Effect of Bamboo Fiber on Mechanical Properties of Fly Ash with Polypropylene Composites. In; Springer, Singapore, 2019; pp. 437–446.

44. Baby, A.; Nayak, S.Y.; Heckadka, S.S.; Purohit, S.; Bhagat, K.K.; Thomas, L.G. Mechanical and morphological characterization of carbonized egg-shell fillers/Borassus fibre reinforced polyester hybrid composites. *Materials Research Express* **2019**, *6*, 105342.

45. Sajith, S.; Arumugam, V.; Dhakal, H.N. Comparison on mechanical properties of lignocellulosic flour epoxy composites prepared by using coconut shell, rice husk and teakwood as fillers. *Polymer Testing* **2017**, *58*, 60–69.

46. Kang, D.J.; Pal, K.; Park, S.J.; Bang, D.S.; Kim, J.K. Effect of eggshell and silk fibroin on styrene–ethylene/butylene–styrene as bio-filler. *Materials & Design* **2010**, *31*, 2216–2219.

47. Khraisheh, M.; Kim, J.; Campos, L.; Al-Muhtaseb, A.H.; Al-Hawari, A.; Al Ghouti, M.; Walker, G.M. Removal of pharmaceutical and personal care products (PPCPs) pollutants from water by novel TiO2–Coconut Shell Powder (TCNSP) composite. *Journal of Industrial and Engineering Chemistry* **2014**, *20*, 979–987.

48. Severa, L.; Němeček, J.; Nedomová, Š.; Buchar, J. Determination of micromechanical properties of a hen's eggshell by means of nanoindentation. *Journal of Food Engineering* **2010**, *101*, 146–151.

49. Mičicová, Z.; Domčeková, S.; Raník, L.; Liptáková, T. Inorganic Materials and their Use in Polymeric Materials. *Procedia Engineering* **2016**, *136*, 239–244.

50. Shafiur Rahman, G.M.; Aftab, H.; Shariful Islam, M.; Mukhlish, M.Z. Bin; Ali, F.

Enhanced physico-mechanical properties of polyester resin film using CaCO3 filler. *Fibers and Polymers* **2016**, *17*, 59–65.

51. Ji, G.; Zhu, H.; Qi, C.; Zeng, M. Mechanism of interactions of eggshell microparticles with epoxy resins. *Polymer Engineering & Science* **2009**, *49*, 1383–1388.

52. Bootklad, M.; Kaewtatip, K. Biodegradation of thermoplastic starch / eggshell powder composites. *Carbohydrate Polymers* **2013**, *97*, 315–320.

53. Vijayaraghavan, K.; Jegan, J.; Palanivelu, K.; Velan, M. Removal and recovery of copper from aqueous solution by eggshell in a packed column. *Minerals Engineering* **2005**, *18*, 545–547.

54. Tsai, W.-T.; Hsien, K.-J.; Hsu, H.-C.; Lin, C.-M.; Lin, K.-Y.; Chiu, C.-H. Utilization of ground eggshell waste as an adsorbent for the removal of dyes from aqueous solution. *Bioresource Technology* **2008**, *99*, 1623–1629.

55. Köse, T.E.; Kıvanç, B. Adsorption of phosphate from aqueous solutions using calcined waste eggshell. *Chemical Engineering Journal* **2011**, *178*, 34–39.

56. Baláž, M.; Bujňáková, Z.; Baláž, P.; Zorkovská, A.; Danková, Z.; Briančin, J. Adsorption of cadmium(II) on waste biomaterial. *Journal of Colloid and Interface Science* **2015**, *454*, 121–133.

57. Asgari, G.; Dayari, A. Experimental dataset on acid treated eggshell for removing cyanide ions from synthetic and industrial wastewaters. *Data in Brief* **2018**, *16*, 442–452.

58. De Angelis, G.; Medeghini, L.; Conte, A.M.; Mignardi, S. Recycling of eggshell waste into low-cost adsorbent for Ni removal from wastewater. *Journal of Cleaner Production* **2017**, *164*, 1497–1506.

59. Mittal, A.; Teotia, M.; Soni, R.K.; Mittal, J. Applications of egg shell and egg shell membrane as adsorbents: A review. *Journal of Molecular Liquids* **2016**, *223*, 376–387.

60. Mutavdžić Pavlović, D.; Ćurković, L.; Macan, J.; Žižek, K. Eggshell as a New Biosorbent for the Removal of Pharmaceuticals From Aqueous Solutions. *CLEAN - Soil, Air, Water* **2017**, *45*, 1700082.

61. Foo, K.Y.; Hameed, B.H. Coconut husk derived activated carbon via microwave induced activation: Effects of activation agents, preparation parameters and adsorption performance. *Chemical Engineering Journal* **2012**, *184*, 57–65.

62. Cosgrove, D.J. Growth of the plant cell wall. *Nature Reviews Molecular Cell Biology* **2005**, *6*, 850–861.

63. Sekirifa, M.L.; Hadj-Mahammed, M.; Pallier, S.; Baameur, L.; Richard, D.; Al-Dujaili, A.H. Preparation and characterization of an activated carbon from a date stones variety by physical activation with carbon dioxide. *Journal of Analytical and Applied Pyrolysis* **2013**, *99*, 155–160.

64. Hong, S.-M.; Jang, E.; Dysart, A.D.; Pol, V.G.; Lee, K.B. CO2 Capture in the Sustainable Wheat-Derived Activated Microporous Carbon Compartments. *Scientific Reports* **2016**, *6*, 34590.

65. Li, B.; Zhang, H.; Zhang, W.; Huang, L.; Duan, J.; Hu, J.; Ying, W. Cost effective activated carbon treatment process for removing free chlorine from water. *Asia-Pacific Journal of Chemical Engineering* **2009**, *5*, n/a-n/a.

66. Jain, A.; Balasubramanian, R.; Srinivasan, M.P. Hydrothermal conversion of biomass waste to activated carbon with high porosity: A review. *Chemical Engineering Journal* **2016**, *283*, 789–805.

67. Gaya, U.I.; Otene, E.; Abdullah, A.H. Adsorption of aqueous Cd(II) and Pb(II) on activated carbon nanopores prepared by chemical activation of doum palm shell. *SpringerPlus* **2015**, *4*, 458.

68. Abioye, A.M.; Ani, F.N. Recent development in the production of activated carbon electrodes from agricultural waste biomass for supercapacitors: A review. *Renewable and Sustainable Energy Reviews* **2015**, *52*, 1282–1293.

69. Zhang, Y.-J.; Xing, Z.-J.; Duan, Z.-K.; Meng Li; Wang, Y. Effects of steam activation on the pore structure and surface chemistry of activated carbon derived from bamboo waste. *Applied Surface Science* **2014**, *315*, 279–286.

70. Smets, K.; De Jong, M.; Lupul, I.; Gryglewicz, G.; Schreurs, S.; Carleer, R.; Yperman,

J. Rapeseed and Raspberry Seed Cakes as Inexpensive Raw Materials in the Production of Activated Carbon by Physical Activation: Effect of Activation Conditions on Textural and Phenol Adsorption Characteristics. *Materials* **2016**, *9*, 565.

71. Yang, K.; Peng, J.; Srinivasakannan, C.; Zhang, L.; Xia, H.; Duan, X. Preparation of high surface area activated carbon from coconut shells using microwave heating. *Bioresource Technology* **2010**, *101*, 6163–6169.

72. Amuda, O.S.; Giwa, A.A.; Bello, I.A. Removal of heavy metal from industrial wastewater using modified activated coconut shell carbon. *Biochemical Engineering Journal* **2007**, *36*, 174–181.

73. Khalil, H.P.S.A.; Noriman, N.Z.; Ahmad, M.N.; Ratnam, M.M.; Fuaad, N.A.N. Polyester Composites Filled Carbon Black and Activated Carbon from Bamboo (Gigantochloa scortechinii): Physical and Mechanical Properties. *Journal of Reinforced Plastics and Composites* **2007**, *26*, 305–320.

74. Mohd Din, A.T.; Hameed, B.H.; Ahmad, A.L. Batch adsorption of phenol onto physiochemical-activated coconut shell. *Journal of Hazardous Materials* **2009**, *161*, 1522–1529.

75. Isah A., U.; Abdulraheem, G.; Bala, S.; Muhammad, S.; Abdullahi, M. Kinetics, equilibrium and thermodynamics studies of C.I. Reactive Blue 19 dye adsorption on coconut shell based activated carbon. *International Biodeterioration & Biodegradation* **2015**, *102*, 265–273.

76. Raj, K.G.; Joy, P.A. Coconut shell based activated carbon–iron oxide magnetic nanocomposite for fast and efficient removal of oil spills. *Journal of Environmental Chemical Engineering* **2015**, *3*, 2068–2075.

77. Tahir, D.; Liong, S.; Bakri, F. Molecular and structural properties of polymer composites filled with activated charcoal particles. In Proceedings of the AIP Conference Proceedings; AIP Publishing LLC, 2016; Vol. 1719, p. 030024.

78. Giorcelli, M.; Khan, A.; Pugno, N.M.; Rosso, C.; Tagliaferro, A. Biochar as a cheap and environmental friendly filler able to improve polymer mechanical properties. *Biomass and Bioenergy* **2019**, *120*, 219–223.

79. Mahdy Samar, M.; El-Kalyoubi, M.H.; Khalaf, M.M.; Abd El-Razik, M.M. Physicochemical, functional, antioxidant and antibacterial properties of chitosan extracted from shrimp wastes by microwave technique. *Annals of Agricultural Sciences* **2013**, *58*, 33–41.

80. Sagheer, F.A. Al; Al-Sughayer, M.A.; Muslim, S.; Elsabee, M.Z. Extraction and characterization of chitin and chitosan from marine sources in Arabian Gulf. *Carbohydrate Polymers* **2009**, *77*, 410–419.

81. Kucukgulmez, A.; Celik, M.; Yanar, Y.; Sen, D.; Polat, H.; Kadak, A.E. Physicochemical characterization of chitosan extracted from Metapenaeus stebbingi shells. *Food Chemistry* **2011**, *126*, 1144–1148.

82. Abdou, E.S.; Nagy, K.S.A.; Elsabee, M.Z. Extraction and characterization of chitin and chitosan from local sources. *Bioresource Technology* **2008**, *99*, 1359–1367.

83. Paul, S.; Jayan, A.; Sasikumar, C.S.; Cherian, S.M. Extraction and purification of chitosan from chitin isolated from sea prawn Fenneropenaeus indicus. *EXTRACTION* **2014**, *7*.

84. Kumari, S.; Rath, P.K. Extraction and Characterization of Chitin and Chitosan from (Labeo rohit) Fish Scales. *Procedia Materials Science* **2014**, *6*, 482–489.

85. Yen, M.-T.; Yang, J.-H.; Mau, J.-L. Physicochemical characterization of chitin and chitosan from crab shells. *Carbohydrate Polymers* **2009**, *75*, 15–21.

86. Hamdi, M.; Hajji, S.; Affes, S.; Taktak, W.; Maâlej, H.; Nasri, M.; Nasri, R. Development of a controlled bioconversion process for the recovery of chitosan from blue crab (Portunus segnis) exoskeleton. *Food Hydrocolloids* **2018**, *77*, 534–548.

87. Divya, K.; Jisha, M.S. Chitosan nanoparticles preparation and applications. *Environmental Chemistry Letters* **2018**, *16*, 101–112.

88. Jothimani, B.; Sureshkumar, S.; Venkatachalapathy, B. Hydrophobic structural modification of chitosan and its impact on nanoparticle synthesis – A physicochemical study. *Carbohydrate Polymers* **2017**, *173*, 714–720.

89. Chen, X.; Gao, Y.; Wang, L.; Chen, H.; Yan, N. Effect of Treatment Methods on Chitin

Structure and Its Transformation into Nitrogen-Containing Chemicals. *ChemPlusChem* **2015**, *80*, 1565–1572.

90. Zhang, W.; Zhang, J.; Xia, W. Effect of Ball-Milling Treatment on Physicochemical and Structural Properties of Chitosan. *International Journal of Food Properties* **2014**, *17*, 26–37.

91. Sari, K.; Abraha, K.; Roto; Mashadi; Suharyadi, E. Effect of milling time on microstructures of nano-sized chitosan. *Journal of Physics: Conference Series* **2019**, *1170*, 012058.

92. Tran, T.H.; Nguyen, H.L.; Hao, L.T.; Kong, H.; Park, J.M.; Jung, S.H.; Cha, H.G.; Lee, J.Y.; Kim, H.; Hwang, S.Y.; et al. A ball milling-based one-step transformation of chitin biomass to organo-dispersible strong nanofibers passing highly time and energy consuming processes. *International Journal of Biological Macromolecules* **2019**, *125*, 660–667.

93. Hong, N.H. Introduction to Nanomaterials: Basic Properties, Synthesis, and Characterization. In *Nano-Sized Multifunctional Materials*; Elsevier, 2019; pp. 1–19.

94. Tulinski, M.; Jurczyk, M. Nanomaterials Synthesis Methods. In *Metrology and Standardization of Nanotechnology*; Wiley-VCH Verlag GmbH & Co. KGaA, 2017; pp. 75–98.

95. Banapurmath, N.; Yaradoddi, J.; Hunashyal, A.M.; Ganachari, S. V; Banapurmath, N.R.; Salimath, B.; Yaradoddi, J.S.; Shettar, A.S.; Hunashyal, A.M.; Venkataraman, A.; et al. Synthesis techniques for preparation of nanomaterials Synthesis Techniques for Preparation of Nanomaterials 4.

96. Tsai, W.T.; Yang, J.M.; Hsu, H.C.; Lin, C.M.; Lin, K.Y.; Chiu, C.H. Development and characterization of mesoporosity in eggshell ground by planetary ball milling. *Microporous and Mesoporous Materials* **2008**, *111*, 379–386.

97. Francis, A.A.; Abdel Rahman, M.K. The environmental sustainability of calcined calcium phosphates production from the milling of eggshell wastes and phosphoric acid. *Journal of Cleaner Production* **2016**, *137*, 1432–1438.

98. Wu, S.C.; Hsu, H.C.; Hsu, S.K.; Chang, Y.C.; Ho, W.F. Synthesis of hydroxyapatite from eggshell powders through ball milling and heat treatment. *Journal of Asian Ceramic Societies* **2016**, *4*, 85–90.

99. J Burton The World Leaders In Coconut Production Available online: www. worldatlas.com/articles/the-world-leaders-in-coconut-production. html (accessed on Oct 26, 2019).

100. Kumar Gadgey, K.; Kumar Gadgey Head, K.; Bahekar Head, A.; Professor, A.; Bahekar, A. Studies on extraction methods of chitin from crab shell and investigation of its mechanical properties. *International Journal of Mechanical Engineering and Technology* **2017**, *8*, 220–231.

101. Fu, R.W.; Li, Z.H.; Liang, Y.R.; Li, F.; Xu, F.; Wu, D.C. Hierarchical porous carbons: design, preparation, and performance in energy storage. *Xinxing Tan Cailiao/New Carbon Materials* 2011, *26*, 171–179.

102. Min, J.; Zhang, S.; Li, J.; Klingeler, R.; Wen, X.; Chen, X.; Zhao, X.; Tang, T.; Mijowska, E. From polystyrene waste to porous carbon flake and potential application in supercapacitor. *Waste Management* **2019**, *85*, 333–340.

103. Wen, Y.; Kierzek, K.; Min, J.; Chen, X.; Gong, J.; Niu, R.; Wen, X.; Azadmanjiri, J.; Mijowska, E.; Tang, T. Porous carbon nanosheet with high surface area derived from waste poly(ethylene terephthalate) for supercapacitor applications. *Journal of Applied Polymer Science* **2019**, 48338.

104. Chao, L.; Liu, Z.; Zhang, G.; Song, X.; Lei, X.; Noyong, M.; Simon, U.; Chang, Z.; Sun, X. Enhancement of capacitive deionization capacity of hierarchical porous carbon. *Journal of Materials Chemistry A* **2015**, *3*, 12730–12737.

105. Zsigmondy, R.; Scherrer, P. Bestimmung der inneren Struktur und der Größe von Kolloidteilchen mittels Röntgenstrahlen. In *Kolloidchemie Ein Lehrbuch*; Springer Berlin Heidelberg, 1912; pp. 387–409.

106. Ojha, S, Raghavendra, G., & Acharya, S.K. Utilization of waste carbon as reinforcement in thermoset composites. *Spherical and Fibrous Filler Composites* **2016**, *9*, 203-229.

107. Kumar Pal, A.; Das, A.; Katiyar, V. Chitosan from Muga silkworms (Antheraea assamensis) and its influence on thermal degradation behavior of poly (lactic acid) based biocomposite films. *Journal of Applied Polymer Science* **2016**, *133*.

108. Khenifi, A.; Bouberka, Z.; Sekrane, F.; Kameche, M.; Derriche, Z. Adsorption study of an industrial dye by an organic clay. *Adsorption* **2007**, *13*, 149–158.

109. Ahmed, M.J.; Dhedan, S.K. Equilibrium isotherms and kinetics modeling of methylene blue adsorption on agricultural wastes-based activated carbons. *Fluid Phase Equilibria* **2012**, *317*, 9–14.

110. Rivera, E.M.; Araiza, M.; Brostow, W.; Castaño, V.M.; Díaz-Estrada, J.R.; Hernández, R.; Rodríguez, J.R. Synthesis of hydroxyapatite from eggshells. *Materials Letters* **1999**, *41*, 128–134.

111. Naemchan, K.; Meejoo, S.; Onreabroy, W.; Limsuwan, P. Temperature effect on chicken egg shell investigated by XRD, TGA and FTIR. In Proceedings of the Advanced Materials Research; 2008; Vol. 55–57, pp. 333–336.

112. Carvalho, J.; Araujo, J.; Castro, F. Alternative low-cost adsorbent for water and wastewater decontamination derived from eggshell waste: An overview. *Waste and Biomass Valorization* 2011, *2*, 157–167.

113. Park, S.; Baker, J.O.; Himmel, M.E.; Parilla, P.A.; Johnson, D.K. Cellulose crystallinity index: Measurement techniques and their impact on interpreting cellulase performance. *Biotechnology for Biofuels* **2010**, *3*, 1–10.

114. Emmerich, F.G.; De Sousa, J.C.; Torriani, I.L.; Luengo, C.A. Erratum: Applications of a granular model and percolation theory to the electrical resistivity of heat treated endocarp of babassu nut (CARBON (1987) 25:3 (417-424)). *Carbon* 2013, *51*, 439.

115. Wei, T.; Zhang, Q.; Wei, X.; Gao, Y.; Li, H. A Facile and Low-Cost Route to Heteroatom Doped Porous Carbon Derived from Broussonetia Papyrifera Bark with Excellent Supercapacitance and CO 2 Capture Performance. *Scientific Reports* **2016**, *6*.

116. Louarn, G.; Zegzouti, A.; Tahiri, N.; Khouchaf, L.; Elaatmani, M.; Louarn, G.; Zegzouti, A.; Daoud, M. Study of the thermal treatment of SiO2 aggregate Study of the thermal

treatment of SiO 2 aggregate.

117. Keesom, W.H.; Taconis, K.W. On the crystal structure of chlorine. *Physica* **1936**, *3*, 237–242.

118. Moreira, J.C.; Santa, R.A.A.B.; Nones, J.; Riella, H.G. Synthesis of zeolite 4a for obtaining zeolite 5A by ionic exchange for full utilization of waste from paper industry. *Brazilian Journal of Chemical Engineering* **2018**, *35*, 623–630.

119. Jänes, A.; Kurig, H.; Lust, E. Characterisation of activated nanoporous carbon for supercapacitor electrode materials. *Carbon* **2007**, *45*, 1226–1233.

120. Tsai, W.T.; Yang, J.M.; Lai, C.W.; Cheng, Y.H.; Lin, C.C.; Yeh, C.W. Characterization and adsorption properties of eggshells and eggshell membrane. *Bioresource Technology* **2006**, *97*, 488–493.

121. Ahmad, F.; Daud, W.M.A.W.; Ahmad, M.A.; Radzi, R.; Azmi, A.A. The effects of CO2 activation, on porosity and surface functional groups of cocoa (Theobroma cacao) - Shell based activated carbon. *Journal of Environmental Chemical Engineering* **2013**, *1*, 378–388.

122. Guo, S.; Peng, J.; Li, W.; Yang, K.; Zhang, L.; Zhang, S.; Xia, H. Effects of CO 2 activation on porous structures of coconut shell-based activated carbons. *Applied Surface Science* **2009**, *255*, 8443–8449.

123. Yang, H.; Yan, R.; Chen, H.; Lee, D.H.; Zheng, C. Characteristics of hemicellulose, cellulose and lignin pyrolysis. *Fuel* **2007**, *86*, 1781–1788.

124. Burhenne, L.; Messmer, J.; Aicher, T.; Laborie, M.-P. The effect of the biomass components lignin, cellulose and hemicellulose on TGA and fixed bed pyrolysis. *Journal of Analytical and Applied Pyrolysis* **2013**, *101*, 177–184.

125. Singh, G.; Kim, I.Y.; Lakhi, K.S.; Srivastava, P.; Naidu, R.; Vinu, A. Single step synthesis of activated bio-carbons with a high surface area and their excellent CO2 adsorption capacity. *Carbon* **2017**, *116*, 448–455.

126. Shen, F.; Qiu, M.; Hua, Y.; Qi, X. Dual-Functional Templated Methodology for the Synthesis of Hierarchical Porous Carbon for Supercapacitor. *ChemistrySelect* **2018**, *3*,

586–591.

127. Langmuir, I. The adsorption of gases on plane surfaces of glass, mica and platinum. *Journal of the American Chemical Society* **1918**, *40*, 1361–1403.

128. H. M. F. Freundlich Over the adsorption in solution. *Journal of Physical Chemistry* **1906**, *57*, 385-471.

129. Hall, K.R.; Eagleton, L.C.; Acrivos, A.; Vermeulen, T. Pore- and solid-diffusion kinetics in fixed-bed adsorption under constant-pattern conditions. *Industrial and Engineering Chemistry Fundamentals* **1966**, *5*, 212–223.

130. Islam, M.A.; Ahmed, M.J.; Khanday, W.A.; Asif, M.; Hameed, B.H. Mesoporous activated coconut shell-derived hydrochar prepared via hydrothermal carbonization-NaOH activation for methylene blue adsorption. *Journal of Environmental Management* **2017**, *203*, 237–244.

131. Aljeboree, A.M.; Alshirifi, A.N.; Alkaim, A.F. Kinetics and equilibrium study for the adsorption of textile dyes on coconut shell activated carbon. *Arabian Journal of Chemistry* **2017**, *10*, S3381–S3393.

132. Akbar Babar, A.; Panhwar, I.; Qureshi, S.; Memon, S.; Siddiqui, Z. *Utilization of Biomass (Rice Straw) to Produce Activated Charcoal Through Single Stage Pyrolysis Process*; 2019; Vol. 14;.

133. Seidmohammadi, A.; Asgari, G.; … A.D.-P. in C.; 2019 A Comparative Study for the Removal of Methylene Blue Dye from Aqueous Solution by Novel Activated Carbon Based Adsorbents. *progress in color, colorants and coatings* **2019**, *12*, 133–144.

134. Wu, J.; Zhong, F.; Li, Y.; Shoemaker, C.F.; Xia, W. Preparation and characterization of pullulan–chitosan and pullulan–carboxymethyl chitosan blended films. *Food Hydrocolloids* **2013**, *30*, 82–91.

135. Luo, B.; Yang, J.; Zhao, J.; Hsu, C.; Li, J.; Zhou, C. Rapid synthesis and characterization of chitosan-g-poly (D, L-lactide) copolymers with hydroxyethyl chitosan as a macroinitiator under microwave irradiation. *Journal of Applied Polymer Science* **2012**, *125*, E125–E131.

136. Cunha, R.A.; Soares, T.A.; Rusu, V.H.; Pontes, F.J.S.; Franca, E.F.; Lins, R.D. The molecular structure and conformational dynamics of chitosan polymers: an integrated perspective from experiments and computational simulations. In *The complex world of polysaccharides*; IntechOpen, 2012.

137. Leceta, I.; Guerrero, P.; Ibarburu, I.; Dueñas, M.T.; de la Caba, K. Characterization and antimicrobial analysis of chitosan-based films. *Journal of Food Engineering* **2013**, *116*, 889–899.

138. Abdel-Fattah, W.I.; Jiang, T.; El-Bassyouni, G.E.-T.; Laurencin, C.T. Synthesis, characterization of chitosans and fabrication of sintered chitosan microsphere matrices for bone tissue engineering. *Acta Biomaterialia* **2007**, *3*, 503–514.

139. Abdellaoui, H.; Raji, M.; Bouhfid, R.; Qaiss, A. el kacem Investigation of the deformation behavior of epoxy-based composite materials. In *Failure Analysis in Biocomposites, Fibre-Reinforced Composites and Hybrid Composites*; Elsevier, 2019; pp. 29–49.

140. Fu, S.Y.; Lauke, B.; Mäder, E.; Yue, C.Y.; Hu, X. Tensile properties of short-glass-fiber- and short-carbon-fiber-reinforced polypropylene composites. *Composites Part A: Applied Science and Manufacturing* **2000**, *31*, 1117–1125.

141. Safi, S.; Zadhoush, A.; Masoomi, M. Effects of chemical surface pretreatment on tensile properties of a single glass fiber and the glass fiber reinforced epoxy composite. *Polymer Composites* **2016**, *37*, 91–100.

142. Hwang, H.Y. Electromechanical characteristics of unidirectional glass fiber epoxy composites. *Polymer Composites* **2011**, *32*, 558–564.

143. Jefferson, A.J.; Srinivasan, S.M.; Arockiarajan, A. Effect of multiphase fiber system and stacking sequence on low-velocity impact and residual tensile behavior of glass/epoxy composite laminates. *Polymer Composites* **2019**, *40*, 1450–1462.

144. Elleithy, R.H. Hierarchical structure and flexure behavior of woven carbon fiber epoxy composite. *Polymer Composites* **2000**, *21*, 716–723.

145. Liu, W.; Zhang, S.; Li, B.; Yang, F.; Jiao, W.; Hao, L.; Wang, R. Improvement in

interfacial shear strength and fracture toughness for carbon fiber reinforced epoxy composite by fiber sizing. *Polymer Composites* **2014**, *35*, 482–488.

146. Raghavendra, G.; Ojha, S.; Acharya, S.K.; Pal, S.K. Jute fiber reinforced epoxy composites and comparison with the glass and neat epoxy composites. *Journal of Composite Materials* **2014**, *48*, 2537–2547.

147. Latha, P.S.; Rao, M.V.; Kumar, V.V.K.; Raghavendra, G.; Ojha, S.; inala, R. Evaluation of mechanical and tribological properties of bamboo–glass hybrid fiber reinforced polymer composite. *Journal of Industrial Textiles* **2016**, *46*, 3–18.

148. Okubo, K.; Fujii, T.; Yamamoto, Y. Development of bamboo-based polymer composites and their mechanical properties. In Proceedings of the Composites Part A: Applied Science and Manufacturing; 2004; Vol. 35, pp. 377–383.

149. Yang, H.S.; Kim, H.J.; Son, J.; Park, H.J.; Lee, B.J.; Hwang, T.S. Rice-husk flour filled polypropylene composites; mechanical and morphological study. *Composite Structures* **2004**, *63*, 305–312.

150. Sapuan, SM, M Harimi and Maleque, M..- Mechanical properties of epoxy/coconut shell filler particle composites. *Arabian Journal for Science and Engineering. Section B: Engineering;* **2003**, *28.*, 171–181.

151. Geethamma, V.G.; Kalaprasad, G.; Groeninckx, G.; Thomas, S. Dynamic mechanical behavior of short coir fiber reinforced natural rubber composites. *Composites Part A: Applied Science and Manufacturing* **2005**, *36*, 1499–1506.

152. Panchal, M.; Raghavendra, G.; Prakash, M.O.; Ojha, S.; Chandra Bose, P.S. Moisture Absorption Behavior of Treated and Untreated Eggshell Particulate Epoxy Composites. *Silicon* **2018**, *10*, 859–867.

153. Panchal, M.; Raghavendra, G.; Prakash, M.O.; Ojha, S. Effects of Environmental Conditions on Erosion Wear of Eggshell Particulate Epoxy Composites. *Silicon* **2018**, *10*, 627–634.

154. Xu, Z.; Chu, Z.; Yan, L.; Chen, H.; Jia, H.; Tang, W. Effect of chicken eggshell on the flame-retardant and smoke suppression properties of an epoxy-based traditional APP-

PER-MEL system. *Polymer Composites* **2019**, *40*, 2712–2723.

155. Bootklad, M.; Kaewtatip, K. Biodegradation of thermoplastic starch/eggshell powder composites. *Carbohydrate Polymers* **2013**, *97*, 315–320.

156. Sutapun, W.; Pakdeechote, P.; Suppakarn, N.; Ruksakulpiwat, Y. Application of Calcined Eggshell Powder as Functional Filler for High Density Polyethylene. *Polymer - Plastics Technology and Engineering* **2013**, *52*, 1025–1033.

157. Prabhakar, M.N.; Rehaman Shah, A.U.; Song, J. Il Fabrication and characterization of eggshell powder particles fused wheat protein isolate green composite for packaging applications. *Polymer Composites* **2016**, *37*, 3280–3287.

158. Rahman, M.M.; Netravali, A.N.; Tiimob, B.J.; Rangari, V.K. Bioderived "green" composite from soy protein and eggshell nanopowder. *ACS Sustainable Chemistry and Engineering* **2014**, *2*, 2329–2337.

159. Saeb, M.R.; Ramezani-Dakhel, H.; Khonakdar, H.A.; Heinrich, G.; Wagenknecht, U. A comparative study on curing characteristics and thermomechanical properties of elastomeric nanocomposites: The effects of eggshell and calcium carbonate nanofillers. *Journal of Applied Polymer Science* **2013**, *127*, 4241–4250.

160. Ghabeer, T.; Dweiri, R.; Al-Khateeb, S. Thermal and mechanical characterization of polypropylene/eggshell biocomposites. *Journal of Reinforced Plastics and Composites* **2013**, *32*, 402–409.

161. Kumar, R.; Dhaliwal, J.S.; Kapur, G.S.; Shashikant Mechanical properties of modified biofiller-polypropylene composites. *Polymer Composites* **2014**, *35*, 708–714.

162. Suhas Y. Nayak, Srinivas Shenoy H., Pratul Sharma, Iqbal Aman, S.D. Use of egg shell particulate as fillers in e-glass/epoxy composites. In Proceedings of the Proceedings of International Conference on Mechanical Engineering and Industrial Automation ; Dubai, 2015; pp. 21–25.

163. Hiremath, P.; Shettar, M.; Shankar, M.C.G.; Mohan, N.S. Investigation on Effect of Egg Shell Powder on Mechanical Properties of GFRP Composites. In Proceedings of the Materials Today: Proceedings; Elsevier Ltd, 2018; Vol. 5, pp. 3014–3018.

164. Ellis, B. Introduction to the chemistry, synthesis, manufacture and characterization of epoxy resins. In *Chemistry and Technology of Epoxy Resins*; Springer Netherlands, 1993; pp. 1–36.

165. Leong, Y.W.; Abu Bakar, M.B.; Mohd Ishak, Z.A.; Ariffin, A. Characterization of talc/calcium carbonate filled polypropylene hybrid composites weathered in a natural environment. *Polymer Degradation and Stability* **2004**, *83*, 411–422.

166. Guermazi, N.; Haddar, N.; Elleuch, K.; Ayedi, H.F. Effect of filler addition and weathering conditions on the performance of PVC/CaCO3composites. *Polymer Composites* **2016**, *37*, 2171–2183.

167. Li, X.H.; Tjong, S.C.; Meng, Y.Z.; Zhu, Q. Fabrication and properties of polypropylene carbonate)/calcium carbonate composites. *Journal of Polymer Science, Part B: Polymer Physics* **2003**, *41*, 1806–1813.

168. Adeosun, S.O.; Usman, M.A.; Ayoola, W.A.; Bodud, M.A. Physico-Mechanical Responses of Polypropylene-$CaCO_3$ Composite. *Journal of Minerals and Materials Characterization and Engineering* **2013**, *1*, 145–152.

169. Abdullah A. Hussein, R.D.S. and A.A.S. Water absorption and mechanical properties of high - density polyethylene / egg shell composite. *Journal of Basrah Researches (Sciences)* **2011**, *37*, 36–42.

170. Siti Shuhadah and AG Supri LDPE-Isophthalic Acid-Modified Egg Shell Powder Composites (LDPE/ESPI). *Journal of Physical Science* **2009**, *20*, 87–98.

171. Soutis, C. Fibre reinforced composites in aircraft construction. *Progress in Aerospace Sciences* 2005, *41*, 143–151.

172. McDanels, D.L.; Serafini, T.T.; DiCarlo, J.A. Polymer, metal, and ceramic matrix composites for advanced aircraft engine applications. *Journal of Materials for Energy Systems* **1986**, *8*, 80–91.

173. Mangalgiri, P.D. Composite materials for aerospace applications. *Bulletin of Materials Science* **1999**, *22*, 657–664.

174. Feraboli, P.; Masini, A. Development of carbon/epoxy structural components for a high

performance vehicle. *Composites Part B: Engineering* **2004**, *35*, 323–330.

175. Brøndsted, P.; Lilholt, H.; Lystrup, A. Composite materials for wind power turbine blades. *Annual Review of Materials Research* **2005**, *35*, 505–538.

176. Barkoula, N.M.; Karger-Kocsis, J. Processes and influencing parameters of the solid particle erosion of polymers and their composites. *Journal of Materials Science* 2002, *37*, 3807–3820.

177. Patnaik, A.; Satapathy, A.; Chand, N.; Barkoula, N.M.; Biswas, S. Solid particle erosion wear characteristics of fiber and particulate filled polymer composites: A review. *Wear* **2010**, *268*, 249–263.

178. Yilmaz, M.G.; Unal, H.; Mimaroglu, A. Study of the strength and erosive behavior of $CaCO_3$ / glass fiber reinforced polyester composite. **2008**, *2*, 890–895.

179. Hassan, T.A.; Rangari, V.K.; Jeelani, S. Mechanical and thermal properties of bio-based $CaCO_3$ /soybean-based hybrid unsaturated polyester nanocomposites. *Journal of Applied Polymer Science* **2013**, *130*, 1442–1452.

180. Fu, S.Y.; Feng, X.Q.; Lauke, B.; Mai, Y.W. Effects of particle size, particle/matrix interface adhesion and particle loading on mechanical properties of particulate-polymer composites. *Composites Part B: Engineering* **2008**, *39*, 933–961.

181. Chow, T.S. The effect of particle shape on the mechanical properties of filled polymers. *Journal of Materials Science* 1980, *15*, 1873–1888.

182. Fu, S.; Feng, X.; Lauke, B.; Mai, Y. Effects of particle size , particle / matrix interface adhesion and particle loading on mechanical properties of particulate – polymer composites. **2008**, *39*, 933–961.

183. Mishra, S.; Sonawane, S.H.; Singh, R.P. Studies on characterization of nano CaCO3 prepared by thein situ deposition technique and its application in PP-nano CaCO3 composites. *Journal of Polymer Science Part B: Polymer Physics* **2005**, *43*, 107–113.

184. Alamri, H.; Low, I.M. Effect of water absorption on the mechanical properties of nano-filler reinforced epoxy nanocomposites. *Materials and Design* **2012**, *42*, 214–222.

185. Pradeep, T.; Anshup Noble metal nanoparticles for water purification: A critical review. *Thin Solid Films* 2009, *517*, 6441–6478.

186. Jahanshahi, M.; Rahimpour, A.; Peyravi, M. Developing thin film composite poly(piperazine-amide) and poly(vinyl-alcohol) nanofiltration membranes. *Desalination* **2010**, *257*, 129–136.

187. Xu, C.; Cui, A.; Xu, Y.; Fu, X. Graphene oxide-TiO2 composite filtration membranes and their potential application for water purification. *Carbon* **2013**, *62*, 465–471.

188. Bao, Q.; Zhang, D.; Qi, P. Synthesis and characterization of silver nanoparticle and graphene oxide nanosheet composites as a bactericidal agent for water disinfection. *Journal of Colloid and Interface Science* **2011**, *360*, 463–470.

189. Taha, A.A.; Wu, Y. na; Wang, H.; Li, F. Preparation and application of functionalized cellulose acetate/silica composite nanofibrous membrane via electrospinning for Cr(VI) ion removal from aqueous solution. *Journal of Environmental Management* **2012**, *112*, 10–16.

190. Li, B.; Cao, H. ZnO/graphene composite with enhanced performance for the removal of dye from water. *Journal of Materials Chemistry* **2011**, *21*, 3346–3349.

191. Upadhyay, R.K.; Soin, N.; Roy, S.S. Role of graphene/metal oxide composites as photocatalysts, adsorbents and disinfectants in water treatment: A review. *RSC Advances* 2014, *4*, 3823–3851.

192. Tesh, S.J.; Scott, T.B. Nano-composites for water remediation: A review. *Advanced Materials* 2014, *26*, 6056–6068.

Publications

Journals

1. **Panchal, M**., Raghavendra, G., Prakash, M. O., & Ojha, S. (2018). Effects of environmental conditions on erosion wear of eggshell particulate epoxy composites. Silicon, 10(2), 627-634. DOI 10.1007/s12633-016-9505-x. SCI journal
2. **Panchal, M**., Raghavendra, G., Prakash, M. O., Ojha, S., & Bose, P. S. C. (2018). Moisture absorption behavior of treated and untreated eggshell particulate epoxy composites. Silicon, 10(3), 859-867. DOI 10.1007/s12633-016-9541-6. SCI journal.
3. **Panchal, M**., Gujjala, R., Ojha, S., Omprakash, M., & Acharya, S. K. (2019). A single step process to synthesize ordered porous carbon from coconut shells-eggshells biowaste. Materials Research Express. 6 115613. DOI 10.1088/2053-1591/ab4cb3. SCI Journal.
4. **Manoj Panchal**, G. Raghavendra, M. Ompraksh S. Ojha , B. Vasavi. (2020) Effect of Eggshell particulate reinforcement on Tensile Behavior of Eggshell-Epoxy Composite. Springer lecture notes. 10.1007/978-981-15-2696-1_38. Scopus.
5. **Manoj Panchal**, G. Raghavendra, M. Ompraksh S. Ojha. Experimental investigation of Mechanical and Erosion behavior of eggshell nanoparticulate epoxy Biocomposite. Polymers and polymer composites. (Revised Review)
6. **Manoj Panchal**, G. Raghavendra, M. Ompraksh S. Ojha. Preparation and characterization of Nano chitosan from Crab Shells prepared by planetary ball milling. Arabian Journal of science and engineering (Communicated).
7. **Manoj Panchal**, G. Raghavendra, M. Ompraksh S. Ojha. Effect of environmental conditions on erosion behavior activated carbon epoxy composite. Polymer composites (Communicated).
8. **Manoj** Pa**nchal**, G. Raghavendra, M. Ompraksh S. Ojha. Fabrication and characterization of A novel Silica/Activated carbon /eggshell composite for water treatment. Silicon (Communicated).

International/ National Conferences

1. **Manoj Panchal**, G. Raghavendra, S. Ojha. Characterization of unboiled and boiled eggshells particle. National Symposium of Mechanical Engineering Research Scholars. NIT Warangal Oct. 2016.

2. **Manoj Panchal**, G. Raghavendra, S. Ojha. Utilization of bio waste as bio sorbent for waste water treatment, RAMSA Conference vizag, gayatri Vidhya parishad vizag dec-2017
3. **Manoj Panchal**, G.Raghavendra, S. Ojha Preparation and Characterization of Layered chitosan from crab shells. ICAFMD Feb 2019, NIT Warangal.
4. **Manoj Panchal**, G.Raghavendra, S. Ojha. A novel silica/activated carbon/nano eggshell composite filter for water treatment International Conference on Advances in Minerals, Metals, Materials, Manufacturing and Modelling, Metallurgy and material science department, Sept. 25-27, NIT Warangal.
5. **Manoj Panchal,** P Sai Kumar Reddy, Y Rajesh Kumar, P Sai kiran, G. Raghavendra, Srikar P. Environmental and erosion wear behavior of eggshell nanoparticulate Epoxy Composite. ICPCM, Dec-2019 NIT Rourkela.